POLITECNICO DI TORINO

Master's Degree in Aerospace Engineering

Master's Degree Thesis

Trajectory optimization with chemical propulsion for multiple debris removal missions

Supervisor

Prof. Lorenzo Casalino

Candidate

Daniele Poma

December 2024

Summary

Today, space debris is a natural consequence of any space mission and is originated by launching, operative and end of life phases ranging from debris smaller than 10 cm to big rocket bodies and upper stages. With the great increase of space activities in the last few decades, the crucial concern is that space debris poses a problem not only for future missions but also for present space activities with an increasing risk of in-orbit collisions between a debris and an active payload that, happening at a speed of several km/s, would be destructive; another consequence of these impacts would be the formation of a multitude of other debris with the risk of an exponential increase of the number of objects according to what Kessler Syndrome has predicted. Thanks to some international regulations, today the space sector is trying to reduce the amount of space debris produced during space missions in their whole but these actions are not enough and the actual situation makes Active Debris Removal (ADR) a compelling need. This thesis presents a possible ADR solution being a chemical propulsion spacecraft that rendezvous with several LEO debris objects and makes them de-orbit into Earth's atmosphere where they will destroy; since there is an obvious advantage if a single ADR mission can remove more than a single object, this thesis analyses multiple debris removal missions and in particular gives a strategy to select the optimal debris sequence in order to minimize the propellant consumption. The transfers between the objects exploit the J2 perturbation to further reduce the propellant required and the sequences created, among which the optimal ones are chosen, are characterized by a variable start in time and a variable duration; the algorithm used to optimize the sequences is an Ant Colony Optimization (ACO) algorithm based on ants' foraging behaviour that has been chosen because of its great performances in solving the Travelling Salesman Problem (TSP) to which this thesis' problem can be mapped. The results obtained by first applying the ACO to the global problem and then applying it to the single missions show that this approach is effective in finding a good 4-missions sequence of multiple debris with a reduced consumption of propellant.

Acknowledgements

Voglio ringraziare il mio relatore, il Professor Lorenzo Casalino, per essere riuscito con i suoi corsi ed i suoi insegnamenti ad accrescere in me la passione, già significativa, per il settore spaziale;
lo ringrazio per la disponibilità e la pazienza dimostrate durante il lavoro di questa tesi.

Ma soprattutto, un grande grazie va ai miei familiari ed in particolar modo ai miei genitori che mi sono sempre stati vicini, che hanno fatto e continuano a fare tanto per permettermi di realizzare i miei sogni.

Un ringraziamento particolare va poi a mio fratello Francesco, mio compagno di avventure, senza cui non potrei essere la persona che sono oggi.

Table of Contents

List of Tables VII

List of Figures VIII

Acronyms XI

1 Introduction 1

2 Space Debris 3
- 2.1 Space debris problem . . . 3
- 2.2 What are we doing . . . 7
- 2.3 Achievements and Missions . . . 11
  - 2.3.1 HEO Robotics . . . 12
  - 2.3.2 ClearSpace-1 . . . 12
  - 2.3.3 ADRAS-J . . . 13

3 Fundamentals of Orbital Mechanics and Astrodynamics 14
- 3.1 Two-Body problem . . . 14
  - 3.1.1 Description . . . 15
  - 3.1.2 Constants of motion . . . 18
  - 3.1.3 Classical Elements and other quantities . . . 20
- 3.2 Orbital Perturbations . . . 23
  - 3.2.1 Classification . . . 24
  - 3.2.2 Non-spherical mass distribution and J2 . . . 28
- 3.3 Space Propulsion . . . 31
- 3.4 Orbital Manoeuvres . . . 34

4 Ant Colony Optimization 37
- 4.1 Real ants behaviour . . . 37
- 4.2 ACO Metaheuristic . . . 40

4.3 ACO applied to the Travelling Salesman Problem . . . 42
4.4 Ant System . . . 43
4.5 AS Successors . . . 45
4.5.1 MMAS . . . 46
4.5.2 ACS . . . 47

5 Problem definition 49
5.1 GTOC9 . . . 49
5.2 Variations from the original problem . . . 51
5.3 Analytical model used for transfers . . . 53
5.4 Specific ACO algorithm used . . . 59

6 Calculations and Results 61
6.1 General parameters . . . 61
6.1.1 Analysis of $t1$ . . . 66
6.1.2 Variation of tt . . . 70
6.2 Analysis of α . . . 77
6.3 Analysis of β . . . 82
6.4 4 launches . . . 85

7 Conclusions 100

A The IJK coordinate system 102

B Combinatorial Optimization Problems 103

C Debris orbital elements 105

Bibliography 107

List of Tables

6.1 Results of the general parameters analysis 63
6.2 1% values of case 23 68
6.3 1% values of case 25 68
6.4 Trials results of case 23 with modified tt 71
6.5 Trials results of case 25 with modified tt 71
6.6 1% values of case 23, leg 1 73
6.7 1% values of case 25, leg 1 73
6.8 1% values of case 23, leg 2 74
6.9 1% values of case 25, leg 2 74
6.10 1% values of case 23, leg 3 74
6.11 1% values of case 25, leg 3 74
6.12 Results of the constant α analysis 77
6.13 Results of the discretely variable α analysis 79
6.14 Results of the continuously variable α analysis 81
6.15 Results of the constant β analysis 82
6.16 Results of the discretely variable β analysis 84
6.17 Results of the basic cases analysis 85
6.18 Results of the variable α cases analysis 86
6.19 Results of the modified tt cases analysis 86
6.20 Optimization of case $4L\_1$ 89
6.21 Optimization of case $4L\_2$ 90
6.22 Optimization of case $4L\_3$ 91
6.23 Optimization of case $4L\_4$ 92
6.24 Optimization of case $4L\_5$ 93
6.25 Optimization of case $4L\_6$ 94
6.26 Optimization of case $4L\_7$ 95
6.27 Optimization of case $4L\_8$ 96

List of Figures

2.1 Prediction of the number of catalogued in-orbit objects [1] 9
2.2 One of the pictures taken by ADRAS-J spacecraft [15] 13

3.1 The n-body problem [16] 15
3.2 The two-body problem [17] 17
3.3 Classical orbital elements [17] 21
3.4 The regression of the line of nodes [17] 30
3.5 Comparison between combined and separate manoeuvres 36

4.1 Experimental setup used for the double bridge experiment [18] . . . 38

5.1 Debris orbits 52
5.2 Debris inclinations and semimajor axes 54
5.3 Debris RAAN and semimajor axes 54

6.1 Case 2 63
6.2 Case 12 63
6.3 Case 15 64
6.4 Case 22 64
6.5 Case 23 64
6.6 Case 25 64
6.7 Case 27 64
6.8 Case 36 64
6.9 Case 38 65
6.10 Case 40 65
6.11 Trend of the maximum pheromone value (T trials) 67
6.12 Trend of the minimum pheromone value (T trials) 67
6.13 1% values positions in trial $T2$ 69
6.14 1% values positions in trial $T10$ 69
6.15 Trial $TT1$ 71
6.16 Trial $TT3$ 71
6.17 Trial $TT7$ 71

6.18 Trial $TT8$ . . . 71
6.19 Trend of the maximum pheromone value (TT trials) . . . 72
6.20 Trend of the minimum pheromone value (TT trials) . . . 72
6.21 1% values positions in trial $TT3$, leg 3 . . . 75
6.22 1% values positions in trial $TT6$, leg 3 . . . 75
6.23 Case A1 . . . 78
6.24 Case A5 . . . 78
6.25 Case A7 . . . 78
6.26 Case A9 . . . 78
6.27 Case A14 . . . 80
6.28 Case A17 . . . 80
6.29 Case A19 . . . 80
6.30 Case A24 . . . 80
6.31 Case A29 . . . 81
6.32 Case A30 . . . 81
6.33 Case B1 . . . 83
6.34 Case B5 . . . 83
6.35 Case B11 . . . 84
6.36 Case B17 . . . 84
6.37 Case $4L\_1$ . . . 86
6.38 Case $4L\_2$ . . . 86
6.39 Case $4L\_3$ . . . 87
6.40 Case $4L\_4$ . . . 87
6.41 Case $4L\_5$ . . . 87
6.42 Case $4L\_6$ . . . 87
6.43 Case $4L\_7$ . . . 87
6.44 Case $4L\_8$ . . . 87
6.45 Case $4L\_1$ optimized . . . 97
6.46 Case $4L\_2$ optimized . . . 97
6.47 Case $4L\_3$ optimized . . . 97
6.48 Case $4L\_4$ optimized . . . 97
6.49 Case $4L\_5$ optimized . . . 97
6.50 Case $4L\_6$ optimized . . . 97
6.51 Case $4L\_7$ optimized . . . 98
6.52 Case $4L\_8$ optimized . . . 98
6.53 First mission of case $4L\_7$ . . . 98
6.54 Second mission of case $4L\_7$ . . . 98
6.55 Third mission of case $4L\_7$ . . . 98
6.56 Fourth mission of case $4L\_7$ . . . 98

A.1 The geocentric equatorial system (IJK) [17] . . . 102

Acronyms

ACO

Ant Colony Optimization

ACP

Annual Collision Probability

ACS

Ant Colony System

ACT

Advanced Concepts Team

ADR

Active Debris Removal

AMR

Area to Mass Ratio

AS

Ant System

ASAT

Anti-SATellite weapons

EAS

Elitist strategy for Ant System

ESA

European Space Agency

GEO

GEOsynchronous orbit

GTOC

Global Trajectory Optimization Competition

ISAS

Institute of Space and Astronautical Science

ISS

International Space Station

JAXA

Japan Aerospace eXploration Agency

JPL

Jet Propulsion Laboratory

LEO

Low-Earth Orbit

MEO

Mid-Earth Orbit

MMAS

Max-Min Ant System

NEI

Non-Earth Imaging

NORAD

NORth american Aerospace Defense command

NP

Non-deterministic Polynomial time

P

Polynomial time

PMD

Post Mission Disposal

RAAN

Right Ascension of the Ascending Node

RPO

Rendezvous and Proximity Operations

TSP

Travelling Salesman Problem

UN

United Nations

USAF

United States Air Force

Chapter 1

Introduction

Environmental issues are becoming more and more important since their effects result being more evident and impacting on both nature and human activities; in recent periods, the focus of the matter has extended from only on-Earth environment to above Earth and space domain. The main issue arisen is strictly connected to the increase of space activities and it probably is the worse threat for their continuity: space debris.

In the last few decades, indeed, the space sector has experienced a great growth with also the rise of several private space companies making the space environment crucial and more commercialized. Even if the situation is improving, today the space activities, in the way they are actually conceived, are characterised by an inherent generation of new space debris that will keep growing in number if the trend continues and no action is taken. In order to solve the situation, reducing the production of new debris is not enough but an effective intervention is needed with the implementation of Active Debris Removal (ADR) missions [1]; one of the possible options is the use of a spacecraft that rendezvous with more debris objects during a single mission in order to make them de-orbit into Earth's atmosphere: this strategy has obvious advantages if compared to a case in which the spacecraft rendezvous with just one object in each mission.

In this thesis, the aforementioned solution is further explored and analysed, in particular, tackling the problem of finding among a group of debris objects the best order to rendezvous with them having the purpose of reducing propellant consumption; the possible sequences among which to choose the most promising ones are generated considering a variable starting date and with a variable duration in order to increase the number of possible sequences and achieve a greater variability. The algorithm used to optimize the itinerary of the spacecraft belongs to the category of Ant Colony Optimization (ACO) algorithms that are metaheuristic methods

inspired by ants' foraging behaviour and based on the coordinated action of a group of artificial agents.

The second chapter of this thesis gives an overview of the actual space debris objects situation with their categorisation and some examples of actual missions launched to deal with them; the third chapter briefly presents some basic notions and conventions of orbital mechanics and astrodynamics, which are useful to understand the problem treated and its criticalities. The fourth chapter presents the general ACO algorithm with an in-depth description of some of its most promising versions; the fifth chapter describes in an extensive way the problem tackled by this thesis and the methods used to solve it, while the sixth chapter presents the main calculations made and the results obtained.

Chapter 2

Space Debris

The term space debris refers to any human made inactive and uncontrolled object that is present in the space environment, from Low Earth Orbit (LEO) to the deep space; it is immediately clear the great variety of elements that belong to this group: from small pieces smaller than 10 cm to big rocket bodies and upper stages. This great size variability is one of the aspects that make the space debris issue a pretty hard one to be tackled and solved; despite this, the debris problem has been pretty evident since the beginning of the space program, generating several studies with the goal of solving it and tickling the collective imagination at the point of creating even a science fiction manga that focuses on this issue: *Planetes*. This chapter wants to give a general look to the space debris problem explaining what are the risks connected and the accidents already happened; subsequently, it presents the actual studies, the future programmed missions and the direction that the space sector is taking in order to solve the problem.

2.1 Space debris problem

The space debris problem has been tackled, at least from a theoretical and study point of view, from a relatively early stage in the space program history. Indeed, a paper of the 1978 [1] already tried to face the issue; it predicted that the fragments from random collisions between objects in LEO would become a relevant source of debris starting from the year 2000 producing a greater hazard than the one from natural meteoroids and, more importantly, making the number of debris increase exponentially in time, even if a zero net input condition would be actuated and maintained. It is scary how this 40 years old paper (whose conclusions were more recently confirmed by [1]) states that even keeping the number of orbiting satellites constant, the situation will worsen making the space environment even riskier for space missions; and if it is considered that in the last years the space

activities have seen a rapid growth with the launch of an always growing number of missions, it is particularly worrying for the future (but actually also present) of the space sector. That paper conclusions are based on the concept of collisional cascading of objects in orbit that emerged during the studies on the origin of the solar system, on ring formation around the planets and on meteoroids origin: it states that any two orbiting objects being at the same distance from the main attracting body represent an unstable condition; the objects, indeed, are predicted to eventually collide and create a great number of small fragments that, themselves, will share the same distance from the main body; these events, considering the orbital perturbations actions that modify the orbit characteristics (in particular for the LEO environment, where the atmospheric drag may cause initial different orbits to reach the same altitude), result having an even higher risk of happening. It is clear how, already in that period, the space debris was a real threat for the missions operability and, today, the situation is even worse; it was so evident the gravity of the problem, that it was even created a specific term to refer to that situation: the Kessler Syndrome. This expression, today becomes popular and sometimes misused, refers exactly to the collisional cascading event that risks to happen in the future: from the collision of two intact (and maybe even active) satellites, a great cloud of fragment would be produced posing an hazard also for the other orbiting satellites with the risk of starting a cascade destruction. The Kessler Syndrome, today, represents probably one of the worst threats for space activities with the risk of compromising the space environment or even of making it inaccessible; it is clear the need of taking action in order to, at least, mitigate this real risk.

To better understand what the problem deals with, the first step is to classify the in-orbit debris objects, a process that can be made considering different debris aspects to determine its origin, its actual conditions and potential orbit evolution [2]:

- orbit characteristics: debris pieces are basically related to the orbits where any space mission is or has been conducted (with the eventuality of variations from the original trajectories due to the perturbations, particularly for older debris); however, the debris, differently from its sizes, is not uniformly spread and is concentrated in the most used orbits with similar altitudes and specific inclinations. In particular, most of the debris objects can be found in LEO and GEO with inclinations at least near to the ones of the most useful orbits for space applications that are Molniya (a highly elliptical orbit with the critical inclination of 63.4°) and sun-synchronous ones (a better description of this type of orbit and of the meaning of critical inclination is given in subsection 3.2.2) [3]. This aspect creates great object clusters in some specific regions of the space environment, with some even more specific cases: an example is the

cluster of SL-8/Kosmos upper stages rocket bodies; the great majority of the 295 in orbit Kosmos upper stages can be found in nearly circular orbits with three distinct groupings of altitude and inclination being 760 km and 74°, 970 km and 83°, 1570 km and 74° [2]. Despite the similar altitudes and inclinations, however, the debris bodies RAAN are spread almost uniformly over the full circle because of the J2 effect causing different drift rates depending on the orbit semimajor axis and inclination. The concentration of debris in specific regions is both a positive and negative aspect: it has the advantage of making a potential ADR mission simpler and requiring a lower ΔV to be accomplished; on the other hand, the downside is that specific orbits (that are the most used and most useful for today's space activities) are rapidly becoming crowded with a higher risk of resulting unusable in a shorter period of time.

- fragmentation: the debris can be intact or fragmented with important consequences on its actual dimensions (meaning the level of damage that, in case of impact, it can cause to other in-orbit objects), on the capability of tracking it and on the complexity of a rendezvous manoeuvre with it.

- material: they may be made by a single material, by a few or they may be composite of many materials; it is important to determine of how many materials and of which materials the debris is made. These characteristics have an important effect on the damages caused in case of impact, on the level of destruction that the debris encounters during a potential atmosphere re-entry and on the technology that can be used to rendezvous and remove it (depending on the strength of the material, some techniques may risk to fragment it).

- size: as said before, the debris may have very different sizes but, generally, three main dimension categories can be identified: debris smaller than 1 mm, debris having dimensions comprised between 1 mm and 1 cm and debris bigger than 1 cm [4]; actually, these values have to be treated as approximations of the real debris dimensions and the particularly important divide size is considered to be 1 cm due to the different consequences that an impact with a debris smaller or bigger than that size can have. Another important reason to determine debris size is the capability of tracking it, an essential aspect of impact mitigation.

- shape: a debris can have a regular convex shape, a regular shape with concavities or an irregular shape; this characteristic is mainly linked to the possibility of rendezvous and docking with the debris and to the effects that perturbations can have on its orbit.

- area to mass ratio (AMR): it is possible to distinguish three main categories:

debris with a high area to mass ratio (HAMR) (>2 m^2/kg), debris with a medium area to mass ratio (MAMR) and debris with a low area to mass ratio (LAMR) (>0.8 m^2/kg); this aspect is linked to the risk of impact posed by a debris (a debris with a higher surface has also a higher probability of impact with other objects), to the effects of orbit perturbations on it and to the evolution of the burning process during a potential atmospheric re-entry.

An essential aspect of the problem and of the collision mitigation action is the ability of tracking the in-orbit debris objects to know their position and predict their trajectories; a crucial role in this sector is played by NORAD (North American Aerospace Defense Command), which monitors a great number of orbiting bodies. This organization provides the NORAD two-line element sets, that are the most comprehensive orbital database available today; however, this database is not complete for different reasons: first of all, it intentionally omits satellites considered essentials for US national security; moreover, it does not report all that objects considered lost since they have not been tracked for the past 30 days; finally, the database does not include a large number of debris pieces that are too small to be even detected or regularly tracked [5]. This last category of debris, in particular, poses a severe problem since there is a great number of debris objects that are too small to be detected but that can represent a serious hazard for other space missions; even if smaller debris bodies impacting a satellite may only cause some damages without destroying it, if they hit a vital component, even if they are smaller than 1 mm, given the high impact speed they may severely compromise a mission. A recent example of a small debris impact is the one happened to the NanoAvionics MP42 microsatellite; in October 2024, thanks to an onboard selfie camera, it was possible to identify a 6 mm hole on one of its solar panels. Despite the impact, the satellite was lucky enough not to experience serious damages and continued performing its mission without interruption [6]. Unluckily, this type of events can not be prevented or predicted given the high number of small debris pieces and the inability of monitoring them; probably, the only solution possible is improving the satellites resilience making them able to withstand these kind of impacts.

During the space program history, several impacts have already happened with the creation of thousands of new orbiting debris objects even if some of them were intentional, as part of anti-satellite tests; all the episodes here presented involved LEO satellites. One of the first events of this kind, and the first time ever that a satellite had been destroyed from an aircraft, is the USAF (United States Air Force) P-78 anti-satellite test of the 1985 intended to destroy an orbiting Solwind P78-1 satellite; the satellite had already completed its gamma ray spectroscopy mission and the test was intended to study the collision breakup evolution in order to develop more accurate models. The impact happened at the right altitude to

get a lot of informations from the breakup: it was high enough to have the time to catalogue most fragments possible but also low enough to make the study of fragments decay possible; the results concluded that a number between 80 and 95 fragments had a mass large enough to destroy another satellite with the same mass of the P78-1 satellite and that the lighter debris were the first to decay from orbit [1] [7].
The impact with the worst consequences, however, was the intentional break-up of the Chinese spacecraft Fengyun-1C happened in 2007; the satellite was hit by a ballistic object launched from Earth creating the most severe artificial debris cloud in a highly populated orbit since the beginning of the space exploration: about 2000 debris objects larger than 10 cm were identified populating long-lived orbits [8].
A much more recent event happened in 2021 when the satellite Cosmos 1408, an electronic signals spying spacecraft no longer operational, was destroyed by a Russian kinetic anti-satellite test; the impact caused about 1500 debris pieces of trackable size intersecting the ISS (Internation Space Station) orbit that forced the astronauts to wear their spacesuits and seek refuge in the crew capsules for the first passages of the cloud [9].
Even if these ASAT (Anti-satellite weapons) tests may have some little positive aspects about the post-impact studies (like for the P78-1 test), however, they have clear, detrimental effects on the debris environment producing large numbers of small objects that could be easily avoided; despite their terrible effects, today an international law banning these types of test does not really exist, and only in 2022 a UN (United Nations) panel formally adopted for the first time a not legally binding resolution to ban destructive ASAT tests to which only some nations committed [10].

Intentional ASAT tests, however, are not the only cause of in orbit impacts; indeed, in 2009 the first unintentional collision of two satellites occurred, involving the operational Iridium-33 and the inoperative Cosmos 2251 spacecrafts. This bad, avoidable accident generated more than 1600 large debris bodies gathered into two separate clouds [11].

2.2 What are we doing

Today, important steps forward have been made in detection and tracking of artificial objects and several studies have already been conducted on possible techniques that can be adopted to mitigate the space debris problem; however, most of these studies have focused on trajectory design and analysis to mitigate in orbit debris assuming a fixed targets sequence or being restricted to general order-of magnitude analyses [2]. This is the reason because this thesis focuses on finding and optimizing

a debris objects sequence so that they can be removed with successive missions.

From a practical point of view, currently, no actual debris removing mission has ever taken place even if important progresses and achievements have happened in the last years. An essential attitude adopted more and more by the international community is the so called Post Mission Disposal policy (PMD) that requires a payload or upper stage to be removed from the orbit within a determined period of time after its operational life end; recent studies have revealed this policy to be essential for the control of the debris number proliferation since it would allow, at least, to actuate a zero net in orbit input condition [1]. The PMD policy is well assumed by the ESA's (European Space Agency) Space Debris Mitigation Requirements [4] that establish also other important behaviours to assume to prevent an exponential growth of the debris number; here are presented the most important standards that can be applied to LEO missions contained in this document.

The PMD requirement imposed by the regulation is that the orbit clearance of a spacecraft shall be achieved by the disposal in an orbit with a natural orbital decay of less than 5 years and with a cumulative collision probability with space objects larger than 1 cm, from the satellite end of life until its re-entry, below 10^{-3}. This specific requirement, actually, applies to spacecraft operating in what is defined LEO protected region: a group of LEO orbits having an altitude going from zero (precisely, from the surface of a spherical Earth with an equatorial radius of 6378 km) up to 2000 km; it is possible to see how restrictive this regulation is and if a spacecraft at its end of life is in an orbit with a decay period longer than 5 years, it needs to perform a de-orbit manoeuvre either for a direct or a delayed de-orbit: in the first case the manoeuvre lowers the orbit perigee to an altitude below the Earth surface and the spacecraft burns directly into the atmosphere (this approach may be used for lower orbits and it is pretty expensive); with the second strategy, the satellite lowers its semimajor axis to an orbit with a natural decay lower than 5 years. Another requirement correlated to the de-orbit phase is that the expected number of casualties at re-entry shall be less than 10^{-4}; the regulation also suggests two possible ways to obtain this value: adopting the design for demise or choosing a controlled re-entry; the first recommendation refers to a spacecraft design practice in which full ablation of elements is achieved during the re-entry phase, the second one is a de-orbit where the time of re-entry is sufficiently controlled so that the impact of any potential surviving debris is confined to a specific area. This regulation, however, is not limited to de-orbit phases but it also contains several recommendations for the operational phase, an essential aspect that often is not considered (in most cases, when talking of debris, only the initial or end of life phases are considered); first of all, it is said that a spacecraft shall be designed not to release space debris during normal operations, reducing the

intentional generation of new objects. Another important requirement applicable to some satellites and missions (like satellites that are part of a constellation or that performs close proximity operations) is that a spacecraft shall have a recurrent manoeuvre capability that is the capability of performing repeatable manoeuvres to modify the orbit in order to avoid a potential impact with a debris; moreover, the regulation states that a spacecraft with manoeuvre capability operating in the LEO protected region shall have an ACP (Annual Collision Probability, it is the probability of having an impact during one year of operations) threshold below the lower value between: 10^{-4} and the collision probability value such to reduce the ACP by at least 90% with respect not performing collision avoidance manoeuvres.

Even if applying the PMD policy is essential, studies showed that implementing only the PMD behaviour is not enough to effectively tackle the debris problem [1]; this is also due to the fact that PMD can be applied to new missions but few objects that currently are already in orbit have this capability; therefore, it is essential also to take action and promote ADR missions, as it can clearly be seen in figure 2.1.

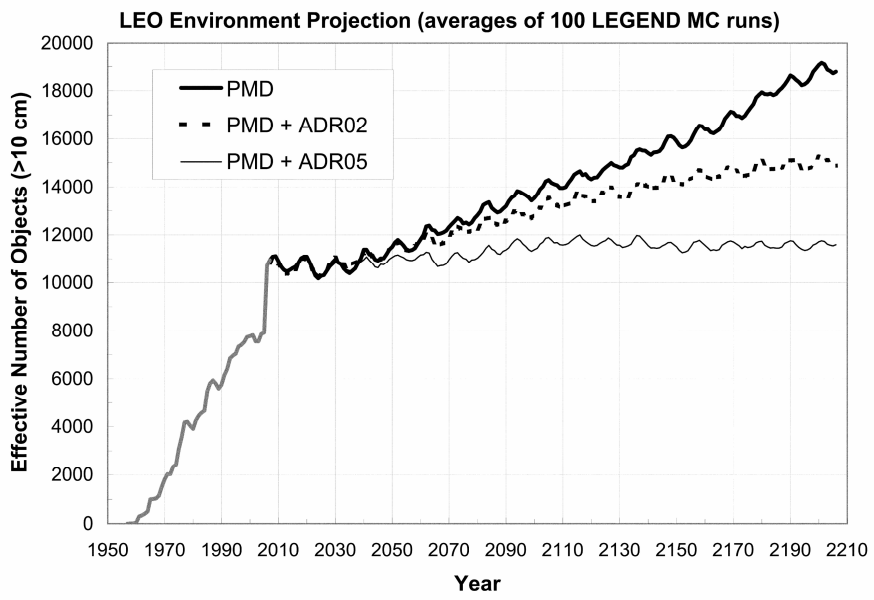

Figure 2.1: Prediction of the number of catalogued in-orbit objects [1]

It represents model predictions of the number of catalogued in-orbit objects bigger than 10 cm for three different scenarios: a case in which only the PMD policy is actuated with a 90% compliance (PMD), a case in which the PMD policy with 90% compliance and the ADR of 2 debris objects per year are actuated ($PMD + ADR02$) and a case in which the PMD policy with 90% compliance and

the ADR of 5 debris objects per year are actuated ($PMD + ADR05$); it is clear the need of operating ADR missions that, if removing 5 debris pieces per year, would be able to prevent the number of catalogued fragments from further increasing.

ADR is a generic term referring to a variety of methods that today are studied to actively remove already existing debris; the main considered are [11]:

- electro-dynamic tethers: this method considers connecting the object that has to be de-orbited to a de-orbiting element via a conductive tether; if both ends have the possibility of providing electrical contact with the ionospheric plasma, the motion will cause a current to flow into the tether. The interaction between the current and the Earth's magnetic field would cause a Lorentz force that, with the proper combination of current and orbital motion directions, can be used to de-orbit the target object. Studies have shown that for low-altitude and high-inclination satellites, this method can drastically reduce the de-orbit time; some negative aspects are the difficulty in attaching the tether and the fact that, with this method, the debris would see a great increase in its cross-sectional area with the risk of more collisions.

- capture and remove: the ADR spacecraft would rendezvous, capture and remove the debris bringing it to a disposal orbit; this method, not very useful for LEO debris, is particularly suited for GEO debris even if the ADR spacecraft should be able to provide a pretty high ΔV.

- momentum exchange tethers: a spacecraft with a higher orbit attaches a tether to a spacecraft at a lower altitude; the difference in the velocity and the perturbations will make the two satellites swing along an arc; if the lower object is released at the point with the greatest retrograde velocity, it will lower the perigee while the higher spacecraft will increase its apogee. This pretty simple solution presents some negative aspects: other than the problems already mentioned for electro-dynamic tethers (that in this case are even worse because this method requires really long cables to obtain a small altitude reduction), the ADR spacecraft would have an orbit pretty difficult to be predicted.

- Lasers: they would be used by an ADR spacecraft to vaporize debris material; this solution presents several criticalities: first of all the need of keeping a very focused beam pointing to a fast moving target for a long period of time; another problem would be producing the required power on board, today an infeasible thing; moreover, this solution would pose several problems with respect to international weapons treaties and UN regulations and could be pretty dangerous since several space debris objects still contain some propellant.

- surface material: it is based on the idea of fishing nets, slowing the objects that would impact with it; the proposed materials are low density ones that should be used as a large, thin surface. However, to prevent the risk of additional fragmentation, the surface should be too thin to produce a significant deceleration on the debris.

- solar sails: they are gaining more attention also as a propulsive system and for ADR they would actually be used to perform a de-orbit manoeuvre; exploiting the photons coming from the Sun, these thin sails would be able to decelerate a debris. They are particularly useful for eccentricity change manoeuvres (since they do not require an energy exchange) that would increase the atmospheric drag on the debris making it lowering its orbit; this system, however, can not be used at altitudes below 800 km because the corrosive nature of the ionosphere would be fatal for the sails; moreover, they would greatly increase the debris surface making a collision more probable.

- de-orbit packages: they may be solid rocket motors and they would be attached to the desired debris to perform a de-orbiting manoeuvre; it is the solution considered for this thesis' work. It presents the disadvantages of increasing the launch mass of the ADR spacecraft and of being complicated to be attached to the debris; it would also require the ability of determining and controlling the debris attitude in order to thrust in the desired direction.

2.3 Achievements and Missions

Even if today no ADR mission is active, however, in the last years the space sector has reached some important achievements for the mitigation and solution of debris problem and some missions are already programmed for a recent future. An interesting example of these steps forward can be considered the satellite LignoSat, a magnolia wood satellite developed by researchers at Kyoto University and the Tokyo-based logging company Sumimoto Forestry; it was delivered to the ISS on 5 November 2024 and it will be later deployed in orbit to gather important data on the satellite health for the following six months. This idea, that firstly could seem absurd, perfectly embodies the idea of design for demise, strongly reducing the pollution generated by satellites during re-entry: conventional satellites, indeed, are made of aluminium that, when burning into the atmosphere, generates aluminium oxides that can affect the Earth's thermal balance and damage the ozone layer [12]. In the following subsections some of the most interesting and promising future missions for debris removal and mitigation are presented.

2.3.1 HEO Robotics

An essential aspect of the debris problem would be debris detection and tracking, an action not always possible from Earth; moreover, considering an ADR mission requiring proximity manoeuvres and rendezvous with the debris, a closer view of the debris itself would be precious: this is exactly what HEO Robotics does. HEO delivers non-Earth imagery and insights of spacecraft of interest and it owns the world's largest commercially available NEI (Non-Earth imaging) dataset and NEI sensor network; partnering with Earth observation satellite constellations, it launches its own NEI cameras as hosted payload. A service today used for early operations, in-orbit support and for de-risking re-entry can clearly be used for debris detection or to help accomplishing ADR missions with minimal modifications; in particular, the characteristic of having NEI cameras hosted on several satellite constellations can be a great advantage having the ability to cover an overall larger field of view and so detecting a higher number of debris objects; moreover, NEI informations can offer something today barely feasible: the detection even of smaller debris. In September 2024, HEO awarded Blacksky (a leading provider of real-time geospatial intelligence) with a space domain awareness contract enabling the capability of getting high-resolution imagery over the middle latitudes; this further increases the NEI capabilities and can be the beginning of even greater collaborations [13].

2.3.2 ClearSpace-1

Promoted by ESA, this mission will be the first ever to remove a space debris from orbit capturing and safely bringing it down for a safe atmospheric re-entry; the mission is developed in team with the Swiss company ClearSpace and is planned to launch in 2028. At first, the target was the conical upper portion of a payload adapter of the Vega launcher called VESPA; it weighted 113 kg but, after having detected other space debris objects in its vicinity (indicating the collision of the target with undetectable debris bodies), the target was chosen to be the PROBA-1 spacecraft. It is the first ESA spacecraft with fully autonomous capabilities, it weights 95 kg and it was launched in 2001 to a LEO sun-synchronous orbit. The ClearSpace spacecraft will initially be launched to a lower 500 km orbit for commissioning; after this, it will raise the orbit to reach the debris, dock to the unprepared target with a four-armed capture mechanism, conduct a perigee decrease manoeuvre and re-enter Earth's atmosphere to burn up. Therefore, the first ADR mission ever will adopt the technique of the rendezvous and docking and it will be a single debris mission ending with the destruction of both the target and the ADR spacecraft; it will be the first step in the yet unexplored world of ADR missions and, if successful, a great result in orbital manoeuvring considering the challenges posed by the rendezvous and docking with an uncontrolled object. Moreover, this

mission will be essential for the ESA's Zero Debris Approach that poses the goal of notably limiting the production of new debris in Earth and Lunar orbits by 2030 for all future missions [14].

2.3.3 ADRAS-J

Figure 2.2: One of the pictures taken by ADRAS-J spacecraft [15]

Successfully concluded on July 2024, this mission made the history of debris removal techniques and, even if it did not remove any debris, it was an essential step forward towards a complete ADR mission. Astroscale Japan partnered with JAXA (the Japan Aerospace Exploration Agency) to conduct the ADRAS-J mission (Active Debris Removal by Astroscale-Japan); the goal of the mission, brilliantly reached, was to approach and characterize a large debris through Rendezvous and Proximity Operations (RPO). The target was an upper stage of a H-IIA rocket weighting about 3 tonnes and being at an altitude of about 600 km; it was unprepared and it could not provide any GPS data, meaning that the location and orbital position needed for an RPO mission were not available, requiring the ADRAS-J spacecraft to determine them by itself; starting from the initial ground based observation data, the spacecraft had to use its rendezvous payload sensors to conduct a safe approach. The spacecraft successfully conducted a close approach (within 50 m) to the target and completed three fly-around observations to gather data and images about the target (the mission was not intended to dock with the debris). The success of the mission, came with some amazing pictures of the target (figure 2.2), was the first essential step of a future ADR mission: before operating on the debris, it is essential to acquire most data possible about itself, from the orbit and the attitude to the spinning rate and the integrity conditions [15].

Chapter 3

Fundamentals of Orbital Mechanics and Astrodynamics

In this chapter, a brief and basic explanation of the most important aspects of orbital mechanics and astrodynamics is given; its content is useful to better understand the physics and dynamics laying behind the problem treated in the thesis but also to clearly define some conventions and some symbols used throughout the thesis.

The first section presents the basis of orbital mechanics with a description of the simplest model that can be used and some of its peculiarities; in the second section, the theoretical two-body problem model is brought closer to reality with the introduction and the explanation of the most important real-world perturbing phenomena. The third section treats space propulsion from both an analytical and a descriptive point of view, while the last section delves into the fundamentals of astrodynamics and presents the concepts lying behind some of the most used orbital manoeuvres.

3.1 Two-Body problem

Orbital mechanics is the essential basis for any space mission, since it governs the motion of spacecrafts but also of planets and of all other celestial bodies; at first, this was a discipline based on human observations made throughout the centuries but, for a quantitative study, a mathematical model is needed and the first person to elaborate one was Newton. The simplest model to predict orbital motions is the two-body problem based on Newton's universal law of gravitation; this model,

even if it makes several approximations and simplifications, it can well describe some of the phenomena of greatest interest, like Earth's motion around the Sun, Moon's motion around the Earth and a spacecraft motion around the Earth, giving an idea of how the two body interact and move one with respect to the other one.

3.1.1 Description

To clearly understand the two-body problem, it may be useful to start from the general description of a more complex and complete problem from which, through some simplifications, the two-body problem can be derived; this more complex model is the n-body problem.

The n-body problem models the interactions and the motion of n orbital bodies considering, in the most general version, all forces acting on each body; at the base of this model there are two Newton's laws hereafter expressed in vector notation: Newton's second law and his universal law of gravitation

$$\sum \vec{F} = \frac{d(m\vec{v})}{dt} = m\vec{a} \tag{3.1}$$

$$\vec{F}_{gj} = -G\frac{m_i m_j}{r_{ji}^2}\frac{\vec{r}_{ji}}{|\vec{r}_{ji}|} \tag{3.2}$$

where the first one indicates that the sum of all the forces acting on a body is equal to the rate of change of the body's momentum and, in case of constant mass, is equal to the mass times the acceleration of that body; in the second equation $\vec{F}_{gj}$ is the gravitational force acting on a generic body (of mass m_i) due to the body of mass m_j and r_{ji} is the distance vector from m_j to m_i.

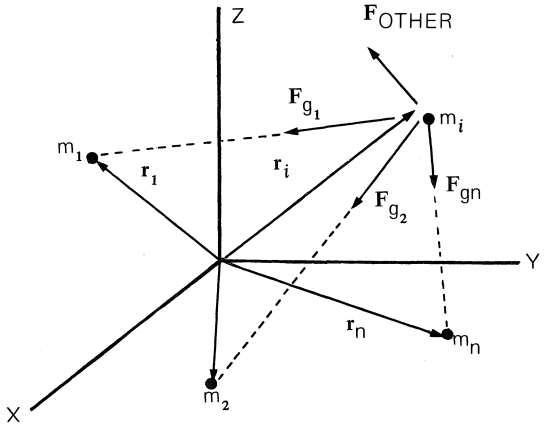

Figure 3.1: The n-body problem [16]

If it is considered a number n of bodies and the presence of other forces (indicated as $\vec{F}^*$, F_{OTHER} in figure 3.1) over the gravitational one, the total force acting on body i and due to all the other n bodies is

$$\vec{F} = \vec{F}^* + \sum_{\substack{j=1 \\ j\neq i}}^{n} -G\frac{m_i m_j}{r_{ji}^2}\frac{\vec{r}_{ji}}{|\vec{r}_{ji}|} = \vec{F}^* - Gm_i \sum_{\substack{j=1 \\ j\neq i}}^{n} \frac{m_j}{r_{ji}^2}\frac{\vec{r}_{ji}}{|\vec{r}_{ji}|} \tag{3.3}$$

that is the equation of the n-body problem. Considering an inertial coordinate system (X,Y,Z in figure 3.1), it is possible to apply equation 3.1 and, making the hypothesis of $m_i = constant$, this substitution can be made

$$\vec{F} = \frac{d(m_i\vec{v}_i)}{dt} = m_i\ddot{\vec{r}}_i \tag{3.4}$$

where $\ddot{\vec{r}}_i$ is the double time derivative of the position vector of m_i in the inertial coordinate system; therefore, it is clear that equation 3.3 represents $3n$ second order, scalar, ordinary differential equations without an exact solution.

Given the complexity of the exact n-body problem, it is possible to make a preliminary study of orbital bodies' motion with the simplified model of the two-body problem, being characterised by analytical solutions. This model is based on some simplifying assumptions:

- the problem considered is characterized by only two masses, m_1 (the primary body) and m_2 (the secondary body), with $m_1 >> m_2$; this is reasonable, for example, for an artificial satellite (m_2) that orbits around Earth (m_1)
- the two bodies considered have a spheric symmetry (both a geometrical symmetry and a mass distribution symmetry); this enables them to be considered as point masses
- the gravitational force is the only force acting on the system considered ($\vec{F}^* = 0$)
- the problem is studied from an inertial coordinate system; this is essential for derivations since it allows to differentiate vectors removing the derivatives of the coordinate system itself. In the case of interest for this thesis, a spacecraft orbiting around the Earth, the geocentric equatorial system (better described in A) is suitable for this purpose (even if it actually is a pseudoinertial frame)

From these hypotheses, is then possible to determine the two-body equation hereafter illustrated. Analysing a more specific situation which suits the thesis' problem, it is possible to consider m_1 as the mass of the Earth ($m_\oplus$) and m_2 as the mass of a satellite (m_{sat}) orbiting the Earth; starting from the inertial coordinate

system XYZ, it is possible to identify the Earth-centred IJK, which is displaced from XYZ but it does not rotate or accelerate with respect to it (a more precise description of the coordinate system IJK is given in A). The vector that indicates the relative position of the satellite with respect to the Earth is

$$\vec{r} = \vec{r}_{sat} - \vec{r}_{\oplus}$$

where $\vec{r}_{\oplus}$ is the position vector of the centre of the Earth and $\vec{r}_{sat}$ is the position vector of the satellite, both with respect to XYZ coordinate system. From this, it is possible to simply determine the satellite acceleration relative to the centre of the Earth; since IJK is an inertial coordinate system, it is enough to calculate the second derivative of the above equation

$$\ddot{\vec{r}} = \ddot{\vec{r}}_{sat} - \ddot{\vec{r}}_{\oplus}$$

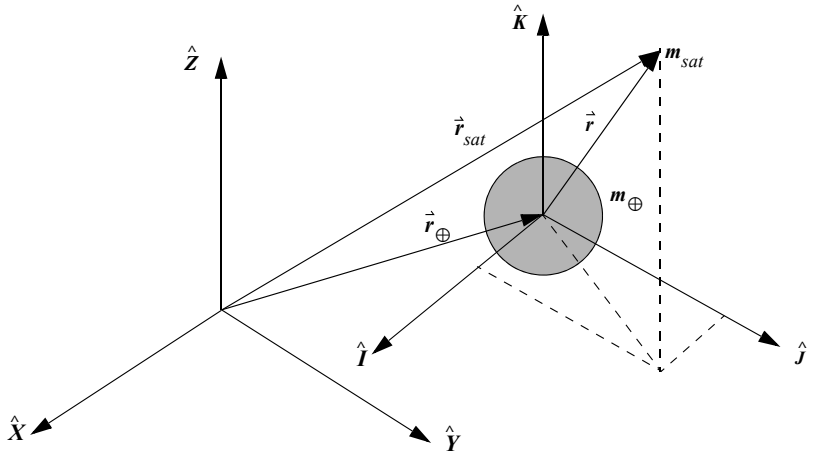

Figure 3.2: The two-body problem [17]

Using Newton's second law and his gravitational law it is possible to write the gravitational force acting on the satellite and the one acting on the Earth respectively

$$\begin{aligned} \vec{F}_{g_{sat}} &= m_{sat}\ddot{\vec{r}}_{sat} = -G\frac{m_{\oplus}m_{sat}}{r^2}\frac{\vec{r}}{|\vec{r}|} \\ \vec{F}_{g_{\oplus}} &= m_{\oplus}\ddot{\vec{r}}_{\oplus} = G\frac{m_{\oplus}m_{sat}}{r^2}\frac{\vec{r}}{|\vec{r}|} \end{aligned} \tag{3.5}$$

After simplifying m_{sat} in the first equation and $m_{\oplus}$ in the second one, by subtracting

the second equation from the first one it is possible to obtain

$$\ddot{\vec{r}} = -G\frac{m_\oplus + m_{sat}}{r^2}\frac{\vec{r}}{|\vec{r}|} \tag{3.6}$$

Since the mass of the smaller body is much smaller than the mass of the bigger one, it is possible to assume $m_\oplus + m_{sat} \approx m_\oplus$ and so $G(m_\oplus + m_{sat}) \approx Gm_\oplus$; it is convenient to introduce the Earth's gravitational constant $\mu \triangleq Gm_\oplus$ that, substituted in 3.6, leads to the two-body problem equation

$$\ddot{\vec{r}} = -\frac{\mu}{r^2}\frac{\vec{r}}{|\vec{r}|} \tag{3.7}$$

often referred to as the relative form because it describes the motion of the smaller body referenced to the primary attracting body.

3.1.2 Constants of motion

It is useful to calculate two constants of the two-body problem orbital motion that can give some important informations about the smaller body motion and that can help to predict a satellite orbit behaviour.

The first quantity is the specific angular momentum that can be easily obtained by cross-multiplying equation 3.7 with the position vector

$$\vec{r} \times \ddot{\vec{r}} = -\vec{r} \times -\frac{\mu}{r^2}\frac{\vec{r}}{|\vec{r}|}$$

Because $\vec{r} \times \vec{r} = 0$, the second term is equal to 0; the first term can be rewritten considering the following differential

$$\frac{d}{dt}(\vec{r} \times \dot{\vec{r}}) = \dot{\vec{r}} \times \dot{\vec{r}} + \vec{r} \times \ddot{\vec{r}} = \vec{r} \times \ddot{\vec{r}}$$

Substituting this differential in the original equation it is possible to say that the integral quantity is a constant, since the second term is equal to 0; substituting $\dot{\vec{r}}$ with $\vec{v}$ it is possible to finally obtain

$$\vec{h} = \vec{r} \times \vec{v} = constant \tag{3.8}$$

that indicates that the specific angular momentum, for a body moving accordingly to the two-body problem, remains constant during the time. The angular momentum, as its definition, is perpendicular to both the position vector $\vec{r}$ and the velocity $\vec{v}$ of the smaller orbiting body, meaning that it is perpendicular to the

plane on which these two vectors lie (the orbital plane); therefore, the equation 3.8 indicates that in the two-body problem the orbital plane remains constant but also that $\vec{r}$ and $\vec{v}$ are paired so that, in any position along the orbit and in any moment, their cross-product is constant.

The second quantity of interest is the specific mechanical energy; to obtain this second constant, the first step is to dot multiply both the terms of 3.7 with the velocity vector $\dot{\vec{r}}$

$$\dot{\vec{r}} \cdot \ddot{\vec{r}} = -\dot{\vec{r}} \cdot \frac{\mu}{r^2} \frac{\vec{r}}{|\vec{r}|}$$

The satellite, in its motion along the orbit, is characterized by an only-radial (so parallel to the position vector $\vec{r}$) component of the acceleration meaning that the angle between $\dot{\vec{r}}$ and $\ddot{\vec{r}}$ and the angle between $\dot{\vec{r}}$ and $\vec{r}$ are the same and so it is possible to write the previous equation as

$$\dot{r}\ddot{r} + \frac{\mu}{r^3}\dot{r}r = 0 \quad \Rightarrow \quad v\dot{v} + \frac{\mu}{r^2}\dot{r} = 0$$

in which two derivatives can be recognized

$$\frac{d}{dt}\left(\frac{v^2}{2}\right) = v\dot{v} \qquad \frac{d}{dt}\left(-\frac{\mu}{r}\right) = \frac{\mu}{r^2}\dot{r}$$

The first one is the derivative of the specific kinetic energy while the second one is the derivative of the specific potential energy; substituting, it is possible to obtain

$$\frac{d}{dt}\left(\frac{v^2}{2}\right) + \frac{d}{dt}\left(-\frac{\mu}{r}\right) = 0 \quad \Rightarrow \quad \frac{d}{dt}\left(\frac{v^2}{2} - \frac{\mu}{r}\right) = 0 \tag{3.9}$$

The sum of the specific kinetic and the specific potential energy is the specific mechanical energy and since its rate of change is zero, it means that the specific mechanical energy along the orbit is constant

$$\epsilon = \frac{v^2}{2} - \frac{\mu}{r} = constant \tag{3.10}$$

The constant (often indicated as c) has an arbitrary value and depends on where the zero potential energy is chosen to be; in orbital mechanics it has been chosen to put $c = 0$ meaning that the potential energy is set to be zero at infinity and that the specific potential energy of a body along its orbit will always be negative. If, for example, it is considered an elliptic orbit, according to this equation, when the satellite is at the periapsis (the nearest point in the orbit from the centre of attraction) it has high kinetic energy (meaning high speed) and low potential energy while, when at the apoapsis (the farthest point in the orbit from the centre

of attraction), it has low kinetic energy (and so low speed) and high potential energy.
Since the specific mechanical energy is constant along the orbit followed by the satellite, it is useful to define ϵ in terms of the semimajor axis a (a better description of this quantity is given in 3.1.3). If, for simplicity, it is considered the situation at the periapsis of the orbit, $\vec{r}$ and $\vec{v}$ are parallel, the specific angular momentum is $h_p = r_p v_p$ and so, substituting in equation 3.10

$$\epsilon = \frac{v^2}{2} - \frac{\mu}{r} = \frac{h^2}{2r_p^2} - \frac{\mu}{r_p}$$

It is possible to use the equalities $r_p = a(1-e)$ and $h = \sqrt{\mu a(1-e^2)}$ to obtain

$$\epsilon = \frac{\mu a(1-e^2)}{2a^2(1-e)^2} - \frac{\mu}{a(1-e)}$$

that solved, gives the following result (valid for orbits other than parabolic since in that case $a \to \infty$)

$$\epsilon = -\frac{\mu}{2a} \tag{3.11}$$

This result, if combined with equation 3.10, gives the traditional form of the vis-viva equation

$$v^2 = \mu\left(\frac{2}{r} - \frac{1}{a}\right) \tag{3.12}$$

3.1.3 Classical Elements and other quantities

Starting from the equation of motion of the two-body problem previously obtained (3.7), it is possible to integrate it and obtain the trajectory equation, which gives a great insight into orbital motion

$$r = \frac{h^2/\mu}{1 + B/\mu\cos\nu} = \frac{p}{1 + e\cos\nu} \tag{3.13}$$

This is the polar form of a conic section, meaning that the orbit of a body in the two-body problem can only be a conic section: circle, ellipse, parabola or hyperbola; the result here obtained actually verifies and extends Kepler's first law according to which the orbit of a planet is an ellipse. For the purpose of this thesis, from now on, the subject will focus on elliptical orbits.

Analysing this equation more deeply, it is possible to find h, the specific angular momentum, μ, the gravitational constant that depends on the main attracting body, B, a constant of integration and ν, the true anomaly (later explained). The

quantity h^2/μ is equal to the semilatus rectum, p, the distance between the focus where there is the attracting body and the orbit; it is measured perpendicular to the major axis and it is particularly used to describe the scale of a parabolic orbit since in that case $a \to \infty$. The ratio B/μ is equal to the eccentricity of the orbit, e, a fixed constant for a specific orbit that indicates its "roundness"; eccentricity value indicates what type of conic section an orbit is: it is $e = 0$ for circular orbits, $0 < e < 1$ for elliptical orbits, $e = 1$ for parabolic orbits and $e > 1$ for hyperbolic orbits.

In order to define the state of a satellite in space, six quantities are needed; these can be the classical coordinates in a Cartesian coordinate system: three for the position vector and three for the velocity vector. However, the six quantities defined like this are pretty difficult to be understood and not straightforward and it is for this reason that orbital mechanics often uses other six parameters called classical orbital elements (the following descriptions are referred to elliptical orbits around Earth if not differently indicated).

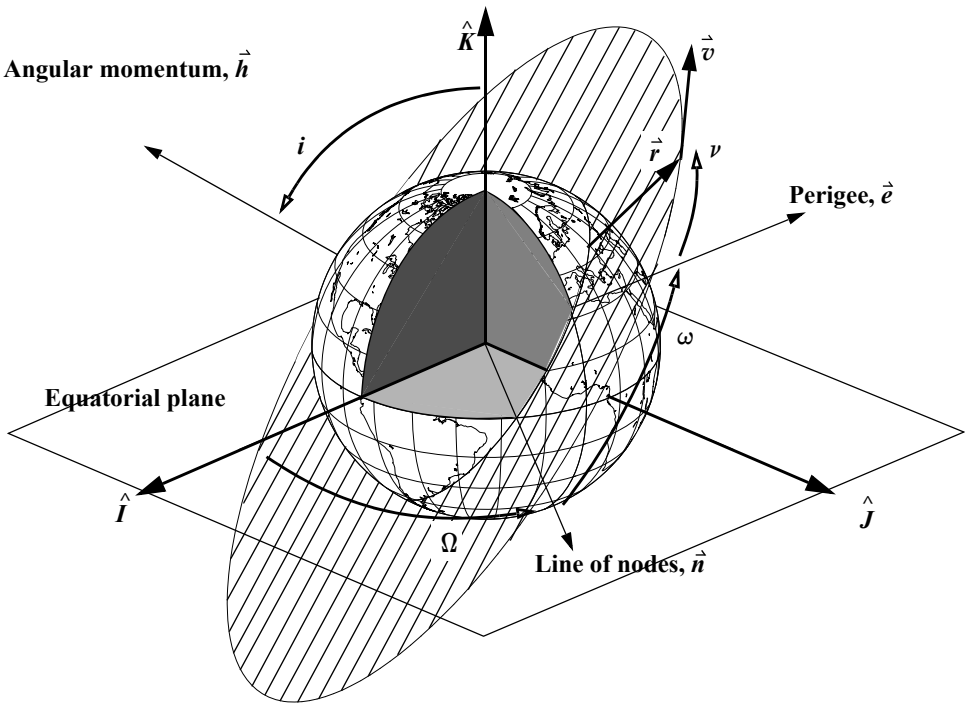

Figure 3.3: Classical orbital elements [17]

- a, the semimajor axis: is half the major axis, gives an idea of orbit dimensions and is univocally linked to the orbit mechanical energy; in case of circular

orbits it is equal to the radius

- e, the eccentricity: is the magnitude of a vector always pointing to periapsis, it defines the shape of the orbit, in particular how the orbit shape is flattened
- i, the inclination: it indicates how much the orbit is tilted with respect to Earth's equatorial plane; it is the angle measured from axis K of the IJK coordinate system (better explained in A) to the angular momentum vector $\vec{h}$ and ranges from 0° to 180°
- Ω, the Right Ascension of the Ascending Node (RAAN): it is the angle counter-clockwise measured on the equatorial plane from axis I to the location of the ascending node; the ascending node is the point on the equatorial plane at which the satellite crosses Earth's equator from south to north and it is opposite to the descending node where the satellite crosses the equator from north to south. The line segment connecting these two points is called line of nodes and has the vector $\vec{n}$ associated. RAAN is not defined for equatorial orbits and its values range from 0° to 360°
- ω, the argument of perigee: it is the angle measured on the plane of the orbit from the ascending node to the orbit periapsis; it is not defined for both circular and equatorial orbits and it ranges from 0° to 360°
- ν, the true anomaly: it locates the satellite on the orbit and it is the angle measured on the orbital plane from the periapsis to the satellite current position vector (starting at the origin of IJK coordinate system); it varies from 0° to 360°

There are two other important quantities needed to solve the direct and inverse time problem to determine the relation between time and angular displacement along the orbit: the eccentric anomaly (E) and the mean anomaly (M).
Considering an elliptical orbit with semimajor axis a_1 and eccentricity e_1, a circle of radius a_1 (called auxiliary circle) can be circumscribed around it; if it is considered a satellite being on the elliptical orbit with a true anomaly ν_1, it is possible to trace a line perpendicular to the semimajor axis intersecting the ellipse in the point where the satellite is and intersecting the circle in a point indicated as C. The angle measured from the semimajor axis to the line segment $\overline{OC}$ (where O is the centre of both the ellipse and the circle) is the eccentric anomaly E_1; there is an equation relating the true and the eccentric anomaly

$$E_1 = 2\tan^{-1}\left[\sqrt{\frac{1-e_1}{1+e_1}}\tan\left(\frac{\nu_1}{2}\right)\right] \tag{3.14}$$

used to solve the direct time problem in which ν_1 is known and the goal is to determine the time t_1 from which the satellite has passed the periapsis.

The mean anomaly can be defined as the angle swept by a satellite from the periapsis if it was moving on the auxiliary circle with a constant speed and with the same orbital period of a body moving on the elliptical orbit; M strongly depends on e and E

$$M = E - e \sin E \tag{3.15}$$

A quantity strictly connected to the mean anomaly is the mean motion n, which represents the mean angular rate of motion of the satellite in orbit

$$n = \sqrt{\frac{\mu}{a^3}} \tag{3.16}$$

From the mean motion it is also possible to define the orbital period, which is the time needed for the satellite to travel along one orbit

$$T = 2\pi\sqrt{\frac{a^3}{\mu}} \tag{3.17}$$

The constant speed to maintain a body on a circular orbit is defined circular speed (v_c) and can be easily obtained from the vis-viva equation (3.12) considering that for a circular orbit $a = r$

$$v_c = \sqrt{\mu\left(\frac{2}{r} - \frac{1}{r}\right)} \quad \Rightarrow \quad v_c = \sqrt{\frac{\mu}{r}} \tag{3.18}$$

Even if this thesis deals only with Low Earth Orbits (LEO), it is useful to present how the orbits are categorized based on their altitude; each category deals with different, specific phenomena and it is of particular interest for several reasons and for different types of missions:

- Low-Earth Orbits (LEO): comprises the lower orbits with an altitude up to about 800 km
- Mid-Earth Orbits (MEO): they have an altitude ranging from 800 km to 30000 km
- Geosynchronous orbits (GEO): they have an altitude of about 35780 km and they are characterised by an orbital period equal to Earth's rotation (24 hours)

3.2 Orbital Perturbations

The two-body problem model gives an idea of how orbiting bodies behave and how they interact one to each other; the problem is that, in reality, there are not

only two orbiting bodies and gravitational force is not the only interaction between them and for these reasons the two-body problem does not predict in an accurate way the orbital motion, especially on long periods of time. The key assumptions at the base of the model, in particular for some specific situations, are too strong and this is the reason for adjusting the two-body problem with the addition of different types of perturbations in order to obtain a more true to reality model; therefore, it is necessary to give a more in-depth description of these forces in order to better understand the effects they can have on the normal, predicted motion.

3.2.1 Classification

Considering the orbital mechanics, with the term perturbations are indicated all the non-gravitational forces or all the interactions with other bodies that make an object behave in a different way from what the two body model predicted; perturbations can be of reduced entity but in several cases they are comparable to the primary attracting force (the gravitational attraction between the primary body and the secondary one), becoming impossible to be neglected and deeply changing the idealized and undisturbed motion. Another aspect to be considered is that the term perturbation seems to indicate something that spoils the predicted motion but it actually is not always like this: in some cases, the perturbations have a positive effect on the satellite motion, for example, enabling it to consume less propellant (this aspect is better described later). In general, the forces causing the perturbative effects on the secondary body motion can be classified into two different categories:

- conservative forces: when this kind of forces act on the satellite, the mechanical energy of the system remains constant; two examples are central-body and third-body gravitational effects in which the main force acting is, again, of gravitational nature
- non-conservative forces: when the system is subjected to this type of perturbations, its mechanical energy may both decrease or increase; some examples are solar-radiation pressure and drag

In a meticulous analysis, a lot of several perturbations can be identified since even the smaller force, in particular in some cases, into the void may have some effects on the satellite motion; however, in this thesis, only the most important perturbative forces related to the orbital motion around the Earth are presented, with a focus on the one of greatest interest. In particular, the main perturbations considered are:

- irregularities of the gravity field of the central body: they are caused by the non-spherical mass distribution of the Earth, their description and their effects are presented in the next section

- third body effects: they are caused by the gravitational interactions between the two main bodies and a third one
- atmospheric drag: particularly relevant for lower orbits
- solar-radiation pressure: exceeds the effects of atmospheric drag in higher orbits

All these perturbations are pretty difficult to be modelled and studied in a precise way and because of this, propagating orbits with high accuracy is complicated; to succeed in this challenging task, there are two different approaches to consider the perturbative effects on the satellite motion (potentially, a third method, which is a combination of the other two, can also be considered):

- special perturbation techniques
- general perturbation techniques

The special perturbation techniques use numerical methods to integrate the equations of motion including all the perturbing accelerations; they are called special because they produce a specific solution valid only for a certain situation. Thanks to the computing power it has been achieved and the fact that these approaches can give very accurate results, today they are the most used methods, even if they suffer from their specificity; among these techniques, there are two of particular interest: Encke's formulation and Cowell's formulation. The first one today is not very used because of the precise numerical solutions that computers can achieve, however, it has a great historical importance since it has been a very popular method for decades having the ability to attain a good level of precision with limited computing capabilities; it is based on the concept of osculating orbit: in a certain instant of time, it is the two-body orbit that a satellite would follow if the perturbing forces were removed in that precise instant; so, at each point in time, it is possible to identify the corresponding osculating elements for the satellite. Starting with an osculating orbit, Encke's formulation integrates in Cartesian elements just the difference between the two-body acceleration and the perturbed acceleration; in this way, it actually integrates only the perturbations that, having a pretty small magnitude, make a greater computational precision achievable. After a while, this process needs a rectification point where the osculating elements are re-initialized since, otherwise, the osculating orbit would become excessively different from the actual trajectory.
The Cowell's formulation continues to gain favour and, today, it is pretty commonly used to set up the equations of motion for numerical integration; it adds the perturbing accelerations directly to the two-body equation of motion to produce more accurate results and has the great advantage of making possible to incorporate any

kind of perturbation and of any entity (differently from Encke's formulation based on the reduced value of perturbing accelerations). Some disadvantages associated to this method can be the difficulty in finding the expression for a particular perturbation, since it can be pretty complex and computationally intensive, or also the struggle in obtaining the necessary data for a model able to characterize a specific perturbation.

The general perturbation techniques produce approximate (general) results valid for a limited time interval but with the ability of accepting any initial input condition (differently from special perturbation specificity); they are based on analytical approximations of the original equations of motion that permit analytical integration in a simpler and faster process but with decreased accuracy with respect to special perturbation techniques. Another important aspect of these methods is that, since they are based on Keplerian elements, they give a clearer idea of the effects of the perturbations. Special techniques propagate the orbits giving the results in term of position and velocity vectors that are two wide-changing quantities (they experience great variations even during a single orbit in the unperturbed motion); instead, general techniques use Keplerian elements to describe a perturbed orbit since they undergo small variations in the case of perturbations, making the use of analytical methods possible.

Considering the effects on the Keplerian elements and in particular the way they change over time, it is possible to classify the perturbations into three different categories:

- secular variations: they modify the Keplerian elements linearly over time; they are the main cause of the degradation of analytical methods over long intervals of time
- long-periodic variations: they have effects characterised by a cycle significantly longer than one orbital period
- short-periodic variations: their effects repeat with a period shorter than the orbital period

With the point of view of the general perturbation techniques, it is now possible to give a better description of the main perturbations and of their effects on the Keplerian elements.
The third-body perturbations refer in particular to the gravitational effects caused by the presence of the Moon, since it is the nearest attracting body other than the Earth, and the Sun, because it is a highly massive body and it can influence Earth-gravitating objects; this type of perturbative forces, however, are pretty small, in particular if compared to Earth's gravity, and to study their effects it

is necessary to consider long periods of time. The effect of the Sun is to create a torque about the line of intersection between the satellite orbital plane and the Sun orbital plane that tends to turn the satellite plane into the ecliptic (the orbital plane of the Earth around the Sun); the resulting gyroscopic effect makes the satellite orbit precess about the pole of the ecliptic with a nodes regression (in this case the nodes are determined by the intersection of the satellite orbital plane and the ecliptic). Similarly, the Moon makes the orbit regress about an axis normal to the Moon's orbital plane inclined of about 5° to the ecliptic. The resulting effect is a regression of the satellite orbit about a mean pole located between the Earth's pole and the ecliptic pole in a process that is relevant particularly for higher orbits; in the case of lower orbits, indeed, even if the third-body effect is still present, these perturbations are overcome by the non-spherical mass distribution of the Earth that causes a similar effect as explained in the next section. Therefore, these perturbations cause secular variations only in Ω and ω of the satellite orbit without any variation in a and are particularly relevant for geosynchronous orbits, whose inclination oscillates for one cycle from 0° to 15° and back in about 53 years [17]

The atmospheric drag is strictly correlated to the atmospheric density and so to the altitude of the orbit and it is, therefore, particularly relevant for lower orbits. The best way to predict its behaviour in an accurate way is to have a precise atmospheric model, particularly of the higher atmospheric layers, but this is a pretty complex task: firstly, calculating density in real-world problems (and in particular the density of these hard-to-reach atmospheric layers) is always extremely complex, secondly the interactions of the Sun with the upper atmosphere and the influence of the Earth's magnetic field make calculations of drag values even more uncertain. The atmospheric drag needs to be studied accurately since for lower orbits it is the predominant perturbation, becoming even larger than the primary attracting force during re-entry; the main negative effect is to shrink the orbit until the point at which the satellite re-enters the atmosphere and hits the Earth. Since drag is a non-conservative force, it makes orbit energy decrease, causing the reduction of a but an interesting aspect is the so called drag paradox [17]: the energy reduction causes the orbit to get closer to the Earth but, in a pretty counter-intuitive way, it makes the satellite go faster; this is due to the fact that a satellite with a smaller a actually moves faster (it can be seen from equation 3.12); in case of elliptical orbits, at perigee the effect of drag is more relevant (since the satellite is lower, the atmosphere is more dense) with the greatest energy drain that causes the orbit to become increasingly circular, with a more relevant reduction of the apogee height. Despite these negative consequences, which if not studied properly can cause a satellite to re-enter too early, the atmospheric drag also has some positive aspects: first of all, it makes satellites destruction after their end of life possible, reducing the quantity of space debris in LEO; strictly correlated

to this aspect, there is the protection that the atmosphere offers to the life on Earth preventing unpredicted space debris pieces or asteroids to reach the surface. Finally, the drag is used in some interplanetary missions as aerobraking and it is an essential component during the re-entry phase of manned missions since it can slow down the capsule before landing without the need to use any propellant. Overall, the atmospheric drag causes secular changes in a, e, i and periodic changes in all orbital elements, particularly i, Ω and ω; the orbital parameters most sensitive to it, however, are eccentricity, apogee and perigee altitude and orbital period.

The solar-radiation is any kind of electromagnetic wave emitted by the Sun and that propagates into the space until reaching a surface, like the one of a satellite, where it can be absorbed or reflected depending on the characteristics of the surface itself. According to Maxwell's theory, an electromagnetic wave carries momentum that, when transferred to the surface it strikes, generates a pressure; this perturbation is usually pretty small but can become important in outer space where it is the only force acting on a spacecraft other than gravity. The perturbative force resulting on a satellite depends on the surface exposed to the Sun (meaning the attitude of the satellite), on its reflectivity (in case of total reflection the momentum change doubles) and on the solar flux arriving; this last aspect is pretty complicated to be studied since it requires a good knowledge of the solar cycles and the variations that sometimes, like in the case of solar storms, are unpredictable. Radiation pressure causes periodic variations in all orbital elements with effects becoming even more complex in the case in which the satellite passes through the Earth's shadow; an example can be the effect on a (and so the effect on the orbital energy): when the satellite moves towards the Sun, the orbit energy and a decrease because the pressure opposes to spacecraft motion, when the satellite moves away from the Sun, they both increase. Even the solar-radiation pressure does not pose only negative effects on a satellite motion but it can also have some positive aspects; for example, in some cases it can be used for attitude control or even for propulsion in the case of solar sails.

3.2.2 Non-spherical mass distribution and J2

The Earth is not a perfect sphere and its non-spherical mass distribution causes a non-uniform gravitational field; this important difference from the two-body assumption, in which the Earth is considered as a body with spheric symmetry, causes some essential perturbing effects that are particularly relevant for lower orbits. The equipotential surfaces of the gravity field are actually not spherical and it is necessary to consider a geoid instead of a sphere; the geoid is a complex geometrical shape whose surface is perpendicular to the actual direction of the

gravity force. In order to account for Earth's real shape, the assumption of considering its gravitational potential function as $U = \frac{\mu}{r}$ is too simplistic and a more precise, aspherical potential function needs to be determined in order to model in a more accurate way the gravitational field; this is a pretty hard task but, over time, some important progresses have been made towards a model being more and more precise. For the scope of this thesis, here is presented only a brief description of the main properties of the aspherical potential function.

The potential function used to take into account the perturbations (U) is characterised by the sum of a principal term resulting from the spherical symmetry assumption ($\frac{\mu}{r}$) and other three terms considering the real shape of the Earth:

- zonal harmonics: they take into account the additional mass distributed along the latitude
- sectoral harmonics: they consider the extra mass distribution in longitudinal regions
- tesseral harmonics: they try to model specific regions of the Earth which are different from a perfect sphere

Each of these terms are multiplied by a coefficient determined by the geodesy data, among which, the most relevant are the ones of the zonal harmonics indicated as J_n (n is the term of the series considered since each harmonic, theoretically, is an infinite series); the first zonal coefficient is J_2 (since $J_1 = 0$), the greatest one and so the most relevant in the perturbing effects with a dimensionless value of $J_2 = 0.00108263$. It indicates Earth oblateness and since it is almost 1000 times larger than J_3, it is often used as a term to indicate the perturbations caused by the non-spherical mass distribution of the Earth and it is the only zonal coefficient considered in this thesis.

The most important consequence of J_2 is the regression of the line of nodes; to explain this phenomenon, the Earth can be simply approximated as a sphere with an additional concentration of mass at the equator. This added mass causes a stronger gravitational attraction to the equatorial bulge, resulting in a torque that tends to turn the orbital plane towards the equator, as illustrated in figure 3.4. The consequence is a gyroscopic phenomenon: since the torque is along the line of nodes, the angular momentum vector changes its direction in parallel to the torque itself, as indicated in figure 3.4, and the resulting precession, which is perpendicular to the angular momentum, causes the line of nodes to regress.

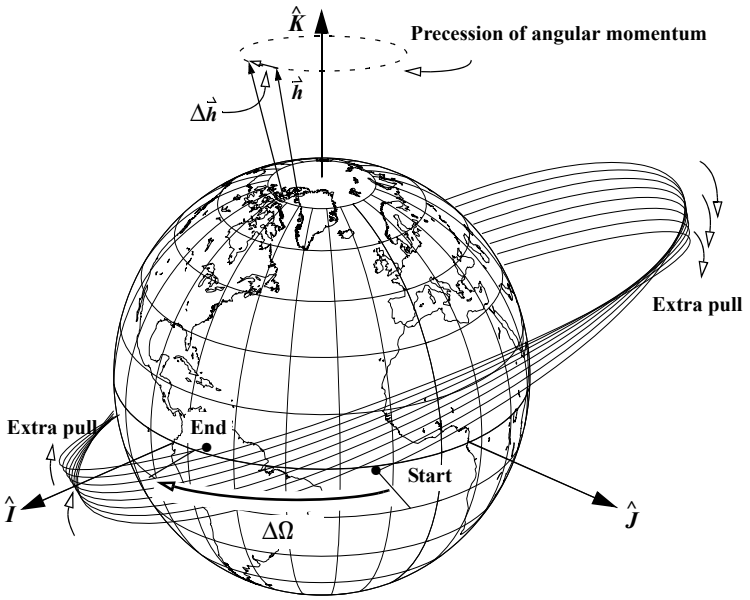

Figure 3.4: The regression of the line of nodes [17]

The variation of Ω can be expressed in a precise way as a function of other orbital elements

$$\frac{d\Omega}{dt} = \dot{\Omega} = -\frac{3}{2}\sqrt{\frac{\mu}{a^3}}\frac{J_2 \cos i}{(1-e^2)^2}\left(\frac{r_E}{a}\right)^2 \tag{3.19}$$

where r_E is Earth's equatorial radius. Since the semimajor axis is at the denominator, it is evident that the higher the orbit, the less the Ω variation is relevant. With the change of Ω in time, J_2 consequences may have a negative impact on some missions, however, this effect has several positive aspects; the first one is the sun-synchronous orbits that, without the regression of the line of nodes, would not even exist. Sun-synchronous orbits exploit a specific combination of a, e and i in order to obtain a $\Delta\Omega$ in one day that is equal to the angle covered by the Earth in its path around the Sun; this makes the line of nodes keep a constant angle with respect to the Sun, allowing the satellite to pass over a determined point on the Earth's surface always at the same hour and with the same lighting conditions, making the sun-synchronous orbit particularly interesting for Earth-observation missions. Moreover, as it is done in this thesis, J_2 effect may also be used to change orbital plane; indeed, this is a really expensive manoeuvre that can be accomplished with a reduced propellant consumption changing a accordingly to the $\dot{\Omega}$ needed: if it is needed to change the plane of a satellite, it is enough to lower a, wait to reach the desired Ω and then increase a again with a resulting propellant consumption that usually is lower than a direct plane-change manoeuvre.

The second major effect of J_2 perturbation is the apsidal precession that is the motion in time of the line connecting the apsides; also this effect has an analytical expression

$$\frac{d\omega}{dt} = \dot{\omega} = \frac{3}{4}\sqrt{\frac{\mu}{a^3}}\frac{J_2\left(5\cos^2 i - 1\right)}{\left(1-e^2\right)^2}\left(\frac{r_E}{a}\right)^2 \tag{3.20}$$

that expresses how the perigee and apogee positions change as a function of the other classical elements; as it can be seen by the equation, this phenomenon has a peculiarity: for orbits with an inclination of 63.4° or 116.6° (called critical inclinations) the effect nullifies.

Another effect of J_2 perturbation is the one on the mean anomaly (M) that changes according to

$$\frac{dM}{dt} = \dot{M} = \sqrt{\frac{\mu}{a^3}} + \frac{3}{4}\sqrt{\frac{\mu}{a^3}}\frac{J_2\left(3\cos^2 i - 1\right)}{\left(1-e^2\right)^{3/2}}\left(\frac{r_E}{a}\right)^2 \tag{3.21}$$

The three effects here presented are secular perturbations but they are not the only consequences of the Earth non-spherical mass distribution; actually, all the orbital elements (a, e, i, Ω, ω, M) are subjected to periodic variations but of reduced entity and with less evident results.

3.3 Space Propulsion

Any kind of propulsion is based on Newton's third law of action equals reaction but because the space is a nearly total vacuum, there are no means to exchange any force with; this is the reason because spacecrafts have to bring with them the propellant that, accelerated through a nozzle, can give the desired thrust. The fact that the propellant needs to be carried on-board is a great disadvantage, since it means that there are less volume and weight available to transport a payload; this is the reason because the mass of propellant needed for a mission is a greatly studied and optimised parameter. The quantity of propellant used to accomplish a certain manoeuvre, then, can be easily correlated, in an approximate and preliminary study, to the ΔV, that is the quantity used to define the cost of a manoeuvre; this is possible thanks to the Tsiolkovsky rocket equation

$$\Delta V = c \ln \frac{m_i}{m_f} \tag{3.22}$$

where m_i is the initial mass of the satellite and m_f is the final mass of the satellite and their difference $m_i - m_f$ is equal to the mass of propellant used. c is an

esteem of the exhaust speed and it is called effective exhaust velocity; it can be written as $c = I_{sp}g_0$ where g_0 is the standard gravity ($9.81\ m/s^2$) and I_{sp} is called specific impulse, a property of the engine installed that measures how efficiently the propellant mass is used by the rocket engine itself. The rocket equation is a very powerful tool, particularly in preliminary mission project phases: knowing the mission that needs to be accomplished (so knowing its ΔV) and the engine used, thanks to this equation it is possible to immediately make an esteem of the total mass of the spacecraft needed; this allows to have an initial idea of the dimensions of the satellite and of the cost of the mission.

The ΔV needed to perform a manoeuvre can be modelled in two different ways, each one more appropriate for a specific type of propulsion: with an impulsive ΔV model and with a continuous ΔV model. The first one is used in the case in which the engine remains operative for a period of time that is short with respect to a characteristic time (like the orbital period of the satellite), meaning that the propellant expulsion is pretty fast; in this case, the thrust is considered to be impulsive and to have a duration that tends to zero while the satellite,theoretically, remains in the same position, in a model that is better suited for chemical propulsion. The continuous model assumes that the engine remains operative for a long period of time during which the spacecraft changes its position; it is better suited for electrical propulsion and brings to a manoeuvres study that is completely different. From here on, only the impulsive model is considered since the thesis' problem is tackled using a spacecraft with chemical propulsion.

Even if useful, the Tsiolkovsky equation gives only an approximation of the real situation without dealing with any of the actual losses acting on the satellite motion; these are generically indicated as velocity losses and can be classified into three different categories: misalignment losses due to the thrust having a different direction from the velocity, aerodynamic losses (actually they are the same of the atmospheric drag perturbation) and gravity losses that are an energy loss due to the gravitational attraction. Taking into account these real effects, the actual ΔV needed increases with respect to the one calculated with the rocket equation.

Today, different types of propulsion are used and there are several ones that are only at a theoretical or at an experimental level; the two most important and most frequently used types of propulsion are the chemical propulsion and the electrical propulsion, each one with its advantages, disadvantages and peculiarities; here, a brief description of them is presented with a focus on the chemical propulsion, the solution of interest for this thesis.
The electrical propulsion makes use of the electrical power generated by on-board solar panels or by a different generator to accelerate the propellant in order to

receive an equal and opposite thrust; they can be of several different types and their effective exhaust velocity, strictly linked to the specific impulse and so to the propellant consumption, is

$$c = \sqrt{\frac{2\eta P_E}{\dot{m}_p}} = \frac{2\eta P_E}{T} \tag{3.23}$$

where P_E is the available electrical power, η is the electrical efficiency, T is the thrust and $\dot{m}_p$ is the propellant mass flow; in order to achieve a higher c (and so I_{sp}, meaning a lower propellant consumption) it is better to have $\dot{m}_p$ and T of small entity and the lower they are, the better it is without, in theory, any limit to c. Indeed, electrical propulsion is characterized by a low thrust that can be perfect for precise manoeuvres and attitude control and an I_{sp} that greatly varies reaching also big values; some negative aspects are that, to achieve great ΔV, the engine needs to thrust for long periods of time and that the value of P_E is limited by the weight of the electrical power source.
The chemical propulsion, for which the energy to accelerate the propellant comes from a chemical reaction, is characterized by

$$c = \sqrt{2E_{ch}} \tag{3.24}$$

where E_{ch} is the energy released during the chemical reaction; it is immediately evident that in this case, differently from electrical propulsion, the c is limited by the type of propellant used. The maximum value that today can be obtained is about $I_{sp} = 450s$ with the combination of liquid oxygen and liquid hydrogen, a value indicating that chemical propulsion has higher propellant consumption than electrical propulsion. The great advantage of this system is the high thrust that it can provide, the reason for which all launchers use this type of propulsion and for which chemical engines need to operate for reduced intervals of time, making the use of the impulsive ΔV model possible; another advantage with respect to the electrical propulsion is that the chemical one only needs the propellant without any external power source, reducing the weight of the propulsive system. According to the propellant state, chemical rockets can be classified into three categories:

- solid rocket motors in which the propellant is solid, they are often used as boosters; they have the advantages of providing high thrust, of having a high density, of being pretty simple and easily storable for long periods of time. The disadvantages are that they can not be reignited, the thrust level cannot be controlled and that they are pretty dangerous to be produced and handled
- liquid rocket engines in which the propellants are liquid; they have the possibility of throttling (that is the regulation of thrust level), they can be reignited, they have medium-high performances and the liquid propellant can be used

for refrigeration. An important disadvantage is the need of tanks for the propellant, meaning additional weight, more complexity and other correlated problems (like the ones requiring ullage motors)

- hybrid rocket engines in which there is the co-presence of solid and liquid propellants, usually with a liquid oxidizer; they are safer than solid rocket motors, have a pretty low cost, can use the liquid propellant for refrigeration and they have intermediate performances. A disadvantage is that they have a low combustion efficiency and they are characterized by some problems in thrust regulation

Analysing more specifically the liquid rocket engines, they work with several types of propellant that can be used without changing composition (like in cold gas thrusters), after decomposition (like monopropellant engines) or after a chemical reaction in which an oxidizer and some fuel are involved. It is also possible to make another distinction based on the type of alimentation system used: pressurized systems or turbo-pump systems; the first one, actually, includes three different solutions: the blow-down system, in which a pressurant gas is inserted inside the propellant tank causing the propellant pressure and the performances to decrease over time, the regulated pressure system, which has a separate tank for the pressurant and a control valve that keeps the pressure of the propellant constant, and the re-pressurization system, similar to the blow-down but with the possibility to re-pressurize the system once. The turbo-pump systems include different, pretty complicated architectures characterized by the use of a turbine and a pump to pressurize the propellant. The choice of one of these two alimentation systems is correlated to the total impulse (I_t) that is needed: for high I_t the propellant tanks are very large and it is better not to have them at a high pressure, making the turbo-pump system preferable (indeed all the launchers have systems like this); in the case of low I_t, the tanks are smaller and so they can be pressurized using a simpler system (this is the solution adopted by all the spacecrafts).

3.4 Orbital Manoeuvres

A spacecraft orbiting around the Earth, continues to move along a conic section as stated by the two-body problem model; in a more realistic simulation, it would be subjected to a modification of its orbit due to orbital perturbations, that are unwanted or at least uncontrollable variations: if a spacecraft wants to change its orbital parameters in a defined way, it needs to use the thrust produced by its engine to modify its velocity. This section presents a general description of the orbital manoeuvres, while the specific model used to calculate the manoeuvres in this thesis' problem is described in chapter 5.

The orbital manoeuvres are an essential part of astrodynamics, since they make a spacecraft not only an inert, orbiting object like an asteroid but a body able to exploit gravitational rules for its purpose. The most important manoeuvres can be divided into two different categories: manoeuvres that cause energy changes and the ones used for plane changes.
The first type of manoeuvres modifies a (indeed, there is a univocal relationship between a and the mechanical energy of the orbit, as expressed by equation 3.11) and can be obtained if the thrust is parallel to the velocity; the energy change can be obtained calculating the derivative of the equation 3.10 making the assumption that the manoeuvre is performed at a constant radius (considering the chemical propulsion, the impulsive ΔV model can be used)

$$dE = V dV \tag{3.25}$$

The result indicates that velocity changes (dV) performed when the speed (V) is larger produce larger energy variations; since the velocity decreases going farther from the attracting body, it means that this type of manoeuvres is more effective if performed at low radii.

The second type of manoeuvres is used to modify Ω and i and are characterised by the equation

$$\Delta V = 2V \sin \frac{\Delta\psi}{2} \tag{3.26}$$

where $\sin\psi = \cos i / \cos\delta$ and ψ is the azimuth angle (δ is the latitude at which the manoeuvre is performed). It can clearly be seen that, at the opposite of energy changing manoeuvres, this manoeuvre is more effective at large radii because, there, V decreases and the same $\Delta\psi$ can be obtained paying a lower ΔV; this equation also indicates that if the change of plane is made with a latitude different from zero (so it is not made at one of the two nodes), the results will not only be a change in the inclination of the orbit but also a change in its RAAN.

There are several relevant impulsive manoeuvres, each one used in different context; the most important are:

- the Hohmann transfer: is the two-impulses manoeuvre between two circular orbits having the lower cost; it connects the arrival and departure orbits with a tangent ellipse and the two impulses, since they change a, are performed at the apsides, parallel to the velocity

- the bielliptic transfer: is a transfer between two circular orbits and is characterized by three impulses; the first one makes the satellite enter on an elliptical orbit that brings it farther than the final orbit. When arrived at

the apoapsis, the satellite performs the second impulse to move on a different ellipse tangent to the arrival orbit; the third impulse is performed at the periapsis of the second ellipse. This transfer exploits the fact that the energy change manoeuvre is more effective at lower radii, performing a higher thrust when at the nearest point from the attracting body; when it is used to transfer to a final orbit way bigger than the departure one, it becomes more efficient than the Hohmann transfer

- the Oberth manoeuvre: it is used to escape from a planet's sphere of influence; it brings the satellite nearer to the main attracting body to exploit the greater effectiveness of the energy change at low radii before performing the second, great thrust

An important strategy that reduces propellant consumption is the combined manoeuvre presented in the left of figure 3.5

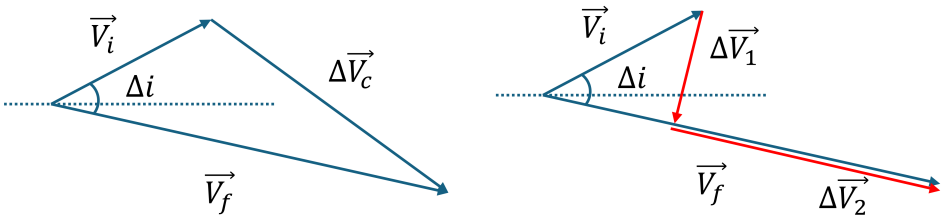

Figure 3.5: Comparison between combined and separate manoeuvres

This type of manoeuvre combines a change of a and i, with a resulting ΔV that is lower if compared to the same manoeuvres performed separately (presented in the right of figure 3.5); $\vec{V_i}$ is the initial velocity, $\vec{V_f}$ is the velocity after the manoeuvre, $\Delta\vec{V_c}$ is the velocity change performed in the combined manoeuvre, $\Delta\vec{V_1}$ and $\Delta\vec{V_2}$ are the two separated impulses needed to perform the same manoeuvre, Δi is the desired change of inclination. This manoeuvre can be used combining a Hohmann transfer and a change of plane manoeuvre and, to further reduce the propellant consumption, it is possible to split the change of inclination in the two impulses of the Hohmann manoeuvre: the first one produces a reduced variation of i, while the second one performs the remaining variation, being more effective because at a large radius.

Chapter 4

Ant Colony Optimization

The goal of this thesis is to find the optimal debris sequence to visit among a group, in order to minimize time and cost; this problem belongs to the wide category of combinatorial optimization problems that consist in finding the optimal solution within a set of discrete possible solutions (a more detailed description of combinatorial optimization problems is given in B). This type of problems can be solved using a great variety of both exact and approximate algorithms but for a large number of elements and so a great variety of possible combinations, as in this case, the latter achieve better performances; among the approximate algorithms a powerful and very promising one is the Ant Colony Optimization (ACO) hereafter explained.

4.1 Real ants behaviour

Ants have always been a symbol of industriousness and teamwork, indeed, more ants together can do things that for a single ant would be impossible, like transporting heavy objects but also finding the shortest path between their nest and food. This form of cooperation is possible also, among the other things, thanks to their communication method.

Unlike other animals, ants communicate one to each other thanks to the use of particular chemicals called pheromones that are released by some ants and detected by the others; one of the most important type of pheromones, particularly for some ant species, is the trail pheromone used to mark a specific path on the ground. An example of pheromone usage is at the base of ants' foraging behaviour: each ant deposits pheromone on the trail it follows from the nest to reach the food, making its path more desirable also for the other ants that follow pheromone trails left on the ground and, in turn, leave other pheromone on their path. This communication technique, based on the modification of the environment is called stigmergy and is

adopted also by other species like termites.

Real ant colonies behaviour has been studied for several years as an inspiration for optimization algorithms, since they are characterized by a highly structured social organization and, even if made by very simple individuals, they can achieve this level of coordination precisely because of stigmergy. The idea is to exploit these self-organizing principles adopted by the ants to coordinate a population of artificial ants in order to solve computational and complex problems [18]. The results of these studies have brought to life different algorithms among which on the most important and successful is the ACO.

ACO bases its working principles on ant colonies' stigmergy and in particular on their foraging behaviour; it is an optimization algorithm with the basic idea of using a form of artificial stigmergy to mimic ant colonies' behaviour and coordinate the action of artificial ants.
In order to better understand ACO algorithms, it can be useful to analyse an interesting controlled experiment conducted to better investigate ant colonies' foraging behaviour [18]. The basic experimental setup, as shown in figure 4.1, was made of a double bridge connecting a nest of ants and a food source with two possible cases:

- (a) the bridge has two branches of equal length
- (b) the bridge has two branches of different length, in particular the lower branch is two times longer than the upper one

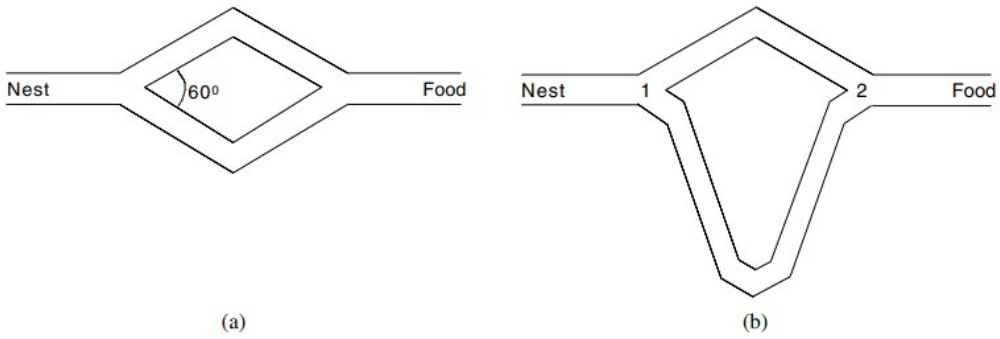

Figure 4.1: Experimental setup used for the double bridge experiment [18]

Ants were left free to move between the nest and the food and the percentage of ants choosing one or another branch was recorded over time.

In the first case (a), at the beginning of the experiment ants randomly chose one branch or the other one with the same ants percentage choosing the upper branch

or the lower branch; after a certain period, an interesting behaviour was observed with all the ants eventually choosing one of the two branches. These results can be explained by the fact that at the beginning there is no pheromone on neither of the two branches and so ants, without having any preferences, choose with the same probability one of the branches; after a while, because of random fluctuations, more ants will end up choosing one of the two branches, increasing the pheromone level on that branch and making more ants to go there into a positive feedback process. This event is an example of the self-organizing behaviour of the ants in which a macroscopic pattern (ants convergence to one of the two branches) emerges thanks to interactions at a microscopic level (leaving and detecting pheromone trails).
In the second experiment (b), after an initial phase of random choice in which about half of the ants chose the upper branch and half the lower branch, ants eventually end up choosing the shorter branch being the most convenient and effective path to reach the food. The explanation is that, during the first tour to the food, an equal number of ants choose the shorter and the longer branch increasing the pheromone level on both the bridges; ants on the shorter path reach the food earlier than ants on the longer one and so they come back to the nest continuing to deposit pheromone. When also longer path ants are back at the nest, the shorter path has an higher level of pheromone because shorter path ants, being back at the nest earlier than the other group, are already coming back to the food; this situation makes the shorter path more desirable, being the preferred path after a short period of time. At the end of the experiment, there is still a small percentage of ants choosing the longer branch in what can be considered a type of path exploration.

An interesting variation was applied to the second case to better understand ants' behaviour: instead of a double bridge, it was proposed a single bridge connection with a long path between the nest and the food; after a while, having a certain level of pheromone accumulated on the single path, a new short connection was inserted between the nest and the food. As a result, only a small percentage of the ants chose the new shorter path because pheromone levels on the longer branch were too high and pheromone evaporation too slow to make them change their choice.
Another interesting observation is that, in order for this way of communication to be effective, ants need to deposit pheromones on both their forward and backward path from the nest to the food; the observation of real ant colonies has shown that depositing pheromones only when returning to the nest make convergence to the shorter path impossible [18].
These two latter observations explain in an even clearer way how important pheromones are for ants communication and how deeply their behaviour is influenced by these chemicals.

4.2 ACO Metaheuristic

Combinatorial optimization problems can be classified depending on their complexity, and so on how difficult it is to find an optimal solution, using the theory of *NP*-completeness (a more in-depth description is given in B); this theory distinguish between two main classes of problems:

- *P*-problems that can be solved in polynomial time
- *NP*-problems that can only be verified in polynomial time (*NP* stands for Nondeterministic-Polynomial time)

The problem treated in this thesis belongs to a particular category of *NP* called *NP*-hard, indicating a problem to which any *NP* problem can be transformed by a polynomial time reduction [18].
As already stated before, combinatorial optimization problems can be solved with exact or approximate algorithms but in the case of *NP*-hard problems exact algorithms can rarely be used because of the poor performance and the time required: in the worst case, it is required an exponential time to find the optimum, a clearly impracticable solution for instances with several elements. Therefore, the only possible solution is to use approximate algorithms often called heuristic. Heuristic methods, even if powerful and suited for several problems, have the disadvantage of generating a pretty limited number of different solutions that, in some cases, can make the algorithm stop at poor-quality local optima; to solve this problem, several approaches have been proposed belonging to the category of metaheuristics.

A metaheuristic is "a set of algorithmic concepts that can be used to define heuristic methods applicable to a wide set of different problems" [18]; basically, a metaheuristic can be considered as a general-purpose heuristic method used to guide a more specific heuristic towards search space regions containing high-quality solutions. Nowadays there are several metaheuristics often used in combinatorial optimization problems such as tabu search, evolutionary computation and the one of interest for this thesis: ACO.
Therefore, ACO algorithms can be defined as a metaheuristic in which a colony of artificial ants, incrementally building a solution, cooperates in solving discrete optimization problems. To apply ACO algorithms, the combinatorial optimization problem is first mapped to another problem characterized by a completely connected graph $G_c = (C, L)$ on which ants, randomly walking, build solutions; the nodes of the graph C are the components of the initial problem that ants have to visit, while the set L fully connects the components. Connections can have associated other two essential elements of ACO algorithms:

- a pheromone trail τ_{ij}
- a heuristic value η_{ij}

The pheromone trail represents a form of long-term memory used by the ants along all the searching process and updated by themselves; the heuristic value, instead, is an a priori information about the problem instance provided by a source outside the ant colony and in many cases represents the cost of adding a new connection to the solution under construction. In this way, the artificial ants, which basically are stochastic constructive procedures that build the solution gradually adding new components and connections, act concurrently and independently and even if they singularly are pretty simple, thanks to collective interaction they can find good-quality solution to complex problems; basically they are not adapting themselves to solve the problem but they gradually modify the way the problem is represented and perceived by other ants.

Generally, an ACO algorithm can be seen as made of three different phases:

- the construction of the solution
- the update of pheromone trails
- the daemon action

During the first phase each ant independently and gradually builds a solution applying a stochastic decision rule that makes use of pheromone and heuristic information to move through neighbour nodes on the construction graph G_C.
After that, pheromone trails are modified, with their value that can basically change in two opposite ways: it can increase thanks to the pheromone deposited by an ant that has passed on that specific connection or it can decrease due to pheromone evaporation; in the first case the probability of a certain connection to be chosen by other ants increases, in the second case the probability decreases avoiding a too fast convergence and fostering the exploration of new connections.
The last (optional) step is related to centralized actions that can not be performed by single ants; an example can be the selection of best performing ants to deposit more pheromone on the next iterations (for other examples of daemon actions, see Section 4.5). After the external action has completed, the process can start again in an iterative way until a certain end-criteria is met.

4.3 ACO applied to the Travelling Salesman Problem

After a general description of ACO working principles, now is possible to analyse its application to some specific, real problems. Today, ACO algorithms have already been used to solve several types of problems, some of which are the sequential ordering problem, the generalized assignment problem, the network routing problem; but one of the most famous, on which ACO was tested at first and to which this thesis' problem can be mapped (as further described in chapter 5) is the Travelling Salesman Problem (TSP).

TSP is a *NP*-hard optimization problem important (not only for ACO algorithms) because arises in several real-world applications, it is easy to be explained and understood and it is used as benchmark for new algorithms. The TSP is the problem of a salesman who has to find the shortest path that takes him from his home town to a set of customer cities and then back home, visiting each city only once.
More formally, the TSP can be represented by a complete weighted graph $G = (N, A)$ with N being the set of nodes (and so of cities to visit) and A the set of arcs connecting the nodes; each arc $(i, j) \in A$ is assigned a value d_{ij} that is the distance between cities i and j, with $i, j \in N$.
The goal in the TSP is to find a minimum length Hamiltonian circuit on the graph (a Hamiltonian circuit is a closed path visiting each node exactly once) and so a solution of the TSP is represented by a permutation of the city indices.
In TSP the pheromone trails are associated with arcs connecting the cities and represent the desirability of visiting a certain city, so, if an artificial ant is at the city i, the pheromone trail value τ_{ij} expresses the desirability to visit city j. The heuristic information is usually set as $\eta_{ij} = \frac{1}{d_{ij}}$.

In the case of TSP, ACO algorithm follows some main steps applied for each ant iteratively:

1. the ant starts from a city chosen with some criterion
2. the ant stochastically choses the next city not yet visited using pheromone and heuristic informations; this operation is iteratively repeated until all the cities have been visited and so a solution has been completely constructed.
3. the ant comes back to the start city
4. when all ants have completed their tour, the pheromone updating phase begins: at first, the pheromone evaporation is applied, then each ant deposits a predetermined value of pheromone on the trail it has followed

In some cases, before the pheromone updating phase, ACO solutions can be improved by the application of a local search algorithm; this is another example of metaheuristic that perturbs an initial solution by moving to a neighbourhood and by finding a new solution from which repeating the process until a certain requirement is met (this would also be an example of a daemon action).

4.4 Ant System

The first ACO algorithm to be invented is the Ant System (AS), firstly tested on TSP [18]; AS is a very basic version of ACO metaheuristic that has been profoundly modified since its birth with the creation of new, more advanced and updated algorithms. However, it represents ACO basis and, thanks to its easy structure, can be useful in understanding more complex and recent ACO algorithms; it is for these reasons that, in this section, a deep analysis of AS is given (for more clarity, the following explanation considers AS algorithm applied to TSP).

AS algorithm can be divided into two main phases: ants' tour construction and pheromone trails update. Before starting the actual algorithm, pheromone trails need to be initialized with a value a bit higher than what each ant is expected to leave on one iteration; a good estimate of that value can be $\tau_{ij} = \tau_0 = \frac{n}{C^{nn}}$ with n being the number of ants and C^{nn} the length of the nearest-neighbour tour (it is an heuristic that builds the solution adding the closest city as the next one). Even if this initialization can seem to be trivial, it is pretty important to choose the proper value: if the initial pheromone trails are too low, ants are quickly biased by the first tours generated, reducing the exploration of different possible solutions; on the other hand, if τ_0 is too high, ants have to wait several iterations for evaporation to reduce pheromones values so that pheromone added by the ants can bias the search.

Tour Construction: considering a total of n ants, at the beginning each one starts from a random chosen city; a fundamental equation for this phase of the algorithm is the random proportional rule, a probabilistic choice rule thanks to which each ant, at every step of the iteration, chooses the next city to move to. This rule can be expressed as

$$p_{ij}^k = \frac{(\tau_{ij})^\beta (\eta_{ij})^\alpha}{\Sigma_{l \in N_i^k} (\tau_{il})^\beta (\eta_{il})^\alpha}, \quad \text{if } j \in N_i^k \tag{4.1}$$

that expresses the probability of ant k, currently in city i to go to city j; η_{ij} is the heuristic value and is an a priori information of the problem (for TSP it usually is $\eta_{ij} = \frac{1}{d_{ij}}$ with d_{ij} being the distance between cities i and j), β and α are two

parameters that determine which one, among the pheromone trail and the heuristic information, has a higher relative weight; N_i^k is the feasible neighbourhood of ant k when it is in city i, meaning the cities that ant k has not visited yet.
With this rule, the probability of choosing city j starting from city i increases with pheromone trail level τ_{ij} and with the heuristic information value η_{ij} (the higher the heuristic information, the nearer the city). About the two parameters: if $\beta = 0$ closest cities have an higher probability to be chosen, reducing ACO to a simple stochastic greedy algorithm; if $\alpha = 0$ only the pheromone information is followed and this often leads to poor quality, stagnating situations in which one of the first paths chosen rapidly becomes the preferred one by all the ants. In general, good values of the parameters are $\beta = 1$ and $2 \leqslant \alpha \leqslant 5$ even if each problem is characterized by an optimal combination of values.

A crucial difference from real ants, but essential for the artificial ones, is that in AS each ant has a memory (M^k) containing the ordered list of cities already visited; this memory is used to define the feasible neighbourhood of each city visited (N_i^k), to compute the path length for each ant (T^k) and to retrace the tour in order to deposit new pheromone.

It has been described the process followed by each ant but, as already said, AS is based on the combined action of several ants that can be achieved in two different way:

- in the parallel implementation at each step every ant moves to the next city
- in the sequential implementation one ant builds a complete tour before another one can start its tour

for AS, however, the two implementations are equivalent without a great influence on the algorithm.

Pheromone Update: after all ants have completed their tours, pheromone trails are updated. The first step mimics pheromone evaporation, lowering the pheromone value an all arcs by

$$\tau_{ij} \leftarrow (1 - \rho)\tau_{ij}, \quad \forall (i, j) \in A \tag{4.2}$$

where $0 < \rho \leqslant 1$ is called pheromone evaporation rate and is used to avoid an excessive pheromone accumulation and to foster new path exploration.

After pheromone reduction, all ants deposit new pheromone on the connections they have crossed during their tour

$$\tau_{ij} \leftarrow \tau_{ij} + \sum_{k=1}^{n} \Delta\tau_{ij}^k, \quad \forall (i, j) \in A \tag{4.3}$$

in which $\Delta\tau_{ij}^k$ is the amount of pheromone deposited by ant k on the arcs it has visited and it is defined as

$$\Delta\tau_{ij}^k = \begin{cases} \frac{1}{C^k}, & \text{if arc } (i,j) \text{ belongs to } T^k \ ; \\ 0, & \text{otherwise;} \end{cases} \tag{4.4}$$

where C^k, the length of the tour T^k built by ant k, is computed as the sum of the single arcs belonging to T^k. It can clearly be seen that, according to equation 4.4, the shorter an ant's tour, the more pheromone that ant is allowed to deposit, following a scheme that favours the shortest tour.

4.5 AS Successors

AS algorithm, even if it performs pretty well for TSP and other problems, has some limit being the first ever ACO metaheuristic; during the years AS has been modified, trying to make it performs better and better and here are some of the variations applied to it.

The first improvement to AS is called Elitist strategy for Ant System (EAS) and is based on the idea of adding a higher value of pheromone to the best tour found since the start of the algorithm (the best-so-far tour T^{bs}) with a clear example of daemon action. The difference is in the pheromone updating phase during which arcs belonging to T^{bs} receive an additional pheromone quantity $\frac{e}{C^{bs}}$ added to the already increased pheromone level; C^{bs} is the length of the best-so-far tour while e is a parameter that defines its weight and, with proper value, can make EAS obtain better results than AS.

Another AS variant is the rank-based version of AS (AS_{rank}) that operates as EAS, with pheromone levels increased on the arcs of T^{bs}, adding the presence of ants ranking. After all ants have completed their tour, they are sorted by increasing tour length and the quantity of pheromone they can deposit depends on their rank; in particular, only a certain number of the best ranked ants and the best-so-far ant are allowed to deposit pheromone in an algorithm that reveals to be really better than AS.

There are other two AS variants that apply great modifications to the basic version: the $MAX - MIN$ Ant System (MMAS) and the Ant Colony System (ACS), two of the best performing variants of AS.

4.5.1 MMAS

MMAS applies four main variations to the basic AS:

- only the iteration-best or the best-so-far ant is allowed to deposit pheromone; this allows a greater exploit of the best tours found but rapidly leads to stagnation, a problem solved by the second modification
- there is a limit for the possible range of pheromone values $[\tau_{min}, \tau_{max}]$
- pheromone trails are initialised to the upper pheromone limit
- pheromone trails are reinitialized when the system faces stagnation

After pheromone evaporation, the deposit of new pheromone is characterized by

$$\tau_{ij} \leftarrow \tau_{ij} + \Delta\tau_{ij}^{best} \tag{4.5}$$

where $\Delta\tau_{ij}^{best}$ can be $\Delta\tau_{ij}^{best} = \frac{1}{C^{bs}}$ (C^{bs} is the length of the best-so-far tour) if only the best-so-far ant is allowed to deposit pheromone or $\Delta\tau_{ij}^{best} = \frac{1}{C^{ib}}$ (C^{ib} is the length of the iteration-best) if only the iteration-best ant can deposit new pheromone.

The choice for the best-so-far or the iteration-best ant to deposit pheromone changes during the iterations and the relative frequency influences the behaviour of the algorithm: when the best-so-far ant is chosen, the search rapidly focuses on the T^{bs} making the algorithm more greedy; on the other hand, when choosing the iteration-best ant, the search is less directed and more explorative.

Pheromone trail limits are a very useful modification in order to avoid stagnation since they limit the probability of selecting the next city and they prevent a too high pheromone level on some arcs.
The choice of initializing pheromone trails level with the upper limit value, with the help of a small evaporation rate, allows the relative difference in the pheromone trail levels to slowly increase, making the initial phase more explorative.
In general, MMAS in the first iterations generates pretty poor solutions, being characterized by a more explorative behaviour, while its final solutions quality is very high [18].

4.5.2 ACS

ACS has three main differences from the original AS:

- it uses a more aggressive action choice rule, exploiting more the experience of the ants
- pheromone evaporation and deposit take place only on the arcs of the best-so-far tour
- each ant moving from one city to the next one removes some pheromone to increase the exploration of alternative solutions

In ACS the tour construction follows the pseudorandom proportional rule; differently from equation 4.1, when ant k is located at city i it choses the next city j according to

$$j = \begin{cases} argmax_{l \in N_i^k} \left[\tau_{il} \left(\eta_{il}\right)^{\alpha}\right], & \text{if } q \leqslant q_0; \\ J, & \text{otherwise;} \end{cases} \tag{4.6}$$

where q is a random variable between [0,1], $0 \leqslant q_0 \leqslant 1$ is a parameter and J is a random variable chosen with the probability distribution given by equation 4.1 with $\beta = 1$. Every time an ant has to choose the next city to move to, it samples a random number q; using this equation, with probability q_0 the ant chooses the arc with the higher pheromone level and the higher heuristic information level, making the best decision possible according to the learned knowledge; with probability $1 - q_0$ it makes a more explorative choice. Choosing a proper value of q_0 can make the algorithm more explorative or more focused on the best-so-far solution.

In ACS only the best-so-far ant is allowed to add pheromone following

$$\tau_{ij} \leftarrow (1 - \rho)\tau_{ij} + \rho\Delta\tau_{ij}^{bs}, \quad \forall (i,j) \in T^{bs} \tag{4.7}$$

It is clear that in ACS both pheromone evaporation and update only apply to the best-so-far tour, reducing the computational complexity of the process.

There is another pheromone update that happens immediately after an ant crosses an arc and that follows the equation

$$\tau_{ij} \leftarrow (1 - \xi)\tau_{ij} + \xi\tau_0 \tag{4.8}$$

in which $0 < \xi < 1$ and τ_0 are two parameters. The local update makes the arcs chosen by the ants less desirable, fostering exploration of new paths and avoiding stagnation behaviour.

Although for other ACO algorithms it is the same to use a parallel or a sequential implementation, for ACS this makes a difference because of the local updating and, in general, parallel implementation is preferred. An interesting aspect is that ACS, even if not explicitly, has both an upper and lower pheromone trail limit exactly as MMAS. In general, ACS reveals to be the most aggressive of the ACO algorithms with a very short computation time and a less explorative behaviour if compared to MMAS [18].

Some interesting experiments have been conducted [19] to show the importance of cooperation between the ants and of pheromone trails to obtain good solutions in an effective way and in a reduced amount of time; this clearly outlines the great similarities that ACO has with real ants and their communication strategies. In all the experiments, ants that could cooperate and exchange pheromone outperformed the other ants with a high probability of finding an optimal solution in less time; another interesting result showed how much pheromone is more important than the heuristic information, since artificial ants operating on a graph without any heuristic value associated could perform better than ants made blind to pheromone anyway.

Chapter 5

Problem definition

This chapter presents an in-depth description of the problem tackled by the thesis and the methodologies adopted, beginning with the presentation and description of the GTOC9, which is the starting point of this work; next, the aspects for which this thesis differs from the original problem and so the peculiarities of the treated case are explained. In the last two sections, a more technical description of the specific model used to evaluate the transfers between the debris objects and of the most important aspects of the ACO algorithm applied is given.

5.1 GTOC9

The Global Trajectory Optimization Competition (GTOC) started in 2006 as an open to everybody event, taking place every one-two years, in which the best aerospace engineers and mathematicians worldwide challenge themselves to solve a problem of trajectory optimization; the winners get a trophy they will keep up to the following edition and are asked to pose the problem that will characterize the following edition [20].
The ninth edition of the competition (GTOC9) was held in 2017, it was organized by a team from the European Space Agency's Advanced Concepts Team (ACT) and JAXA's ISAS (Japan Aerospace eXploration Agency's Institute of Space and Astronautical Science) and focused on multiple space debris removal from LEO; the competition was won by the JPL team whose solution is taken as a reference and a starting point for this thesis' work.

More in detail, the proposed challenge considers an hypothetical, but not too much unlikely, future in which the explosion of a LEO sun-synchronous satellite, triggering the Kessler effect, makes the LEO environment unusable; to restore the possibility of operating in that environment, a set of 123 debris pieces has been

identified and needs to be removed by ADR missions [21]. The problem requires to design a number of missions to remove all the 123 debris exploiting the J2 effect, having an important role since the low altitude, and trying to minimize a specific cost function; one mission is accomplished by a single spacecraft and is made of multiple debris rendezvous, each characterized by the delivery and activation of a de-orbit package. The objective cost function is

$$J = \sum_{i=1}^{n} C_i = \sum_{i=1}^{n} \left[c_i + \alpha \left(m_{0_i} - m_{dry} \right)^2 \right] \tag{5.1}$$

where C_i is the cost of the i-th mission composed of c_i that is a base cost later explained, the total spacecraft mass at the beginning of the i-th mission m_{0_i} and its dry mass m_{dry}: in this way a lighter spacecraft is favoured. The basic cost c_i is strictly correlated to the time of the solution submission and it is

$$c_i = c_m + \frac{t_{submission} - t_{start}}{t_{end} - t_{start}} (c_M - c_m) \tag{5.2}$$

where $t_{submission}$ is the validation date of the solution proposed, t_{start} and t_{end} are the beginning and ending date of the competition, c_m is the minimal basic cost of 45 MEUR and c_M is the maximum cost of 55 MEUR; for each space debris not removed a penalty cost $c_{penalty} = 55.0018$ MEUR is applied. The initial mass of the spacecraft can be split into $m_0 = m_{dry} + N m_{de} + m_p$ with $m_{dry} = 2000$ kg being the spacecraft dry mass, $m_{de} = 30$ kg is the mass of a single de-orbit package, N is the number of packages brought on-board and $m_p = 5000$ kg is the maximum initial propellant mass (if less propellant is used, the mission has a lower cost).
A debris is considered removed if its position and velocity vectors at some epoch coincide with the spacecraft ones and if the spacecraft stays in proximity of the debris for an interval of time $t_w \geqslant 5$ days; the peculiarity is that only during transfers the spacecraft is subjected to J2 perturbation, whereas, while it rendezvous with a debris it has the same position and velocity vectors of the debris itself.
The manoeuvres are considered impulsive, causing an instantaneous change of the velocity vector of the spacecraft and being a good approximation for a chemical propulsion system; it is imposed a limit of 5 impulses within each transfer (also called leg) beyond the departure and arrival ones. The problem formulation is characterized by some temporal constraints: first of all, the total time between two consecutive debris rendezvous reached during the same mission must not exceed 30 days; this means that if t_a is the time of arrival at debris a and t_b is the time of arrival at debris b, it has to be $t_b - t_a \leqslant 30$ days. To avoid operating two missions in parallel, a time of at least 30 days has to pass between two consecutive missions so that $t_j^f + 30 \leqslant t_i^s$ days if $t_i^s > t_j^s$ for all $i \neq j$ where t_j^f is the end epoch of mission j and t_i^s is the start epoch of mission i; a final constraint is imposed on the

total duration of all the missions that has to be included into a window of 8 years [21].

As said before, the JPL team presented the winning solution made of a 10 missions program capable of removing all the 123 debris; the solution, as explained in [22], was achieved thanks to several different methods like a branch-and-bound technique, a customised genetic algorithm and even an ACO algorithm to firstly create a database of transfer costs and later to combine the single transfers into missions and into the final campaign. The results of the JPL team's work are here considered as a starting point and as the correct solution; in particular, the time intervals found by JPL are considered as the base to develop this thesis' algorithm, the ordered debris sequences are taken as an inspiration and the total ΔV found by the team is seen as a term of comparison and as the minimum cost that needs to be achieved.

5.2 Variations from the original problem

The GTOC9 is the base of this thesis' problem but, starting from it, some essential variations are made to obtain a new and challenging study case. The first important difference is the number of total debris pieces: at first, in this thesis are considered only the debris objects belonging to the first three JPL's missions for a total of 47 debris; in a second phase, also the debris bodies of the fourth mission are included, for a total of 58 debris whose orbits can be seen in figure 5.1 (the trajectories are obtained propagating each debris object orbital elements for a single orbit, following the two-body problem rules without the presence of any perturbation in order to get an idea of the orbits). The number of missions adopted is the same of the JPL's solution (so three in the first case and four in the second case) and the reference debris sequences are the following

- $23, 55, 79, 113, 25, 20, 27, 117, 121, 50, 95, 102, 38, 97$
- $19, 115, 41, 26, 45, 82, 47, 85, 7, 2, 11, 77$
- $72, 107, 61, 10, 28, 3, 64, 66, 31, 90, 73, 87, 57, 35, 69, 65, 8, 43, 71, 4, 29$
- $108, 24, 104, 119, 22, 75, 63, 112, 37, 32, 114$

where each line is relative to a single mission and the debris numbers are taken directly from the *.txt* file given to GTOC9 competition participants and containing the orbital elements of each debris at a specific epoch (the file is reported in C).

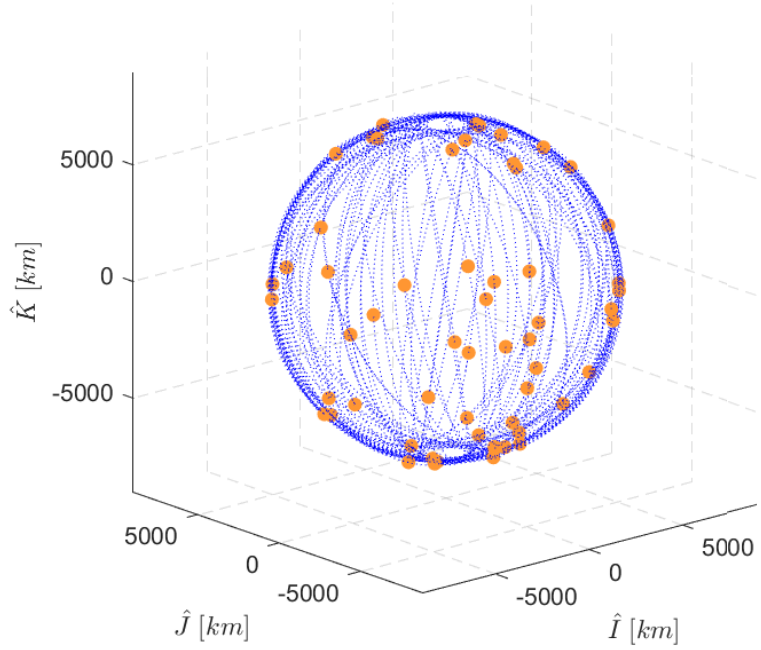

Figure 5.1: Debris orbits

As the GTOC9, also this thesis considers a chemical propulsion spacecraft whose behaviour can be well approximated by impulsive manoeuvres; an important difference from the original problem is relative to the time measure: the basic time unit of measurement considered is of 5 days, meaning that any time interval considered is a multiple of 5 and that the rendezvous time for each debris (previously indicated as t_w) is of exactly 5 days. In this thesis, the GTOC9 objective function is not considered and the only parameter that needs to be reduced is the total ΔV required to accomplish the three or four missions; no considerations about the spacecraft mass and the propellant needed are made, keeping, however, GTOC9's imposed limits as a reference point. The number of impulses considered for each leg are only one or two (as described in detail in the next section) at the beginning or at the end of the transfer; the time constraints are kept the same of the competition.

The most important variation, that makes this thesis' problem a different and more complex study case, is the variable transfers beginning and duration, considered for the evaluation of the total ΔV; before starting the actual ACO algorithm, a 4-D cost matrix (indicated as d) is created, containing all the possible transfers between all the debris objects with any possible start and duration.

The cost matrix, indeed, has the first and second dimensions containing all the debris bodies, to consider all the possible transfers (for example, the entrance (1,2) contains the cost to transfer from debris 1 to debris 2), the third dimension having all the possible starting epoch every 5 days for a total period of about 8 years and the fourth dimension being relative to all the possible transfer durations (from 0 to 25 days as multiples of 5); another essential element is the heuristic matrix (indicated as h, having the same dimensions of d) calculated as the reciprocal of the cost matrix (in this way, the lower the cost of a transfer is, the higher its heuristic value is). After having calculated the cost and the heuristic matrices, the launch dates (indicating the end of a mission and the start of a new one) and the durations of each transfer leg are generated randomly so that the total duration of the campaign and the total number of missions is the same of the JPL's ones; when the necessary time intervals are determined, thanks to the variables *slotl*, which contains transfers durations added to the rendezvous time (5 days), and the variable *slotp*, containing the starting epoch of each leg, the actual ACO algorithm starts. Since this process of creating random time intervals is repeated several times (here indicated as number of repetitions) for a single code run, it is obvious the great variability achieved with respect to the reference solution and the possibility of obtaining better results than the one proposed by JPL.

5.3 Analytical model used for transfers

The first step of the code used to tackle the problem is to create the cost matrix of all the possible transfers between the debris and to do so it has been chosen to use an analytical method that proves to be essential, given the dimensions of the combinatorial problem; in particular, the model used and here explained in details takes inspiration from the one proposed in [23].

Considering that the spacecraft operates in the LEO environment, the J2 effect is much stronger than any other perturbation and it must be considered since, at these altitudes, its effects are not negligible; however, the J2 perturbation does not represent only a disadvantage but, instead, it can be exploited using differential nodal precession rate in order to reduce the cost for changing plane. This, indeed, is the most expensive orbital manoeuvre, becoming prohibitive for large plane changes (it requires a ΔV of about 1.3 km/s per ten degrees [22]); given the fact that the ascending nodes are spread over the full circle, as it can be seen in figure 5.3 where the 58 debris objects semimajor axes and RAAN are presented on a polar diagram, it is essential to exploit J2 effect in order to maintain manoeuvres cost acceptable. Another reason that makes considering J2 necessary can be seen in figure 5.2 where the debris pieces semimajor axes and inclinations are displayed: a

ranges between about 600 km and 900 km of altitude and i ranges between about 96.5° and 101°, resulting in a considerable variation in RAAN change rates, causing the debris bodies to modify their relative angular distribution on the equatorial plane pretty fast.

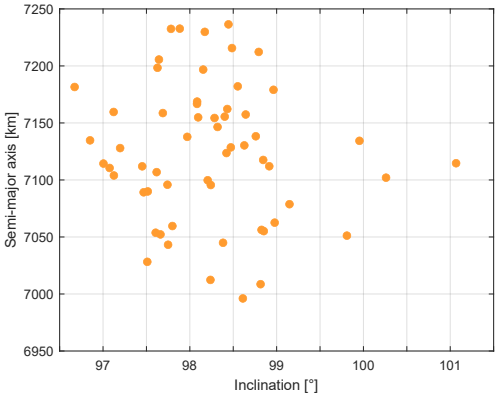

Figure 5.2: Debris inclinations and semimajor axes

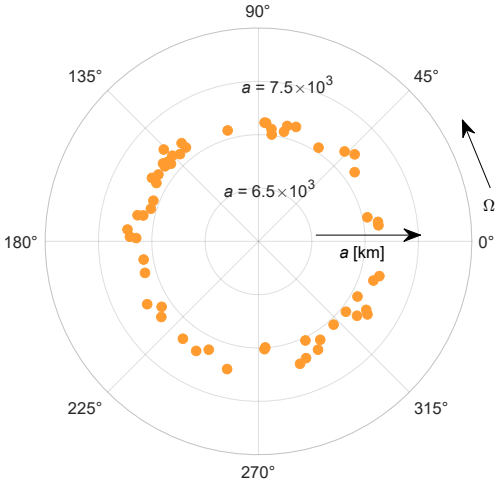

Figure 5.3: Debris RAAN and semimajor axes

In the simplified propagation model used, only secular J2 effects are considered, meaning that a, e and i remain constant while Ω, ω and M vary according to the equations 3.19, 3.20 and 3.21. The debris objects considered have low eccentricity and in this case the RAAN change rate ($\delta\dot{\Omega}$) can be expressed as a function of small changes of a and i (respectively δa and δi); the first step is to take the derivatives of $\dot{\Omega}$ to a and i

$$\frac{\delta\dot{\Omega}}{\delta a} = \frac{21}{4}\frac{\sqrt{\mu}}{a^{9/2}}r_E^2\frac{J_2\cos i}{(1-e^2)^2}\delta a \qquad \frac{\delta\dot{\Omega}}{\delta i} = \frac{3}{2}\frac{\sqrt{\mu}}{a^{7/2}}r_E^2\frac{J_2\sin i}{(1-e^2)^2}\delta i$$

and then, it can be obtained

$$\frac{\delta\dot{\Omega}}{\dot{\Omega}} = \frac{\delta\dot{\Omega}/\delta a + \delta\dot{\Omega}/\delta i}{\dot{\Omega}} = -\frac{7}{2}\frac{\delta a}{a} - \tan i\delta i \tag{5.3}$$

Using this equation and knowing the starting orbital elements values, it is possible to determine the perturbed values at any time. This propagation model has been found to be pretty precise in the evaluation of orbit shape and orientation but with large errors for argument of perigee and mean anomaly; however, given the fact that the orbits considered have a low eccentricity and that phase adjustment manoeuvres have a low cost in term of ΔV thanks to the large number of revolutions during

which each transfer leg takes place [23], this model can be considered adequately accurate for the problem treated.

To evaluate transfer cost, the analytical method used requires the orbital elements of the starting and arrival debris and the epochs at the beginning and at the end of the transfers (respectively indicated as t_s and t_a); not all the orbital elements are necessary, in particular there is the need of having the semimajor axes (a_1 and a_2), the inclinations (i_1 and i_2), the eccentricities (e_1 and e_2), the RAANs (Ω_{ef1} and Ω_{ef2}) and the epochs (ep_1 and ep_2) at which these parameters are measured, that are values all taken from the *.txt* file of the GTOC9 (from here on, the subscript 1 will refer to the starting debris, while the subscript 2 will refer to the arrival debris).
The first step is to evaluate RAAN change rates ($\dot{\Omega}_1$ and $\dot{\Omega}_2$) of the two debris objects using the equation 3.19 and the RAAN values at the beginning of the transfer (the results are then adjusted to be comprised in the interval $[0, 2\pi]$)

$$\begin{aligned} \Omega_{01} &= \dot{\Omega}_1(t_s - ep_1) + \Omega_{ef1} \\ \Omega_{02} &= \dot{\Omega}_2(t_s - ep_2) + \Omega_{ef2} \end{aligned} \tag{5.4}$$

After this, the differences between the initial RAANs ($\Delta\Omega$, the result obtained is then adjusted to be comprised in the interval $[-\pi, \pi]$) and between the initial RAAN change rates ($\Delta\dot{\Omega}$) are calculated

$$\begin{aligned} \Delta\Omega &= \Omega_{02} - \Omega_{01} \\ \Delta\dot{\Omega} &= \dot{\Omega}_2 - \dot{\Omega}_1 \end{aligned} \tag{5.5}$$

these results are used to determine the time (Δt) needed to the starting debris and arrival debris RAANs to become the same because of J2 effect (the result is eventually corrected if the time is negative)

$$\Delta t = -\frac{\Delta\Omega}{\Delta\dot{\Omega}} \tag{5.6}$$

that, added to t_s, gives the arrival time $t = t_s + \Delta t$ for which the required change of RAAN is 0.

In general, the transfer time may be different from Δt and if it is limited, as it often happens, there is the need to manoeuvre in order to modify also the RAAN; the first thing to do is to determine the RAAN values of the starting and arrival debris pieces (respectively Ω_1 and Ω_2) at time t_a (also in this case the results are

adjusted to be comprised in the interval $[-\pi, \pi]$)

$$\begin{aligned} \Omega_1 &= \Omega_{01} + \dot{\Omega}_1(t_a - t_s) \\ \Omega_2 &= \Omega_{02} + \dot{\Omega}_2(t_a - t_s) \end{aligned} \tag{5.7}$$

so that it is possible to determine the RAAN difference at the end of the transfer $\Delta\Omega_{ar} = \Omega_2 - \Omega_1$. At this point, the velocity changes to modify Ω, a and i (indicated respectively as x, y and z) can be calculated with the following equations [23]

$$x = \Delta\Omega_{ar}(\sin i_0)v_0 \tag{5.8}$$

$$y = \frac{a_2 - a_1}{2a_0}(v_0) \tag{5.9}$$

$$z = (i_2 - i_1)v_0 \tag{5.10}$$

where $i_0 = (i_1 + i_2)/2$, $a_0 = (a_1 + a_2)/2$ and $v_0 = \sqrt{\mu/a_0}$.
Because the spacecraft operates with two-impulses manoeuvres (one at the beginning and one at the end of the transfer), it is essential to properly split the total x, y, z between the first and the second impulse in order to obtain an optimized solution; each of the two manoeuvres need to be a combined one to reduce the propellant consumption and, in general, the first impulse can be written as

$$\Delta v_a = \sqrt{(s_x x)^2 + (s_y y)^2 + (s_z z)^2} \tag{5.11}$$

where s_x, s_y and s_z are parameters whose values need to be optimized to split the manoeuvre in the most efficient way; actually, these three values can also be greater than 1, meaning that the semimajor axis and the inclination obtained may be larger than the desired values but this apparently useless and too expensive manoeuvre is actuated in order to take advantage of the J2 effect and to reduce RAAN differences: given the fact that J2 effect on RAAN change rate depends on a and i, it may be useful to control these two orbital elements instead of having to perform a too large change of plane manoeuvre. Modifying the semimajor axis and the inclination, there is a change of RAAN difference (Δx) during the transfer time that can be expressed starting from 5.3

$$\delta\dot{\Omega} = -\frac{7}{2}\frac{\delta a}{a_0}\dot{\Omega}_0 - \tan i_0 \delta i \dot{\Omega}_0$$

$$\delta\Omega = -\frac{7}{2}\frac{\delta a}{a_0}\dot{\Omega}_0 t - \tan i_0 \delta i \dot{\Omega}_0 t$$

where $\dot{\Omega}_0$ is the average RAAN change rate of the starting and arrival debris objects $\dot{\Omega}_0 = (\dot{\Omega}_1 + \dot{\Omega}_2)/2$; substituted in 5.8 leads to

$$\Delta x = -\frac{7}{2}\dot{\Omega}_0 \frac{\delta a}{a_0} v_0 \sin i_0 t - \dot{\Omega}_0 \tan i_0 \delta i v_0 \sin i_0 t$$

that finally, using 5.9 and 5.10 brings to (the sign is changed in order to obtain a positive quantity)

$$\Delta x = 7\dot{\Omega}_0 \sin i_0 t s_y y + \dot{\Omega}_0 \tan i_0 \sin i_0 t s_z z = m s_y y + n s_z z \tag{5.12}$$

The second impulse needed to complete the velocity change can be expressed as

$$\Delta v_b = \sqrt{(x - s_x x - \Delta x)^2 + (y + s_y y)^2 + (z + s_z z)^2} \tag{5.13}$$

where the positive signs in the parentheses of y and z are adopted because s_y and s_z are negative quantities; at this point, the total ΔV can be written as

$$\Delta V = \Delta v_a + \Delta v_b = \\ \sqrt{(s_x x)^2 + (s_y y)^2 + (s_z z)^2} + \sqrt{(x - s_x x - \Delta x)^2 + (y + s_y y)^2 + (z + s_z z)^2} \tag{5.14}$$

At this point, it remains to find the optimal values of s_x, s_y and s_z; since it is difficult to find the minimum of ΔV in closed form, it is possible to use an analytic approximation by squaring the two velocities to remove the square root, neglecting the cross product terms $(2\Delta v_a \Delta v_b)$ [23]

$$\Delta v_a^2 + \Delta v_b^2 = \\ (s_x x)^2 + (s_y y)^2 + (s_z z)^2 + (x - s_x x - \Delta x)^2 + (y + s_y y)^2 + (z + s_z z)^2 \tag{5.15}$$

It is now possible to differentiate it with respect to s_x, s_y and s_z and set the derivatives to zero in order to find the minimum values

$$\frac{\partial(\Delta v_a^2 + \Delta v_b^2)}{\partial s_x} = 4 s_x x^2 - 2x^2 + 2mx s_y y + 2nx s_z z = 0 \tag{5.16}$$

$$\frac{\partial(\Delta v_a^2 + \Delta v_b^2)}{\partial s_y} = 4 s_y y^2 + 2m^2 s_y y^2 + 2mx s_x y + 2mny s_z z + 2y^2 - 2mxy = 0 \tag{5.17}$$

$$\frac{\partial(\Delta v_a^2 + \Delta v_b^2)}{\partial s_z} = 4 s_z z^2 + 2n^2 s_z z^2 + 2nx s_x z + 2mnz s_y y + 2z^2 - 2nxz = 0 \tag{5.18}$$

solving these three equations, it is possible to obtain the optimal values of the parameters

$$s_x = \frac{2x + my + nz}{(4 + m^2 + n^2)x} \tag{5.19}$$

$$s_y = \frac{2mx - (4 + n^2)y + mnz}{(8 + 2m^2 + 2n^2)y} \tag{5.20}$$

$$s_z = \frac{2nx + mny - (4 + m^2)z}{(8 + 2m^2 + 2n^2)z} \tag{5.21}$$

that substituted in 5.14 make it possible to determine the optimal split of the ΔV between the first and the second impulse. What has been said so far is valid for the case of limited transfer time ($t > t_a$) but, in the more favourable case of $t < t_a$ there is not the need of changing RAAN value nor the need of an optimized manoeuvre split and the two impulses become the simpler [23]

$$\Delta v_a = \Delta v_b = \frac{1}{2}\sqrt{y^2 + z^2} \tag{5.22}$$

Another case evaluated by this thesis' code is the possibility of performing one impulse manoeuvres, thrusting only at the start or only at the end of the transfer leg; in this way, the velocity change does not need to be divided and there is not the need to find the optimal values of s_x, s_y and s_z. If the thrust is performed only at the beginning of the transfer the two impulses become

$$\begin{aligned} \Delta v_a &= \sqrt{x_0^2 + y^2 + z^2} \\ \Delta v_b &= 0 \end{aligned} \tag{5.23}$$

where $x_0 = \Delta\Omega \sin i_0 v_0$; on the other hand, if the thrust is performed only at the end of the transfer

$$\begin{aligned} \Delta v_a &= 0 \\ \Delta v_b &= \sqrt{x^2 + y^2 + z^2} \end{aligned} \tag{5.24}$$

To create the initial cost matrix, the code evaluates for each transfer the different possible manoeuvres (two impulses using 5.14 or 5.22, one impulse only at the beginning 5.23, one impulse only at the end 5.24) saving only the least expensive one in order to reduce as much as possible the manoeuvres cost.

5.4 Specific ACO algorithm used

The ACO algorithm used in this thesis' code has an AS algorithm as a basis but it applies several problem-specific modifications to make it more suitable and better performing for the instance considered; in this section the method used is explained in details in each of its phases.

The number of artificial ants considered is the same of the number of debris objects (so 47 for the case of three launches and 58 for four launches) and, after having built the cost and the heuristic matrices and having determined the time intervals of interest, each ant is positioned on a different starting debris. From there, it begins the probabilistic tour construction (meaning the ordered sequence of debris); each ant receives as an input the starting and ending epochs of the leg considered at that step so that it can take into account only the portion of interest of the heuristic matrix (that in this way becomes a 2D matrix): for example, if the starting epoch is indicated as t_1 and the ending one as t_2, the ant considers all the entries of the first two dimensions of the heuristic matrix, fixing the third dimension as t_1 and the fourth dimension as t_2. The pheromone matrix (indicated as tt) is an $n \times n$ matrix (where n is the number of debris considered) containing the pheromone left by the artificial agents after their tour; in general, the used code considers a different pheromone matrix for each launch (and so for each mission) and the matrix is initialized at the beginning of the iterations with the value 1 for each entry. Having the pheromone and heuristic values, each ant can determine the probability of moving to anyone of the other debris bodies using the equation 4.1; the debris with the highest probability given by a combination of the heuristic and pheromone informations is chosen and the ant moves to it. Each ant repeats this process until it has visited all the debris objects and, then, it is followed by the next artificial agent, until all of them have completed a tour.

The next step is to calculate the cost of the tour of each ant as the total ΔV needed to reach all the debris pieces. After this, the process of updating the pheromone matrix begins; first of all the evaporation process takes place reducing all the pheromone entrances of the $(100 \cdot e)\%$ with e being a parameter. Then, the first ant adds to each of its step (each entrance of the pheromone matrix covered

in its path and relative to the specific launch) the quantity

$$\delta t = \frac{dt}{f_i} \tag{5.25}$$

where dt is a parameter and f_i is a quantity relative to the i-th ant calculated as

$$f_i = \frac{cost_i}{min(cost)} - el \tag{5.26}$$

where $cost_i$ is the cost in term of ΔV of the i-th tour, $min(cost)$ is the minimum cost among all the n tours and el is a parameter. When this process ends for the first ant, it is repeated by the second one and so on until all the ants have updated their pheromone matrices.
The final step is to determine the best tour between the n ones built by the artificial ants; this is achieved searching for the lowest cost tour in terms of ΔV.

The process here explained is relative to one single iteration and is repeated 100 times during one repetition, meaning that each artificial agent, at every repetition, travels across a complete tour 100 times before producing a solution. The best result among the 100 iterations is saved as the result of the k-th repetition; after having conducted several repetitions (50 or 100 depending on the case as better explained later) the code finishes giving the best result among all the repetitions done.

Chapter 6

Calculations and Results

After having explained the analytical model used to compute the transfers and the peculiarities of the ACO algorithm involved, this chapter presents the analyses carried out, the calculations done and the results obtained with the code used to try to improve the results proposed by the JPL for the GTOC9. The work done firstly concentrated on finding the most important parameters affecting the code behaviour and results and, in a second moment, tried to find the best combinations of them to optimize as much as possible the code output, both in terms of numerical results (the effective ΔV needed to rendezvous with all the debris objects) and in terms of solution evolution along the iterations. The first studies (reported in 6.1, 6.2 and 6.3) were conducted on the sequence of 47 debris pieces and three missions; the knowledge they made possible to achieve was later applied to the sequence of 58 debris objects and four missions (6.4). The most important parameters identified were *el* of the equation 5.26, *dt* of the equation 5.25, the evaporation coefficient e (these three are indicated as general parameters), α and β of the equation 4.1 and the following sections report the analysis conducted on them.

6.1 General parameters

The results here reported have been obtained using the code previously explained with a number of repetitions $k = 50$ and a number of iterations $iter = 100$; the following table contains the results obtained and the settings used. The first two columns indicate the values of α and β adopted and maintained constant for all the 100 iterations; the columns indicated as *el*, *dt* and e contains the values adopted for these parameters and, as it can be seen, several combinations have been tried in order to better understand how the different parameters influence the results and which combination is the best. The *min* column contains the cost (in terms of ΔV) of the shortest path found during the 50 repetitions; the column *aver* is

relative to the best repetition (the one containing the shortest path) and indicates the average cost calculated over the 100 iterations done; *avg* is the average cost over the 50 repetitions calculated considering the less expensive tour for each repetition. At the end of the table are reported the cases having the minimum *min* value and the minimum *avg* value. The case numbers in red (in the last column) are relative to particularly good results obtained or relative to cases of relevance and are represented after the table in a graph: the graph is relative to the best repetition and on the x-axis reports the iterations whereas on the y-axis reports the cost in terms of ΔV; the orange line is relative to the average cost value, the blue line represents the minimum cost trend.

alpha	beta	el	dt	e	min [m/s]	aver [m/s]	avg [m/s]	case
4	1	0.98	0.01	0.05	1.4776E+04	1.9396E+04	1.9178E+04	1
4	1	0.98	0.01	0.008	1.5935E+04	2.2217E+04	1.8980E+04	2
4	1	0.98	0.01	0.02	1.4875E+04	2.0614E+04	1.8771E+04	3
4	1	0.98	0.01	0.04	1.3948E+04	2.0107E+04	1.9016E+04	4
4	1	0.98	0.01	0.06	1.5441E+04	2.0810E+04	1.8596E+04	5
4	1	0.98	0.01	0.08	1.4621E+04	1.8090E+04	1.8977E+04	6
4	1	0.98	0.01	0.1	1.6213E+04	1.9960E+04	1.9560E+04	7
4	1	0.98	0.01	0.14	1.5959E+04	1.8078E+04	1.9389E+04	8
4	1	0.98	0.01	0.15	1.3868E+04	1.6683E+04	1.8870E+04	9
4	1	0.98	0.01	0.16	1.5566E+04	1.9189E+04	1.9335E+04	10
4	1	0.98	0.01	0.2	1.5837E+04	1.8194E+04	1.9224E+04	11
4	1	0.98	0.01	0.25	1.6551E+04	1.8004E+04	2.0392E+04	12
4	1	0.98	0.006	0.05	1.5755E+04	2.1579E+04	1.8918E+04	13
4	1	0.99	0.006	0.05	1.4999E+04	1.9424E+04	1.8631E+04	14
4	1	0.992	0.006	0.08	1.4035E+04	1.7302E+04	1.7890E+04	15
4	1	0.99	0.006	0.08	1.3671E+04	1.8735E+04	1.8258E+04	16
4	1	0.99	0.006	0.1	1.5051E+04	1.9285E+04	1.8779E+04	17
4	1	0.99	0.006	0.25	1.6450E+04	1.8557E+04	1.9566E+04	18
4	1	0.999	0.006	0.05	1.4090E+04	1.6661E+04	1.8437E+04	19
4	1	0.98	0.007	0.05	1.4108E+04	2.1064E+04	1.8786E+04	20
4	1	0.992	0.007	0.05	1.5484E+04	2.0990E+04	1.8624E+04	21
4	1	0.995	0.007	0.05	1.3329E+04	1.8249E+04	1.8842E+04	22
4	1	0.99	0.007	0.05	1.3330E+04	1.7610E+04	1.8031E+04	23
4	1	0.99	0.007	0.08	1.3847E+04	1.7869E+04	1.8476E+04	24
4	1	0.99	0.007	0.25	1.5323E+04	1.9829E+04	1.8552E+04	25

4	1	0.999	0.007	0.05	1.4730E+04	1.7430E+04	1.8989E+04	26
4	1	0.9999	0.007	0.05	1.6846E+04	1.7739E+04	2.1022E+04	27
4	1	0.98	0.008	0.05	1.5459E+04	1.9683E+04	1.8945E+04	28
4	1	0.98	0.008	0.25	1.5729E+04	1.7618E+04	1.9907E+04	29
4	1	0.999	0.008	0.05	1.6539E+04	1.7143E+04	2.0157E+04	30
4	1	0.98	0.02	0.05	1.5116E+04	2.1191E+04	1.8507E+04	31
4	1	0.98	0.05	0.05	1.3834E+04	1.6997E+04	1.9171E+04	32
4	1	0.98	0.05	0.08	1.5139E+04	1.7743E+04	1.9225E+04	33
4	1	0.99	0.05	0.08	1.6122E+04	1.9129E+04	1.9357E+04	34
4	1	0.98	0.05	0.25	1.5556E+04	1.6243E+04	1.9655E+04	35
4	1	0.96	0.01	0.05	1.6337E+04	2.0100E+04	1.9444E+04	36
4	1	0.97	0.01	0.05	1.3839E+04	1.8318E+04	1.9029E+04	37
4	1	0.97	0.005	0.05	1.5798E+04	2.0353E+04	1.9037E+04	38
4	1	0.97	0.006	0.05	1.5409E+04	2.2348E+04	1.8793E+04	39
4	1	0.97	0.007	0.05	1.5726E+04	2.1082E+04	1.8720E+04	40
4	1	0.97	0.009	0.05	1.5568E+04	2.1238E+04	1.8778E+04	41
4	1	0.99	0.01	0.05	1.4125E+04	1.9492E+04	1.8668E+04	42
minimum min								
4	1	0.995	0.007	0.05	1.3329E+04	1.8249E+04	1.8842E+04	22
minimum avg								
4	1	0.992	0.006	0.08	1.4035E+04	1.7302E+04	1.7890E+04	15

Table 6.1: Results of the general parameters analysis

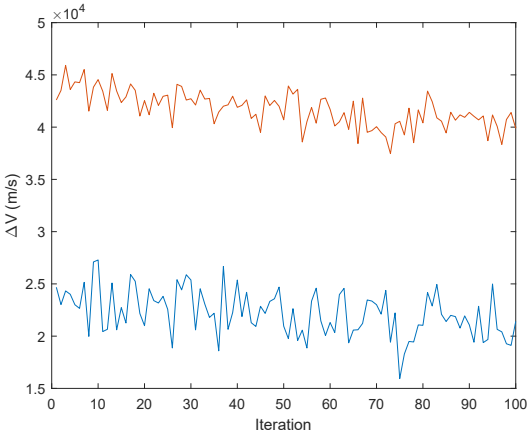

Figure 6.1: Case 2

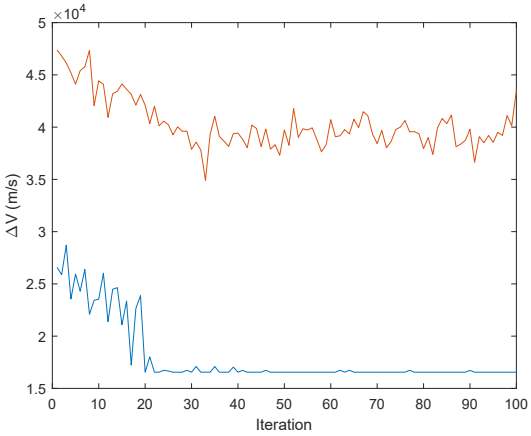

Figure 6.2: Case 12

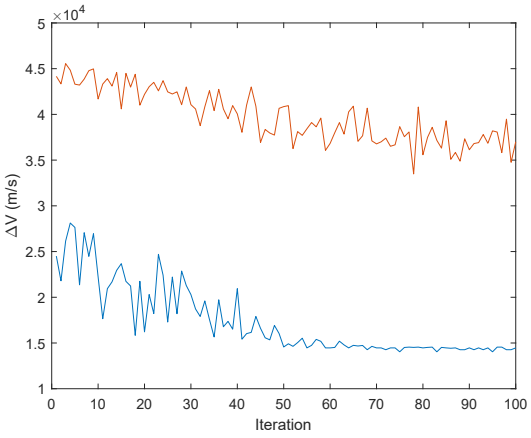

Figure 6.3: Case 15

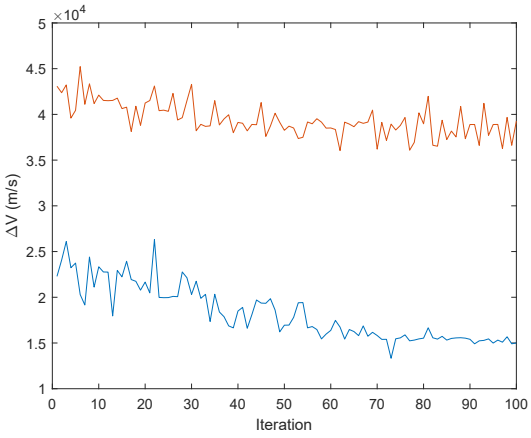

Figure 6.4: Case 22

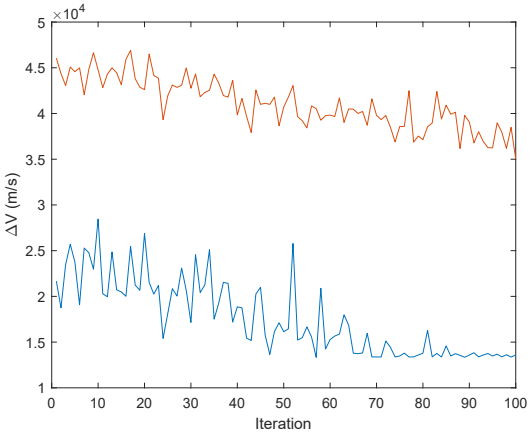

Figure 6.5: Case 23

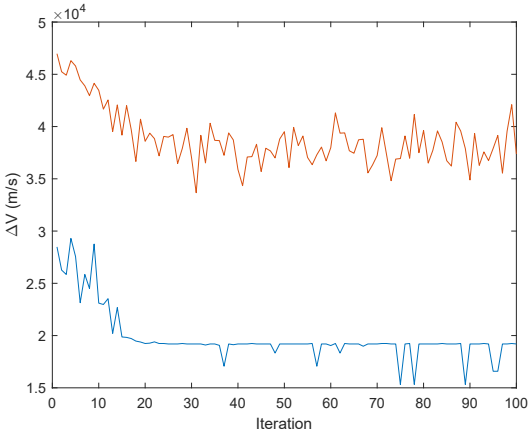

Figure 6.6: Case 25

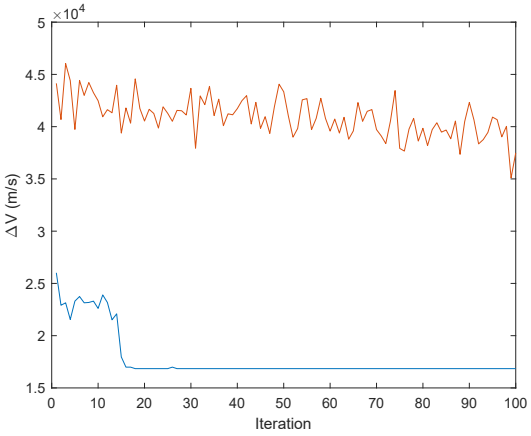

Figure 6.7: Case 27

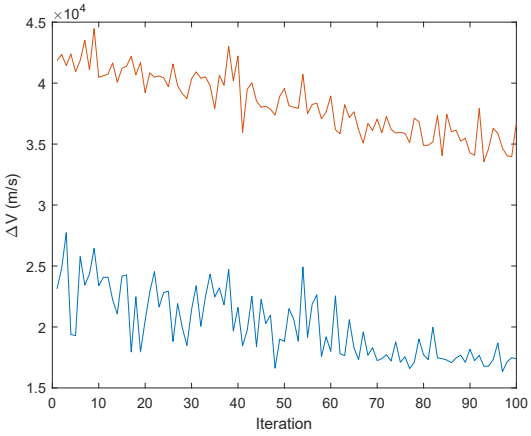

Figure 6.8: Case 36

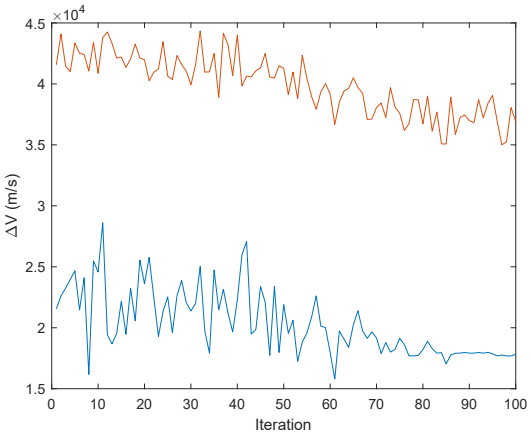

Figure 6.9: Case 38

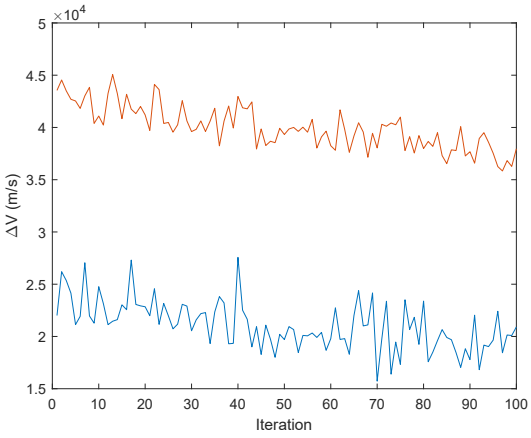

Figure 6.10: Case 40

Considering that the JPL's solution calculated with this algorithm is $\Delta V = 9.5168E+03$ m/s, the best results are obtained with the parameters combination of cases 15, 22 and 23 both for the values obtained and for the solution trends (as it can be seen in the graph); during the 100 iterations, indeed, the cost should at first be higher, indicating a more explorative phase actuated by the artificial ants to analyse the most of the different possible tours, and in the second phase it should start decreasing, indicating the choice of a specific solution. This is particularly clear looking the minimum cost of case 15 that, at the end of the iterations, nearly becomes a line after a good value reduction.

In general, if el is too high it reduces too much f_i, consequently increasing dt; this means that at every iteration too much pheromone is added to the tour, making the ants to rapidly focus on one single poor solution without exploring the remaining ones any more: this behaviour can be clearly seen in the graph of the case 27 in which the minimum becomes constant too fast. On the other hand, if el is too small, the pheromone values increase too slowly, playing a secondary role with respect to the heuristic information; every debris keeps having the same probability of being chosen and a single solution can not emerge (as it can be seen in the graphs of the cases 36 and 40 where the cost continues to oscillate with only a slight reduction thanks to the heuristic information).

The parameter e plays an important role in the permanence time of the pheromone trace and on how rapidly it reduces. If it is too small (case 2) all the possible tours keep having quite the same level of pheromone and the code becomes too much explorative; if the value is big, it causes a much rapid reduction of the pheromone levels on the less covered tours, causing the rapid emerging of a

non-optimal solution (like in case 12). This behaviour is particularly evident in the comparison of case 23 and 25: the second one has an e with a high value causing the rapid stagnation of the code (with some lower peaks) on a non-optimal solution with a cost of about 5000 m/s higher than the solution of case 23 and an average cost that increases instead of decreasing.

If dt is small, it causes a slower increase in the pheromone levels, making the solution more explorative in particular in the first phases (case 38) being characterized by wider oscillations in the minimum value and a less pronounced reduction of the average value (if compared, for example, to the case 36 having a greater dt value).

It is pretty clear the difficulty of determining the best parameters combination, in particular because each one influences the others; these analysis, however, have shown the importance of balancing the values of dt and e in order to make the pheromone trace increase (a process that needs a dt great enough and a e not too high to avoid a fast evaporation) but not too fast (meaning that dt can not have a too high value and e must not be too small making the evaporation too slow); it is also important to notice that a small dt tends to make the algorithm greedy finding low-ΔV solutions but with a reduced exploration level. This balance is needed in order to make the pheromone information acquires the same importance of the heuristic one.

6.1.1 Analysis of $t1$

To better understand how the general parameters influence the algorithm behaviour and in particular to analyse the role played by e, a further study has been conducted; in particular, the goal was to analyse how the pheromone levels changed during the iterations of two pretty similar configurations: case 23 and case 25. These specific cases have been chosen because, even if they have a slightly different parameters configuration ($e = 0.05$ in case 23 and $e = 0.25$ in case 25), the results differences are considerable: the case 23 presents an excellent numerical value, particularly if compared to the other cases, whereas case 25 gives a solution that is nearly the 15% higher. Even looking to the graphs obtained, it is evident the difference: the case 23 is characterized by a better trend with an initial explorative phase, followed by a reduction of the oscillations and of the minimum and average values; on the other hand, the case 25 presents a rapid stagnation on a non-optimal tour with the average value increasing during the last phases.

As said before, the algorithm considers a different pheromone matrix for each mission indicated as t_1, t_2 and t_3 if they respectively refer to mission 1, 2 or 3; to achieve this section task, the matrix t_1 has been considered. From a first observation

of the matrix evolution during the iterations, it resulted an important difference in the minimum and maximum pheromone values obtained at different iterations: the case 23 is characterized by a minimum value reduction of one order of magnitude every about 40 iterations, whereas for the case 25 the same happens every about 10 iterations; this expected behaviour is due to the higher evaporation coefficient of case 25 that rapidly brings the minimum probability of debris choice to values that can basically be considered as 0. The difference is less pronounced for the maximum pheromone value: at the end of the 100 iterations, there is only one order of magnitude difference between the two cases. These behaviours can be observed in figure 6.11 and figure 6.12 representing the maximum and minimum values in the pheromone matrix at the different iterations (both the x-axis and y-axis are in logarithmic scale): the orange line represents the case 23, the blue line reports case 25 behaviour. Already from this preliminary analysis, the lower e advantages started to be clear: they allow higher pheromone levels, in particular at the beginning, granting a more comparable probability among all the different debris objects and a more explorative initial phase.

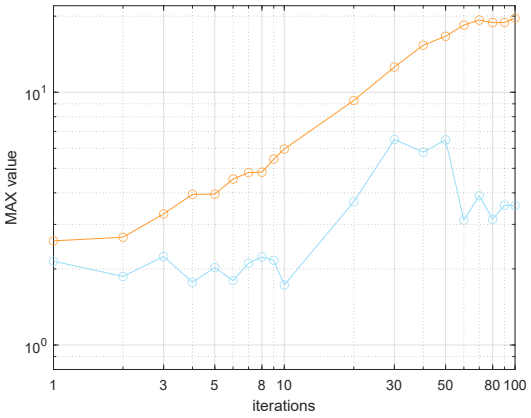

Figure 6.11: Trend of the maximum pheromone value (T trials)

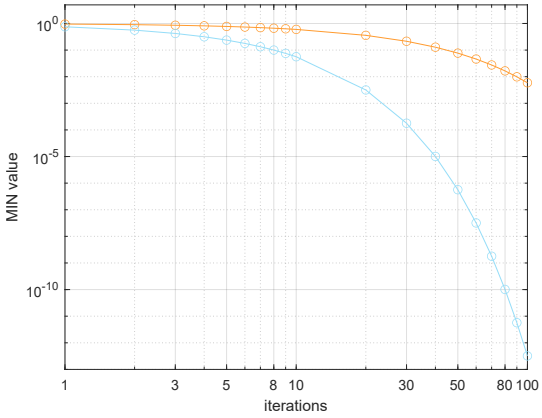

Figure 6.12: Trend of the minimum pheromone value (T trials)

To conduct a more thorough analysis, it was decided to verify, at some fixed iterations, the frequency of the maximum values on every row of the t_1 matrix; this was decided because if on a single row there are more entries with high pheromone levels, different paths have the same probability to be chosen, meaning a higher level of exploration and a higher likelihood of finding the best tour. It was rapidly verified that, both for the case 23 and 25, at each iteration the matrix t_1 presented only one singular maximum value for each row; it was then decided to look for values, at a fixed iteration, that differed for less than 1% from the maximum value of their row at that iteration (from here on these values will be indicated as 1%

values); this percentage was chosen after some trials in order to provide valuable and comprehensive results presented in the following two tables. The first table (6.2) refers to case 23, the second one (6.3) to case 25, the first column indicates the trials done (each with exactly the same parameters configuration of case 23 or 25); the first row displays the iterations considered. Each entrance of the table is given by the number of pheromone matrix entrances that at that single iteration differed for less than 1% from the maximum of their row (basically the sum of 1% values at the indicated iteration); in the last row the average of each column is presented highlighting the higher value among case 23 and case 25. As it can be seen, at the beginning of the algorithm the matrices were considered every single iteration to analyse more in detail their behaviour but, starting from iteration number 10, an evaluation every 10 iterations was considered enough.

case 23	iteration																		
	1	2	3	4	5	6	7	8	9	10	20	30	40	50	60	70	80	90	100
T1	10	5	9	4	2	3	0	0	2	2	2	0	0	0	0	1	0	0	0
T2	100	7	6	5	5	3	2	1	0	1	2	1	0	0	0	1	0	0	3
T3	10	11	10	4	1	1	1	1	2	3	1	0	0	0	1	0	0	1	0
T4	12	17	6	0	1	0	2	3	0	1	4	0	0	0	0	0	0	0	0
T5	2	1	2	1	4	4	1	1	0	1	0	1	0	0	0	0	0	0	0
average	26.8	8.2	6.6	2.8	2.6	2.2	1.2	1.2	0.8	1.6	1.8	0.4	0	0	0.2	0.4	0	0.2	0.6

Table 6.2: 1% values of case 23

case 25	iteration																		
	1	2	3	4	5	6	7	8	9	10	20	30	40	50	60	70	80	90	100
T6	69	4	0	2	1	0	2	0	2	0	0	1	0	0	1	0	0	0	0
T7	14	5	1	3	0	4	2	0	1	0	0	0	0	0	0	0	1	1	0
T8	16	3	0	0	0	0	0	0	0	2	0	0	0	0	0	0	0	0	0
T9	11	4	5	1	1	1	0	0	0	0	1	0	1	0	0	1	0	0	1
T10	103	9	0	3	2	1	2	2	3	0	1	0	0	0	0	0	0	1	1
average	42.6	5	1.2	1.8	0.8	1.2	1.2	0.4	1.2	0.4	0.4	0.2	0.2	0	0.2	0.2	0.2	0.4	0.4

Table 6.3: 1% values of case 25

To have a deeper insight of the 1% values behaviour and to have a clearer idea about their positions during ongoing iterations, a graphical representation is given in the below figures; each small table represents the pheromone matrix at a fixed iteration and the orange coloured entries are relative to the 1% values and to the maximum values of each row. The iterations reported (going left-right, up-down) are iteration number 1, 2, 3, 4, 10, 20, 60 and 100; the most significant trials among the one reported in the before tables have been chosen, in particular: figure 6.13 represents the trial $T2$, figure 6.14 represents the trial $T10$.

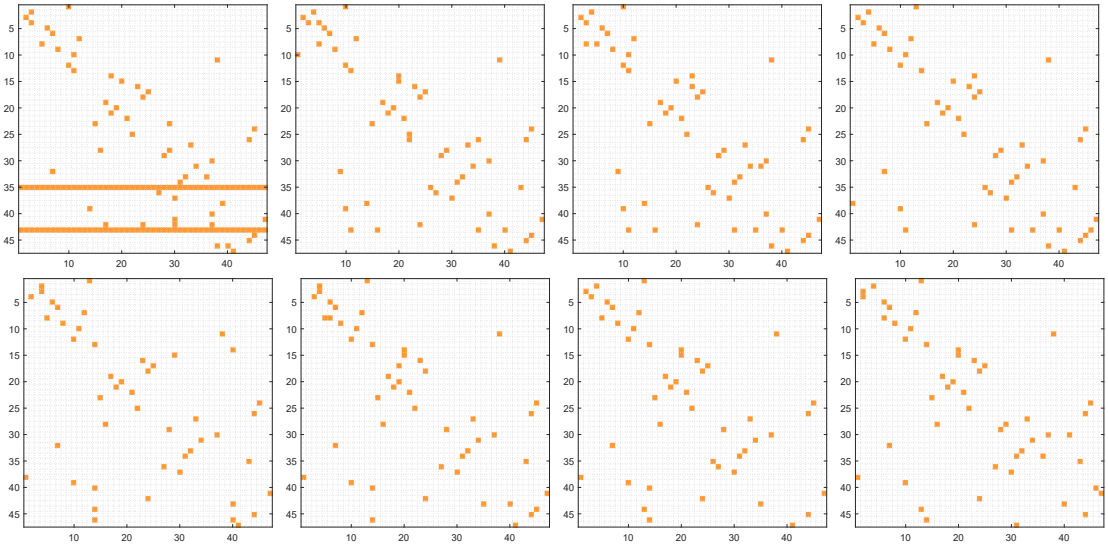

Figure 6.13: 1% values positions in trial $T2$

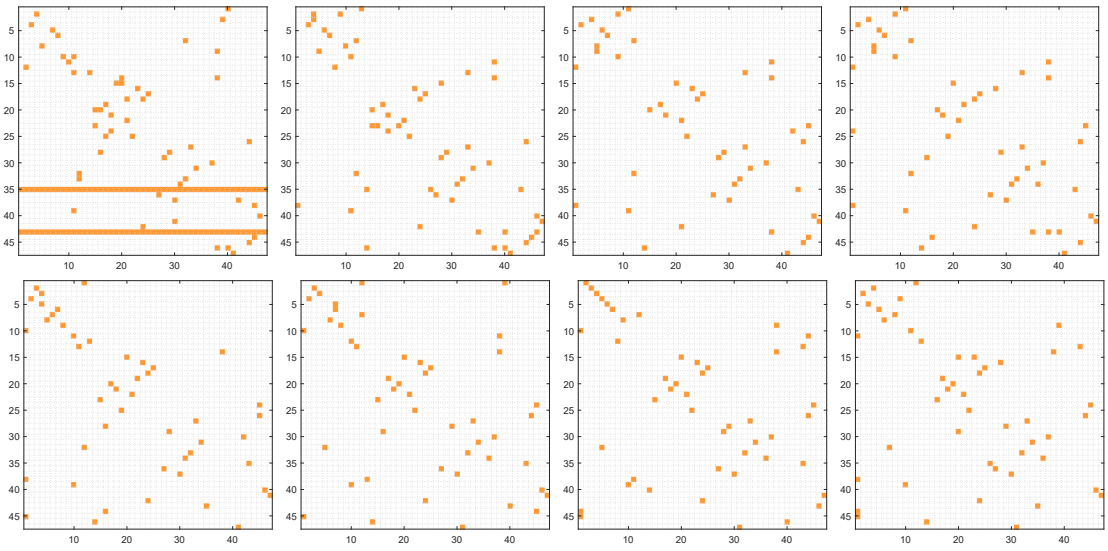

Figure 6.14: 1% values positions in trial $T10$

The tables show how the trials with the parameters configuration of case 23 have on average a higher number of 1% values during the first iterations if compared to the case 25; however, at the end of the algorithm iterations, the number of 1% values of case 23 decrease and the case 25 becomes the one with the higher number of them. This means that during the first phases the case 23 has the good characteristic of being more explorative than the case 25: more entries in the t_1 matrix have the same level of pheromone making the probability of choosing

different paths similar and increasing the possibilities of finding the shortest path possible. On the other hand, during the last iterations the case 23, having less 1% values, focuses on a specific path while the case 25 keeps being characterized by several paths with similar probability. The same conclusions can be made looking to figures 6.13 and 6.14; the matrices of the last iterations show how the case $T10$ keeps changing the positions of 1% and maximum values, indicating that there are still different paths with a similar probability of being chosen; on the opposite, the case $T2$ in the last iterations is characterized by 1% and maximum values having nearly the same position indicating the emerging of a specific path. The continuous lines of the first iterations are relative to debris pieces that have not been chosen and so that have not received any additional pheromone; however, it is interesting to observe how, already at the end of the second iteration, they disappear, meaning that those debris objects have been included in some tour.

6.1.2 Variation of tt

After having analysed the general parameters influence on the algorithm behaviour and after having acquired a better understanding of them, a new configuration was explored: the variation of the pheromone matrix tt. The results presented in this section were obtained using a different pheromone matrix for each leg; this means that, if in the previous trials there were 3 different pheromone matrices, in this case there are 46 different pheromone matrices. Since the analysis focused once again on the behaviour of the pheromone matrix, it was decided to continue considering the cases 23 and 25 and to make different trials for each case continuing to use 50 repetitions and 100 iterations; the promising results obtained are reported in tables 6.4 and 6.5 having the same structure of table 6.1. In the top-left corner it is indicated the case (23 or 25) whose parameters configuration is adopted, each line refers to a different trial; the *min* column contains the ΔV of the shortest path found during the 50 repetitions; the column *aver* is relative to the shortest path repetition and indicates the average cost calculated over the 100 iterations done; *avg* is the average of the cost calculated considering the less expensive tour for each repetition over the 50 repetitions. At the end of the tables are reported the case having the minimum *min* value, the one with the minimum *avg* value and the average of each column (*tot average*). The trial numbers in red (in the first column) are represented after the table in a graph: the graph is relative to the best repetition and on the x-axis reports the iterations whereas on the y-axis reports the cost in terms of ΔV; the orange line is relative to the average cost value, the blue line represents the minimum cost trend.

case 23	min	aver	avg
TT1	1.3557E+04	1.8671E+04	1.7572E+04
TT2	1.4086E+04	1.8321E+04	1.7728E+04
TT3	1.3411E+04	1.7479E+04	1.7868E+04
TT4	1.3986E+04	1.7663E+04	1.7976E+04
TT5	1.3942E+04	1.8063E+04	1.7606E+04
minimum min			
TT3	1.3411E+04	1.7479E+04	1.7868E+04
minimum avg			
TT1	1.3557E+04	1.8671E+04	1.7572E+04
tot average			
	1.3796E+04	1.8039E+04	1.7750E+04

Table 6.4: Trials results of case 23 with modified *tt*

case 25	min	aver	avg
TT6	1.5113E+04	1.6488E+04	1.9403E+04
TT7	1.4797E+04	1.6270E+04	1.9171E+04
TT8	1.5657E+04	1.7295E+04	1.8871E+04
TT9	1.5876E+04	1.8144E+04	1.9446E+04
TT10	1.5864E+04	1.7006E+04	1.9693E+04
minimum min			
TT7	1.4797E+04	1.6270E+04	1.9171E+04
minimum avg			
TT8	1.5657E+04	1.7295E+04	1.8871E+04
tot average			
	1.5461E+04	1.7041E+04	1.9317E+04

Table 6.5: Trials results of case 25 with modified *tt*

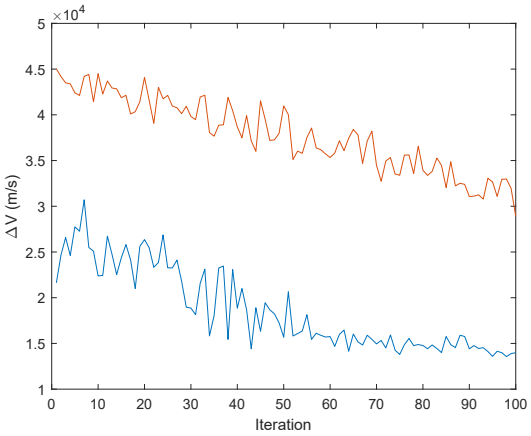

Figure 6.15: Trial $TT1$

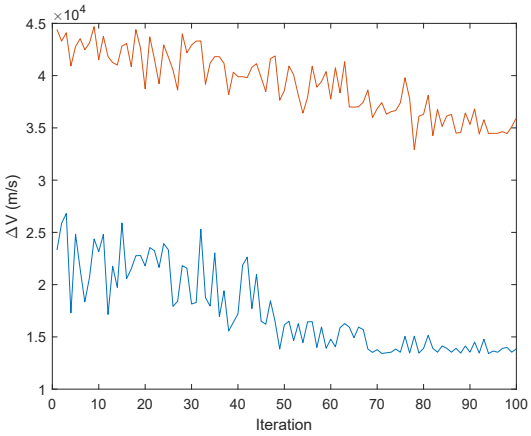

Figure 6.16: Trial $TT3$

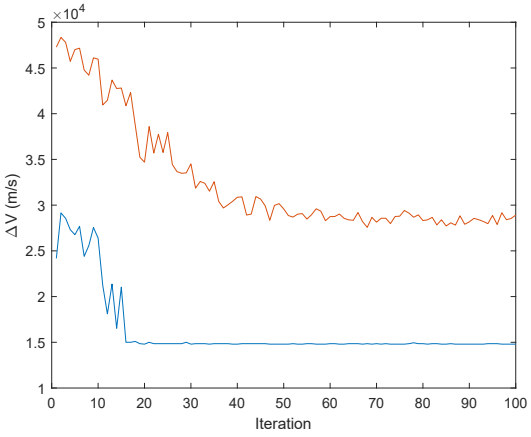

Figure 6.17: Trial $TT7$

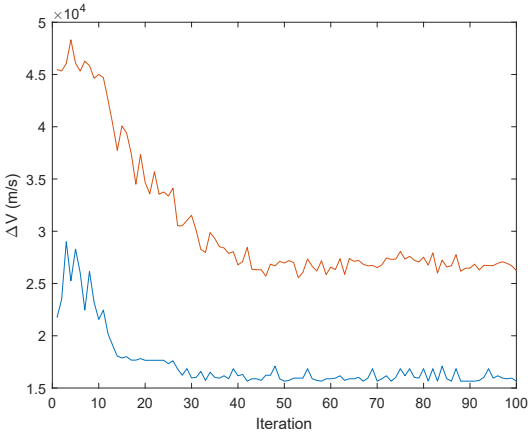

Figure 6.18: Trial $TT8$

The results obtained are better than the ones of the basic algorithm and really promising; the numerical results, if compared with the trials of the previous section, have a reduction of the 9.6% and 5.4% respectively for the *min* and *avg* values of the case 23 and of the 2.7% and 2.6% respectively for the *min* and *avg* values of the case 25 (these percentages are obtained comparing the average of the *min* values and the average of the *avg* values; the comparisons have been made between cases from $T1$ to $T5$ and from $TT1$ to $TT5$ for case 23 and between cases from $T6$ to $T10$ and from $TT6$ to $TT10$ for case 25). Also the graphs present a better trend if compared with figures 6.5 and 6.6: the main difference is the average value lines that for the TT trials present an optimal evolution starting with high values and considerably reducing. These results can be explained by the use of a more specific pheromone matrix: in the T trials there is the possibility that the transfer to a particular debris have a high pheromone level because that debris is reached by several artificial ants, for example, with the sixth leg; however, having a higher probability of being chosen, it is possible that in the following iterations it is selected also as a destination debris of, for example, the third leg; but this choice may not be the best one because from the third to the sixth leg some time passes and the debris at the end of the third leg may not have a favourable position. On the other hand, this risk disappears with the TT trials since each pheromone matrix is used and updated only relatively to a singular, specific leg.

As in the previous section, also for the TT trials a deeper analysis on the pheromone matrix behaviour was conducted; the first observations were made about the maximum and minimum values reached during the iterations (presented in figures 6.19 and 6.20 that are relative to the trials $TT3$ and $TT6$).

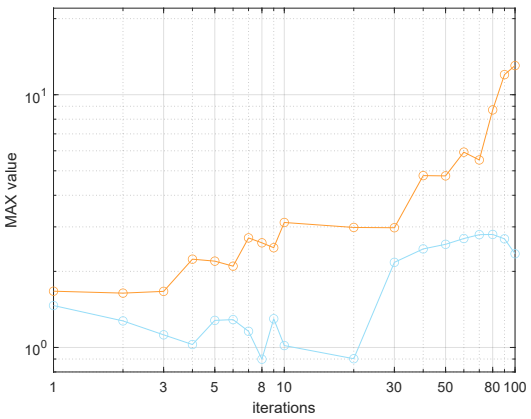

Figure 6.19: Trend of the maximum pheromone value (TT trials)

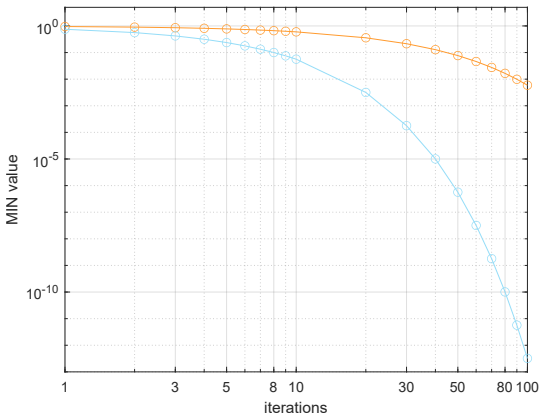

Figure 6.20: Trend of the minimum pheromone value (TT trials)

Also in this case, the minimum value of the case 25 (indicated by a blue line) decreases with a rate of about an order of magnitude every 10 iterations, more rapidly than the one of the case 23 (it decreases of about one order of magnitude every 40 iterations); the interesting aspect is that the TT minimum graph is nearly exactly the same of the one obtained for the T trials. About the maximum, also for the TT trials the difference in the final value assumed is less pronounced, even if there is a greater difference than the one observed for T trials; the TT trials for case 23 have a less linear growth (if compared with T trials) and the ones for case 25 are characterized by an initial reduction of the maximum value.

As already done for T trials, also for TT trials it was decided to analyse the number and positions of the 1% values. However, since in this case the number of pheromone matrices grew considerably, it was considered not enough to study only one single pheromone matrix and, to conduct a more complete comparison and a more comprehensive analysis, the matrices of three different legs were considered; the results obtained are presented in the below tables having the same structure than the ones of the previous section, the only difference is that here, in the up-left corner, there is an indication of both the case (and so the parameters configuration) and the leg considered. The comparison between the average values reported in the last line are made for tables relative to the same leg and if no entrance is highlighted between the two tables (the one of case 23 and the one of case 25), it means that the values are the same.

case 23 (leg 1)	iteration																		
	1	2	3	4	5	6	7	8	9	10	20	30	40	50	60	70	80	90	100
TT1	1702	281	6	8	5	4	3	3	1	2	0	1	1	0	0	0	0	1	0
TT2	874	142	6	1	2	5	1	2	1	3	0	0	0	1	0	0	1	1	0
TT3	1472	141	5	6	3	4	2	2	1	1	0	1	0	1	0	0	0	0	0
TT4	1426	415	52	50	7	4	2	1	3	0	0	1	0	0	0	0	1	0	0
TT5	1518	140	142	51	10	6	6	2	2	4	0	0	0	0	0	0	0	0	0
average	1398	224	42.2	23.2	5.4	4.6	2.8	2	1.6	2	0	0.6	0.2	0.4	0	0	0.4	0.4	0

Table 6.6: 1% values of case 23, leg 1

case 25 (leg 1)	iteration																		
	1	2	3	4	5	6	7	8	9	10	20	30	40	50	60	70	80	90	100
TT6	920	188	6	0	1	1	2	4	2	0	0	0	0	0	0	0	0	0	0
TT7	1196	6	6	4	2	2	2	1	0	0	0	0	0	0	0	0	0	0	0
TT8	1334	50	6	6	3	1	2	0	0	1	0	0	0	0	0	0	0	0	0
TT9	736	49	4	0	3	1	0	2	0	0	0	0	0	0	0	0	0	0	0
TT10	1104	141	6	7	2	2	0	1	0	0	0	0	0	0	0	0	0	0	0
average	1058	86.8	5.6	3.4	2.2	1.4	1.2	1.6	0.4	0.2	0	0	0	0	0	0	0	0	0

Table 6.7: 1% values of case 25, leg 1

case 23	iteration																		
(leg 2)	1	2	3	4	5	6	7	8	9	10	20	30	40	50	60	70	80	90	100
TT1	1752	657	561	343	287	191	195	192	143	146	98	46	48	49	47	46	48	47	47
TT2	1107	743	567	384	339	246	244	194	193	192	53	50	49	49	49	50	48	49	48
TT3	1521	744	383	384	337	293	294	248	198	194	51	50	4	1	1	2	0	0	0
TT4	1473	928	568	481	384	293	246	153	144	149	142	48	48	1	1	1	0	0	1
TT5	1611	1022	618	394	259	251	203	202	199	150	144	95	47	47	46	47	46	46	46
average	1493	819	539	397	321	255	236	198	175	166	97.6	57.8	39.2	29.4	28.8	29.2	28.4	28.4	28.4

Table 6.8: 1% values of case 23, leg 2

case 25	iteration																		
(leg 2)	1	2	3	4	5	6	7	8	9	10	20	30	40	50	60	70	80	90	100
TT6	1016	608	382	290	191	187	96	94	95	94	93	92	92	92	92	92	92	92	92
TT7	1292	614	237	242	144	143	145	143	144	139	138	92	93	92	93	92	92	92	92
TT8	1383	704	193	150	139	141	97	48	47	47	46	46	47	46	46	46	46	46	46
TT9	924	428	286	235	240	234	237	234	231	187	92	92	92	92	92	93	92	92	92
TT10	1199	420	338	243	239	144	141	139	141	95	93	92	92	92	92	93	92	92	92
average	1163	555	287	232	191	170	143	132	132	112	92.4	82.8	83.2	82.8	83	83.2	82.8	82.8	82.8

Table 6.9: 1% values of case 25, leg 2

case 23	iteration																		
(leg 3)	1	2	3	4	5	6	7	8	9	10	20	30	40	50	60	70	80	90	100
TT1	1659	1017	560	518	329	187	98	98	53	54	47	46	2	2	2	0	0	0	0
TT2	1292	838	658	521	426	284	284	145	144	96	1	4	0	2	0	0	0	0	0
TT3	1567	883	653	606	467	375	327	242	194	147	51	6	1	1	1	0	0	0	0
TT4	1336	1064	746	473	287	280	281	236	189	187	7	6	0	3	1	0	0	0	0
TT5	1474	884	694	468	330	283	243	154	152	150	7	3	3	5	2	1	0	0	0
average	1466	937	662	517	368	282	247	175	146	127	22.6	13	1.2	2.6	1.2	0.2	0	0	0

Table 6.10: 1% values of case 23, leg 3

case 25	iteration																		
(leg 3)	1	2	3	4	5	6	7	8	9	10	20	30	40	50	60	70	80	90	100
TT6	1243	608	375	285	100	96	51	51	51	52	48	46	46	46	46	46	46	46	46
TT7	1198	607	335	280	232	187	142	142	141	95	93	47	46	46	46	46	46	47	47
TT8	1566	835	514	286	234	141	97	48	48	49	1	1	1	1	1	1	1	1	1
TT9	1106	836	464	419	278	187	184	140	139	93	47	46	46	46	46	47	46	48	47
TT10	1245	649	426	195	97	97	49	49	48	48	1	0	0	0	1	0	0	0	0
average	1272	707	423	293	188	142	105	86	85.4	67.4	38	28	27.8	27.8	28	28	27.8	28.4	28.2

Table 6.11: 1% values of case 25, leg 3

Also for the *TT* trials it was considered useful to have a better idea of the positions of the 1% values and of the row maximum; in a way similar to what has been done in the previous section, here below are reported a schematic representation of the pheromone matrices at iterations 1, 2, 3, 4, 10, 20, 60, 100 (going left-right, up-down) with the 1% and maximum values indicated in orange; the first set of

images are relatives to the trial $TT3$, the second set is relative to the trial $TT6$ both representing the leg number 3, considered the most interesting to analyse.

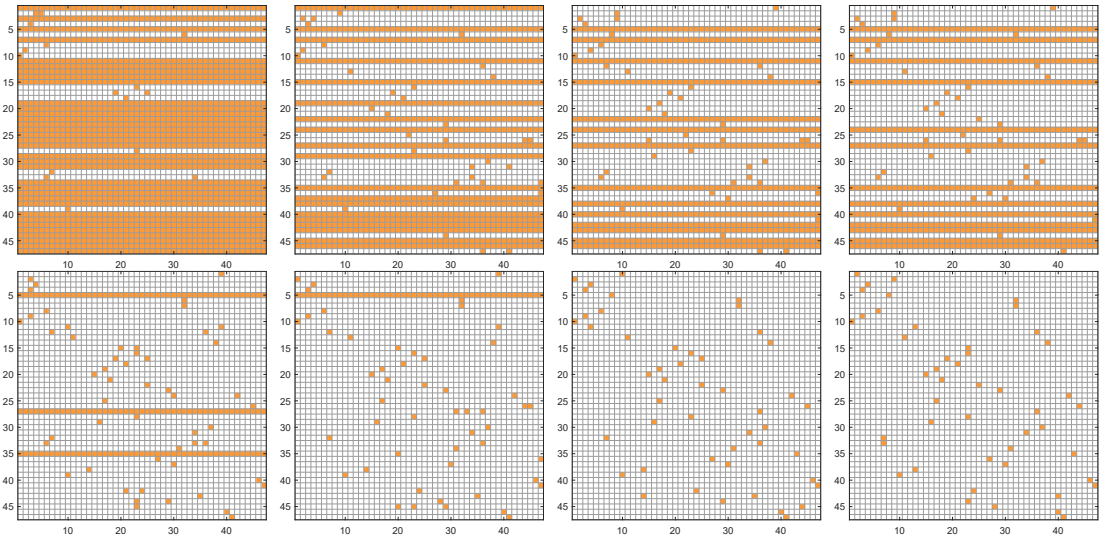

Figure 6.21: 1% values positions in trial $TT3$, leg 3

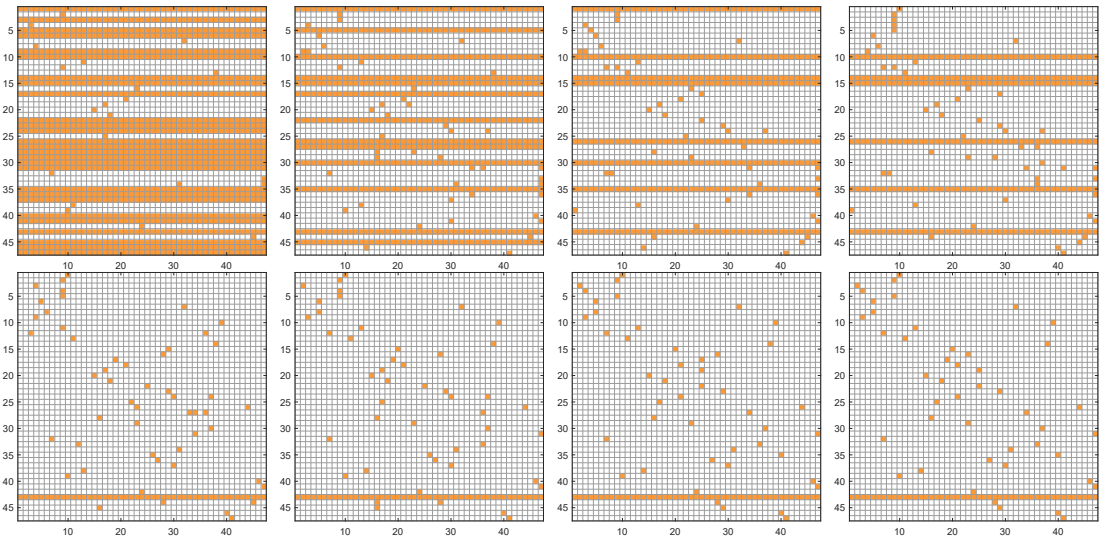

Figure 6.22: 1% values positions in trial $TT6$, leg 3

The tables show an interesting behaviour: excluding the leg 1 that can be considered a particular case, in the leg 2 and 3 during the first iterations the case 23 presents a higher number of 1% values while, during the last iterations, it is the case 25 that has more 1% values whose number remains nearly constant until the

end; the same tendency is evident comparing the figures 6.21 and 6.22: at first, the $TT3$ trial has more orange entries but, during the last tens of iterations, the $TT6$ trial, differently from the $TT3$ one, keeps having an orange line. This behaviour can probably be explained by the higher value of the evaporation coefficient in the case 25: during the last tens of iterations the pheromone levels of not chosen debris is too low to be compared to the levels of other debris, making them nearly impossible to be chosen and subjected only to the evaporation effect (this explains the nearly constant number of 1% values during the last phases of the path construction); the orange line that can be seen until the last iteration, indeed, is relative to a debris that has nearly never been chosen during the search process. On the other hand the case 23, with this kind of pheromone matrix, presents a nearly ideal trend: it starts from a very explorative phase ending to choose the most favourable tour; this can be seen in the reduction of the number of 1% values but, even in a clearer way, from figure 6.21: from an all orange matrix, at the end there is not even a single orange line, meaning that all the debris pieces have been chosen during the tour construction process; this is a result that could have been achieved thanks to the right value of the evaporation coefficient.

Comparing the results here obtained with the ones of T trials, it is possible to immediately see a basic difference: the number of 1% values during the firsts iterations is much higher for TT trials (or, equivalently, the schematic representation of the pheromone matrix is much more orange); this is a natural consequence of the higher specificity of the pheromone matrix for TT trials that, being related to a single leg, in the firsts phases can not see a great difference in the pheromone levels, since the artificial ants can not explore all the debris yet and so, many debris objects are subjected only to the evaporation effect (leading to several orange lines). However, this characteristic is inherently beneficial because the debris bodies have a more similar pheromone level and so the exploration of new paths is favoured; this great explorative level is confirmed also by the considerable reduction of the number of orange lines for TT trials.

6.2 Analysis of α

After having deeply analysed and understood the influence of the general parameters on the algorithm behaviour, it remains to study one of the most important parameters whose setting determines the quality of the solution obtained: α. It appears in the probabilistic choice rule (4.1) that is applied at every step by the artificial agents and it determines the importance of the heuristic information in choosing the next debris (for this specific problem, it determines how much importance to give to the ΔV cost of a transfer). All the cases presented until here were characterised by $\alpha = 4$ but to better understand the role of this parameter and to see if there could be a better value, an analysis using different α values was conducted.

At first, it was chosen to vary α (also changing some other parameters) in an interval between 2 to 5 as suggested by the literature [18]. Below are reported the results obtained running the algorithm for 50 repetitions and 100 iterations, in terms of numeric values: the first line reports the parameters configuration adopted, *min*, *aver* and *avg* have the same meaning of table 6.1; the last lines indicate the case with the minimum value of *min* and the one with the minimum value of *avg*; the red case numbers indicate the results that are reported in the graphs below the table. The orange line of the graphs is relative to the average cost, the blue line is relative to the minimum cost.

alpha	beta	el	dt	e	min [m/s]	aver [m/s]	avg [m/s]	case
1	1	0.98	0.01	0.05	2.3945E+04	4.5553E+04	2.8812E+04	A1
1	1	0.98	0.006	0.05	2.2873E+04	4.8859E+04	3.1126E+04	A2
2	1	0.98	0.01	0.05	1.6013E+04	2.4435E+04	2.1310E+04	A3
2	1	0.98	0.01	0.1	1.5643E+04	2.3028E+04	2.0921E+04	A4
2	1	0.99	0.007	0.05	1.5527E+04	2.5764E+04	2.1009E+04	A5
2	1	0.5	0.01	0.1	1.9179E+04	3.3079E+04	2.3167E+04	A6
3	1	0.98	0.01	0.05	1.5115E+04	2.0819E+04	1.9398E+04	A7
5	1	0.98	0.01	0.05	1.5039E+04	1.9824E+04	1.8452E+04	A8
5	1	0.99	0.007	0.05	1.4248E+04	1.9098E+04	1.7975E+04	A9
minimum min								
5	1	0.99	0.007	0.05	1.4248E+04	1.9098E+04	1.7975E+04	A9
minimum avg								
5	1	0.99	0.007	0.05	1.4248E+04	1.9098E+04	1.7975E+04	A9

Table 6.12: Results of the constant α analysis

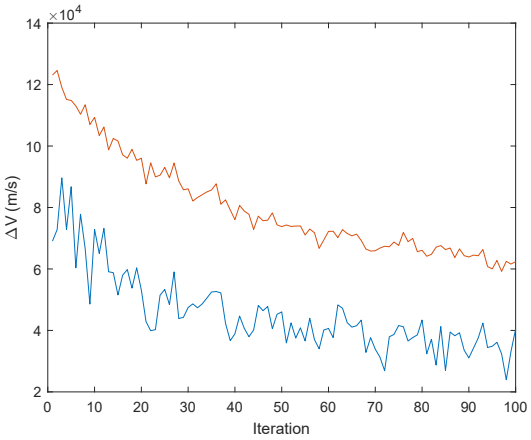

Figure 6.23: Case A1

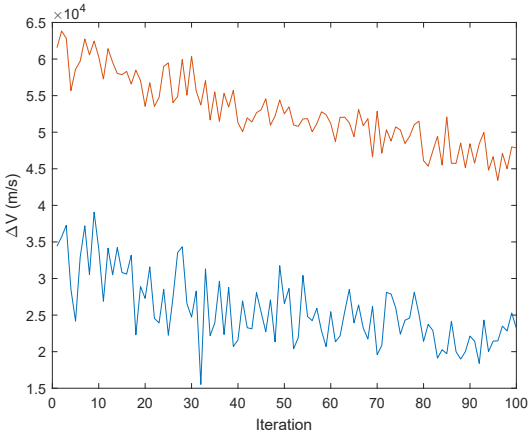

Figure 6.24: Case A5

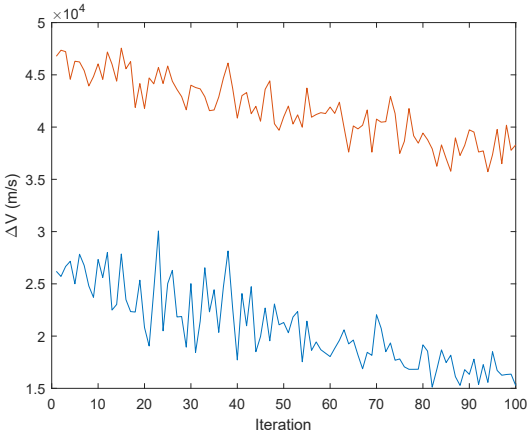

Figure 6.25: Case A7

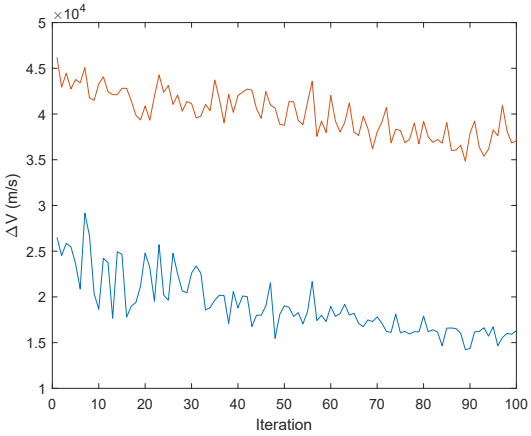

Figure 6.26: Case A9

With low values of α the numerical values obtained are pretty high because a lower importance is given to the heuristic information (and so to the cost of the tour) and the pheromone trace overcomes in the choice for the next debris; it is also true that this configuration is characterized by a good trend of the solutions over the iterations: as it can be seen in figure 6.23, since the pheromone plays an essential role, at first the search is highly explorative being the pheromone level still pretty low; with the progress of the iterations the pheromone left by the ants increases and the solution improves. In the case of an average α value (like cases $A5$ and $A7$) the numerical results improve since the heuristic information starts playing a more important role but, at the same time, the reduction of the solution values is less emphasised because the less expensive path has a higher probability of being chosen already since the start of the tour construction (figures 6.24 and 6.25). Finally, high α values ensure a shorter path because the heuristic information has a higher influence than the pheromone trails on ants choice; a negative aspect is that the solution

during the iterations remains nearly the same, presenting only a slight reduction because the acquired knowledge, given by the pheromone, has a too low importance.

Given the good results obtained, it was decided to try giving the heuristic information a dynamic importance; this could have been achieved adopting an α value that changed during the iterations. The first trials were done adopting a first value for a fixed number of iterations and changing it for the remaining iterations; the results obtained are reported in the table below indicating the first and the second value that α assumes (respectively $alpha1$ and $alpha2$) and the number of iterations for which that value is adopted (after the underscore): for example, the first case adopts $\alpha = 2$ for the first 50 iterations and then, $\alpha = 4$ for the remaining 50 iterations. The columns report the same kind of results of the table 6.12 and also in this case the most interesting configurations are represented graphically, below the table.

alpha1	alpha2	beta	el	dt	e	min [m/s]	aver [m/s]	avg [m/s]	case
2_50	4_50	1	0.98	0.01	0.05	1.5696E+04	2.3878E+04	1.9376E+04	A10
2_60	4_40	1	0.98	0.01	0.05	1.5329E+04	2.3246E+04	1.9704E+04	A11
2_80	4_20	1	0.98	0.01	0.05	1.6107E+04	2.6897E+04	1.9912E+04	A12
2_40	4_60	1	0.98	0.01	0.05	1.4859E+04	2.4082E+04	1.9449E+04	A13
2_20	4_80	1	0.98	0.01	0.05	1.4817E+04	2.1809E+04	1.8964E+04	A14
4_50	2_50	1	0.98	0.01	0.05	1.6466E+04	2.3238E+04	1.9379E+04	A15
4_60	2_40	1	0.98	0.01	0.05	1.5126E+04	2.0073E+04	1.9527E+04	A16
4_80	2_20	1	0.98	0.01	0.05	1.5492E+04	2.2410E+04	1.8893E+04	A17
4_40	2_60	1	0.98	0.01	0.05	1.5700E+04	2.1528E+04	1.9484E+04	A18
1_50	4_50	1	0.98	0.01	0.05	1.5530E+04	3.3947E+04	1.9199E+04	A19
1_60	4_40	1	0.98	0.01	0.05	1.7062E+04	3.8695E+04	2.0218E+04	A20
1_80	4_20	1	0.98	0.01	0.05	1.7276E+04	4.1624E+04	2.1797E+04	A21
1_40	4_60	1	0.98	0.01	0.05	1.6129E+04	3.3299E+04	1.9801E+04	A22
4_50	1_50	1	0.98	0.01	0.05	1.6499E+04	2.8762E+04	1.9706E+04	A23
4_60	1_40	1	0.98	0.01	0.05	1.4167E+04	2.3714E+04	1.9044E+04	A24
4_80	1_20	1	0.98	0.01	0.05	1.6423E+04	2.2132E+04	1.9336E+04	A25
4_40	1_60	1	0.98	0.01	0.05	1.6501E+04	2.8593E+04	1.9858E+04	A26
minimum min									
4_60	1_40	1	0.98	0.01	0.05	1.4167E+04	2.3714E+04	1.9044E+04	A24
minimum avg									
4_80	2_20	1	0.98	0.01	0.05	1.5492E+04	2.2410E+04	1.8893E+04	A17

Table 6.13: Results of the discretely variable α analysis

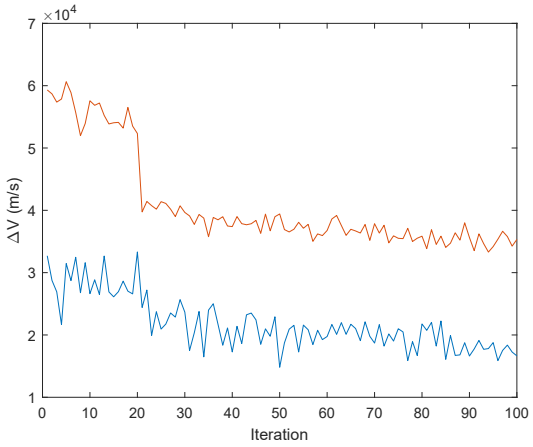

Figure 6.27: Case A14

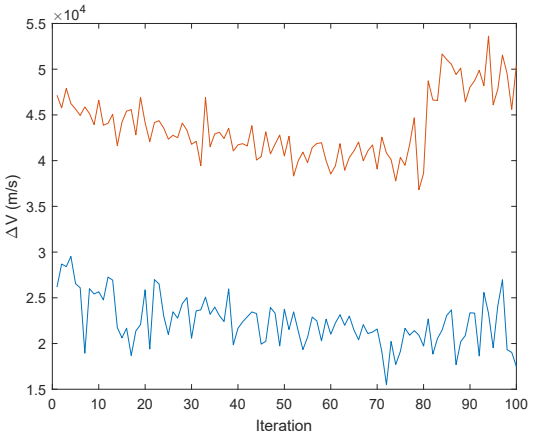

Figure 6.28: Case A17

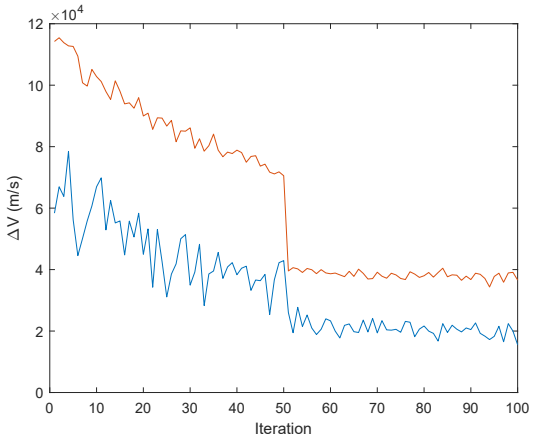

Figure 6.29: Case A19

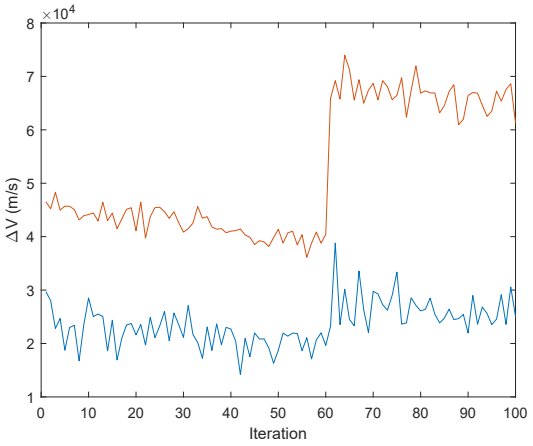

Figure 6.30: Case A24

The results obtained are pretty good in terms of numerical values with case $A24$ and $A14$ being the best ones; a peculiar aspect that can be immediately seen from the graphs is that the point of transition from a value of α to another one is characterized by an evident difference in the results trend, particularly for the average value. It is a behaviour typical of all the trials considered, indicating a transition from less greedy choices to choices based on the cost of the total tour; in particular, the change happens following this order in the case of a growing α value: after the discontinuity, the cost of the tour becomes more important leading to a preference for less expensive transfers and so to a reduced total cost. When the α is lower, during the first phases, the path is more random depending on the tour followed by the other ants and presenting a slower reduction in the total cost. In general, it is possible to say that cases with an increasing α value are characterized by better results.

The last possibility explored was chosen in order to avoid a discontinuity in the average results value and adopted a continuously variable α; in particular, it was decided to adopt an α that changed every single iteration making the influence of the heuristic information really dynamic. The first column ($alpha1$) indicates the α value used at the first iteration, the second column ($alpha2$) contains the α value assumed at the last iteration; below the table, the red numbers cases get a graphical representation.

alpha1	alpha2	beta	el	dt	e	min [m/s]	aver [m/s]	avg [m/s]	case
5	4	1	0.98	0.01	0.05	1.4594E+04	1.9699E+04	1.8520E+04	A27
4	2	1	0.98	0.01	0.05	1.5392E+04	2.1260E+04	1.9272E+04	A28
4	1	1	0.98	0.01	0.05	1.5439E+04	2.5135E+04	2.0178E+04	A29
1	4	1	0.98	0.01	0.05	1.6123E+04	2.9769E+04	2.0204E+04	A30
2	4	1	0.98	0.01	0.05	1.6101E+04	2.2025E+04	1.9663E+04	A31
4	5	1	0.98	0.01	0.05	1.5927E+04	2.0565E+04	1.9387E+04	A32
minimum min									
5	4	1	0.98	0.01	0.05	1.4594E+04	1.9699E+04	1.8520E+04	27
minimum avg									
5	4	1	0.98	0.01	0.05	1.4594E+04	1.9699E+04	1.8520E+04	A27

Table 6.14: Results of the continuously variable α analysis

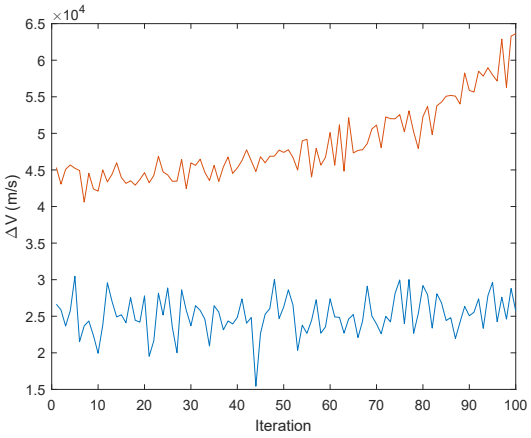

Figure 6.31: Case A29

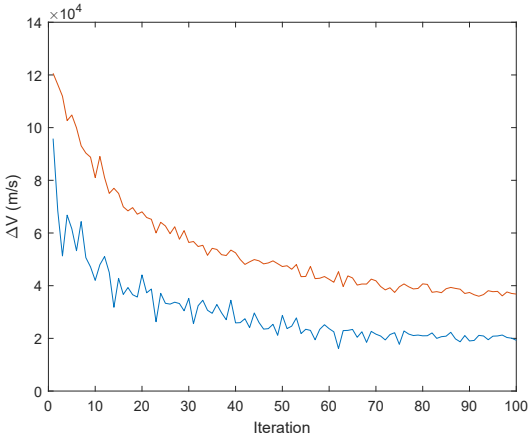

Figure 6.32: Case A30

The numerical results are similar to the discretely variable α trials but in this case the graphical trends are better; also in this case, an increasing α seems to be the best choice making possible to obtain a nearly ideal results trend (as it can be seen in figure 6.32). An important aspect that needs to be noticed, however, is the tendency of the results to start from high values that can be explained by the

initial low values of α (meaning a lower importance given to the total path length).

In conclusion, it is possible to say that choosing a variable α can offer some advantages, in particular for the solution trend; the results obtained are slightly worse than the cases with a fixed α, however, the best configuration possible (with a variable α) would be the continuously increasing α.

6.3 Analysis of β

The last parameter that needs to be examined is β; even this one, as α, appears in the probabilistic choice rule (4.1) but β indicates the importance that the pheromone trails assumes when an artificial ant has to choose the next debris to move to. It is essential that α and β assume values having the right proportion in order to give the correct importance to the heuristic and pheromone information and to avoid having an imbalanced algorithm. At first, several values of β (combined with the variation of some other parameters) were tried in order to understand how it affects the algorithm behaviour; the numerical results of the 50 repetitions and 100 iterations are reported in the table below, having the same structure of the previous ones. Also for this analysis the red numbered cases are represented on the graphs below the table.

alpha	beta	el	dt	e	min [m/s]	aver [m/s]	avg [m/s]	case
4	2	0.98	0.01	0.05	1.6256E+04	1.9714E+04	1.9594E+04	B1
4	4	0.98	0.01	0.05	1.7545E+04	1.7820E+04	2.0960E+04	B2
1	2	0.98	0.0005	0.05	2.2372E+04	5.3028E+04	2.9697E+04	B3
1	2	0.98	0.001	0.05	2.0956E+04	5.0898E+04	2.8674E+04	B4
1	2	0.98	0.01	0.05	2.1702E+04	3.4750E+04	2.8555E+04	B5
2	2	0.99	0.007	0.05	1.8207E+04	2.2460E+04	2.2632E+04	B6
2	2	0.98	0.01	0.05	1.6803E+04	1.9733E+04	2.2874E+04	B7
2	2	0.98	0.1	0.05	2.0502E+04	2.1124E+04	2.6189E+04	B8
minimum min								
4	2	0.98	0.01	0.05	1.6256E+04	1.9714E+04	1.9594E+04	B1
minimum avg								
4	2	0.98	0.01	0.05	1.6256E+04	1.9714E+04	1.9594E+04	B1

Table 6.15: Results of the constant β analysis

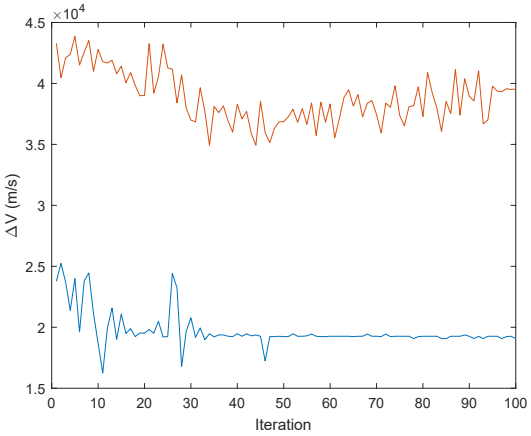

Figure 6.33: Case B1

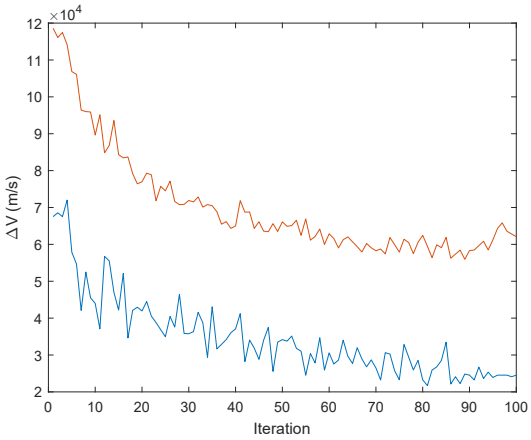

Figure 6.34: Case B5

It is possible to see that the numerical results are not really good, in particular for cases with a β greater than α: this means that the pheromone information has the precedence over the path cost in every choice and so it is normal that the total cost is relevant; better results can be obtained with a β smaller than α (like the case $B1$), similar to the basic configuration of $\alpha = 4$ and $\beta = 1$; this makes understand that the heuristic information, in general, needs to have a greater importance to obtain good results. On the other hand, the graphical results of some cases (like case $B5$), even if starting from pretty high costs, present a really good trend with the reduction of the cost with the ongoing iterations.

As already done for α, also for β it was tried to study a dynamic behaviour; it was decided to adopt a discretely variable β assuming one value ($beta1$) for a number of iterations (it is the number after the underscore indicated in the table) and a second value ($beta2$) for the remaining iterations. This time, α was kept equal to 4 for all the cases to focus the study on β; the number of repetitions considered is again 50 and the number of iterations is 100. The numerical results are presented in the below table having the same structure of the previous tables and reporting the same quantities of the already exposed studies; the red numbered cases are also represented graphically below the table.

alpha	beta1	beta2	el	dt	e	min [m/s]	aver [m/s]	avg [m/s]	case
4	1_50	3_50	0.98	0.01	0.05	1.5433E+04	2.0960E+04	1.9361E+04	B9
4	1_60	3_40	0.98	0.01	0.05	1.5832E+04	2.1491E+04	1.9414E+04	B10
4	1_80	3_20	0.98	0.01	0.05	1.4414E+04	1.8125E+04	1.8737E+04	B11
4	1_40	3_60	0.98	0.01	0.05	1.6292E+04	1.9514E+04	1.9255E+04	B12
4	1_20	3_80	0.98	0.01	0.05	1.6174E+04	1.8343E+04	2.0314E+04	B13
4	3_50	1_50	0.98	0.01	0.05	1.5836E+04	1.7870E+04	2.0072E+04	B14
4	3_60	1_40	0.98	0.01	0.05	1.6427E+04	2.0691E+04	2.0014E+04	B15
4	3_80	1_20	0.98	0.01	0.05	1.7355E+04	1.8169E+04	2.0205E+04	B16
4	3_40	1_60	0.98	0.01	0.05	1.3336E+04	1.7868E+04	1.9203E+04	B17
4	3_30	1_70	0.98	0.01	0.05	1.5980E+04	2.1141E+04	1.9383E+04	B18
4	3_20	1_80	0.98	0.01	0.05	1.6193E+04	1.8926E+04	1.8961E+04	B19
minimum min									
4	3_40	1_60	0.98	0.01	0.05	1.3336E+04	1.7868E+04	1.9203E+04	B17
minimum avg									
4	1_80	3_20	0.98	0.01	0.05	1.4414E+04	1.8125E+04	1.8737E+04	B11

Table 6.16: Results of the discretely variable β analysis

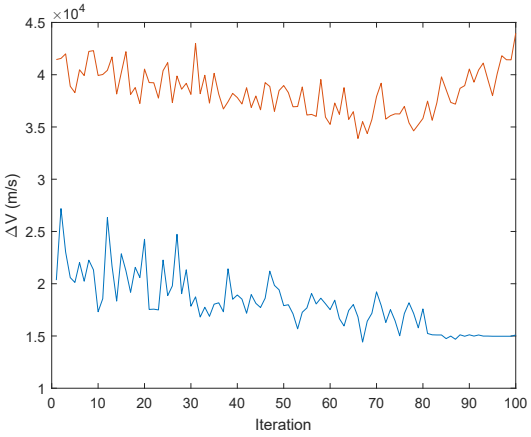

Figure 6.35: Case B11

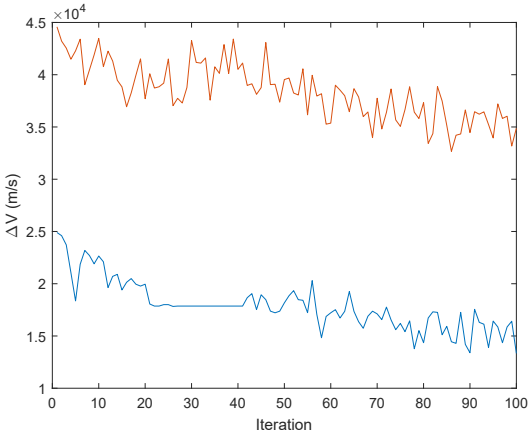

Figure 6.36: Case B17

The numerical results are pretty good, in particular for the case $B17$ presenting an excellent minimum value; however, the same can not be said about the graphs: the iteration at which the β value transition happens is evident and, in general, the trend is not really good, being characterized, in some cases (like case $B11$) even by a growing average value towards the end. In general, it seems to be better adopting a reducing β value (at the opposite of what it is for α) even if the advantages given by a β higher than 1 are not many; it is for this reason that an analysis on a continuously variable β has not been conducted.

6.4 4 launches

After having better understood the influence that each parameter has on the algorithm behaviour and solution quality, at this point is is possible to apply the acquired knowledge to increase the number of debris objecta and missions in order to get a step further towards the complete solution of the GTOC9; this section presents an analysis conducted on a total of 58 debris pieces (the first 58 individuated by the JPL team, indicated in section 5.2) that have to be reached with 4 missions: this means that there is a difference in the problem dimensions (and in the number of artificial ants) but also in the general setup, since now the debris bodies can be reached with 4 missions. The first step was to identify the best parameters configurations that had to be adopted for the extended study and the best cases considered were case 15, 22, 23, 25 (presented in the section 6.1), $A27$, $A30$ (presented in the section 6.2), 23 and 25 (these last two with the modified pheromone matrix that changes at every leg, presented in the subsection 6.1.2); these cases, from here on, will be respectively indicated as $4L\_1$, $4L\_2$, $4L\_3$, $4L\_4$, $4L\_5$, $4L\_6$, $4L\_7$ and $4L\_8$.

The algorithm used is exactly the same of the 47 debris objects and 3 missions with the needed changes; also in this case, the repetitions considered are 50 and the iterations are 100. The results obtained are displayed in the below tables in which the cases are grouped basing on their characteristics; the structure of the tables and the presented quantities (*min*, *aver* and *avg*) are the same of the studies already done. Below the tables, there are the graphs of all the 8 cases presenting the average value (orange line) and the minimum value (blue line) trends during the 100 iterations.

Basic								
alpha	beta	el	dt	e	min [m/s]	aver [m/s]	avg [m/s]	case
4	1	0.992	0.006	0.08	2.1438E+04	2.8524E+04	2.5414E+04	4L_1
4	1	0.995	0.007	0.05	2.1420E+04	2.6422E+04	2.5205E+04	4L_2
4	1	0.99	0.007	0.05	2.2310E+04	2.8408E+04	2.5159E+04	4L_3
4	1	0.99	0.007	0.25	2.3757E+04	3.0531E+04	2.6240E+04	4L_4
minimum min								
4	1	0.995	0.007	0.05	2.1420E+04	2.6422E+04	2.5205E+04	4L_2
minimum avg								
4	1	0.99	0.007	0.05	2.2310E+04	2.8408E+04	2.5159E+04	4L_3

Table 6.17: Results of the basic cases analysis

Variable alpha									
alpha1	alpha2	beta	el	dt	e	min [m/s]	aver [m/s]	avg [m/s]	case
5	4	1	0.98	0.01	0.05	2.1658E+04	3.2236E+04	2.5275E+04	4L_5
1	4	1	0.98	0.01	0.05	2.3040E+04	4.6140E+04	2.7196E+04	4L_6
minimum min									
5	4	1	0.98	0.01	0.05	2.1658E+04	3.2236E+04	2.5275E+04	4L_5
minimum avg									
5	4	1	0.98	0.01	0.05	2.1658E+04	3.2236E+04	2.5275E+04	4L_5

Table 6.18: Results of the variable α cases analysis

tt that varies with leg								
alpha	beta	el	dt	e	min [m/s]	aver [m/s]	avg [m/s]	case
4	1	0.99	0.007	0.05	1.8807E+04	2.5981E+04	2.4574E+04	4L_7
4	1	0.99	0.007	0.25	2.1823E+04	2.5523E+04	2.6936E+04	4L_8
minimum min								
4	1	0.99	0.007	0.05	1.8807E+04	2.5981E+04	2.4574E+04	4L_7
minimum avg								
4	1	0.99	0.007	0.05	1.8807E+04	2.5981E+04	2.4574E+04	4L_7

Table 6.19: Results of the modified tt cases analysis

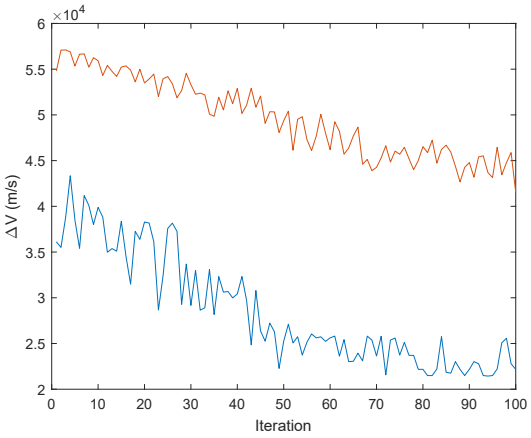

Figure 6.37: Case $4L\_1$

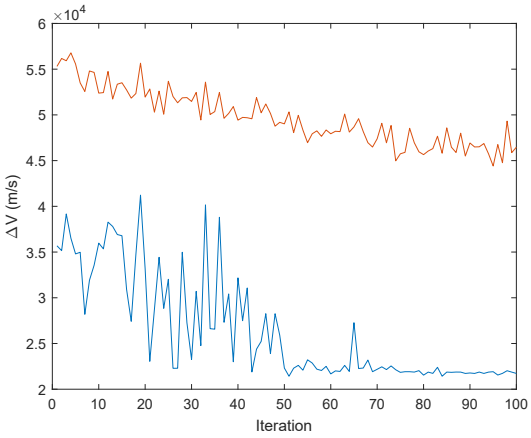

Figure 6.38: Case $4L\_2$

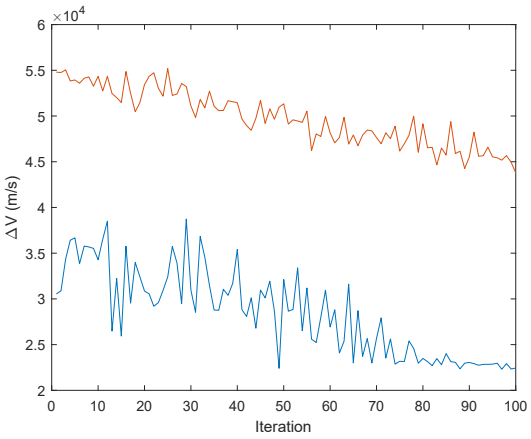

Figure 6.39: Case 4*L*_3

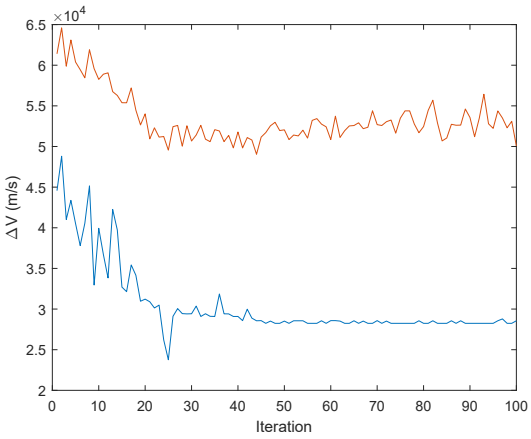

Figure 6.40: Case 4*L*_4

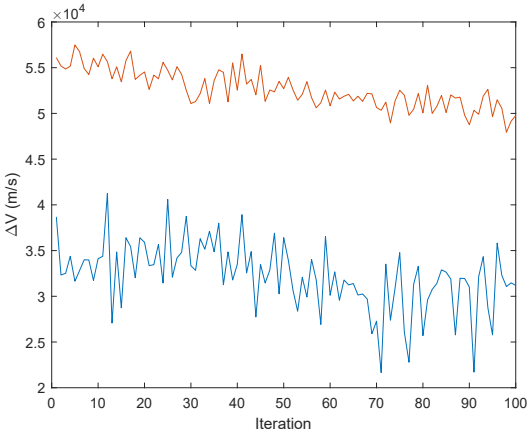

Figure 6.41: Case 4*L*_5

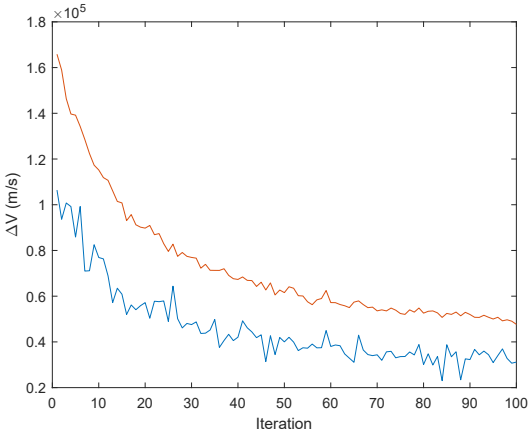

Figure 6.42: Case 4*L*_6

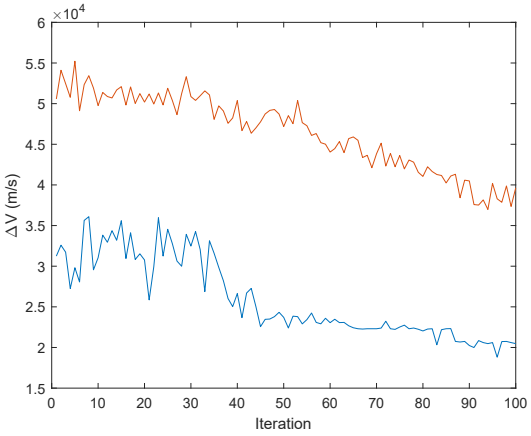

Figure 6.43: Case 4*L*_7

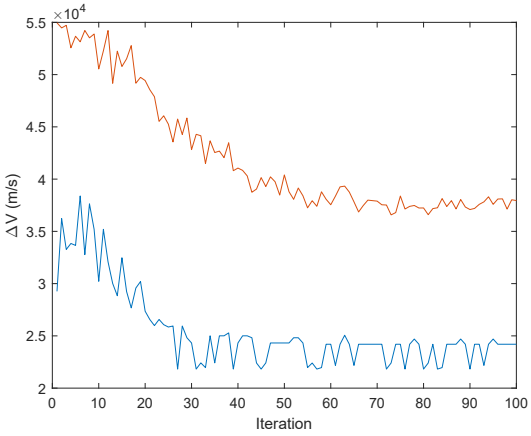

Figure 6.44: Case 4*L*_8

Before making any consideration on the obtained results, it is useful to know that the JPL solution for 4 missions calculated with this algorithm is of $1.3651E+04$ m/s; the results obtained are pretty good, particularly for the case $4L\_7$ in which the minimum value gets pretty near to the JPL's one. Nearly all the graphs, but in particular the ones of cases $4L\_6$ and $4L\_8$, present a good trend with the results values that, after a first phase being higher, then they decrease smoothly. These results, if compared with the equivalent cases for the 3 missions algorithm, are characterized by better values; the minimum value of the best case of the 4 missions algorithm ($4L\_7$), indeed, constitutes an increase of the JPL solution of only the 27%, while the best solution for the 3 missions (case 22) constitutes an increase of nearly the 29%. This can have two different possible explanations: the first one is that the ants, having the possibility to choose between a larger number of debris, in the 4 missions algorithm perform better since there are new paths with a possible lower cost; the second one can be related to the number of ants that, in the case of 58 debris, increases, making the pheromone trace evolution more dynamic and the exploration of new tours more probable.

The final analysis conducted had the intention to further reduce the costs obtained for the 4 missions using again the same ACO algorithm; indeed, it often happens that applying the same metaheuristic again to the single parts of an overall solution, it is possible to further optimize the problem solution itself. As said, the ACO algorithm used was the same with the only difference of being repeated for 100 repetitions and 100 iterations and of being applied to the single 4 missions. Another important variation was made in the time interval between the missions: until here, it was always considered a fixed time of 30 days between the end of one mission and the beginning of the next one; in this case, the time between the missions was imposed in order to obtain a total program duration that was as near as possible to the one proposed by the JPL. In particular, 30 days are considered between the first and the second mission, 35 days between the second and the third one and 75 days between the third and the fourth mission. The results of this optimization are presented in the following tables each one indicating the reference case and, for each mission: the debris pieces sequence obtained applying the algorithm to all the 58 debris (*sequence_base*), the debris pieces sequence after the optimization of the single mission (*sequence_opt*, these two sequences report the debris bodies id of the *.txt* file of the GTOC9 reported in C), the optimized sequence (*sequence_grow*) indicating the debris objects of the global optimization as a growing scale (1, 2, 3, ... to give a more immediate idea of the sequence changes), the intervals of time between two successive rendezvous before and after the local optimization (*slotl* is an algorithm variable that, if multiplied by 5, indicates the days between two successive debris objects plus 5 days of rendezvous with the first debris) and the single mission cost before and after the optimization with the reduction expressed

as a percentage. At the end of each mission table there is the cost of all the program before and after the local optimization and the reduction expressed as a percentage.

Case 4L_1				
alpha	**beta**	**el**	**dt**	**e**
4	1	0.992	0.006	0.08

mission 1	**sequence_base**	97	87	114	22	38	95	23	50	121	117									
	sequence_opt	97	87	114	22	38	95	23	50	121	117									
	sequence_grow	1	2	3	4	5	6	7	8	9	10									
	slotl_base	5	5	1	6	6	6	1	3	6										
	slotl_optimized	6	6	2	6	6	2	6	3	2										
	cost_base	2804.37										**reduction**					13.88%			
	cost_optimized	2415.16																		
mission 2	**sequence_base**	20	27	25	79	113	55	57	3	29	64	90	28	66	73	10	69	61	107	
	sequence_opt	20	27	25	79	113	55	57	3	29	64	28	73	10	66	69	107	61	90	
	sequence_grow	1	2	3	4	5	6	7	8	9	10	12	14	15	13	16	18	17	11	
	slotl_base	6	2	2	4	3	6	6	6	3	5	2	3	3	5	4	4	6		
	slotl_optimized	3	3	6	5	6	6	6	4	5	6	3	2	2	2	3	5	3		
	cost_base	6161.03										**reduction**					11.65%			
	cost_optimized	5443.49																		
mission 3	**sequence_base**	65	31	71	43	72	19	8	4	115	77	102								
	sequence_opt	31	65	71	43	72	19	8	4	115	77	102								
	sequence_grow	2	1	3	4	5	6	7	8	9	10	11								
	slotl_base	4	5	3	6	6	4	6	6	4	6									
	slotl_optimized	3	6	5	3	6	4	5	6	6	6									
	cost_base	4999.42										**reduction**					13.44%			
	cost_optimized	4327.30																		
mission 4	**sequence_base**	32	2	26	11	47	119	85	108	104	24	37	63	112	75	45	82	41	35	7
	sequence_opt	2	32	26	11	47	85	119	104	24	108	37	63	112	75	45	35	41	82	7
	sequence_grow	2	1	3	4	5	7	6	9	10	8	11	12	13	14	15	18	17	16	19
	slotl_base	6	6	2	5	6	4	5	5	5	6	6	6	1	1	4	1	4	5	
	slotl_optimized	6	6	5	5	5	6	3	3	6	2	3	1	5	6	2	5	3	6	
	cost_base	7473.52										**reduction**					12.80%			
	cost_optimized	6516.83																		
TOT	**cost_base**	21438.35										**reduction**					12.76%			
	cost_optimized	18702.78																		

Table 6.20: Optimization of case $4L\_1$

Case 4L_2				
alpha	**beta**	**el**	**dt**	**e**
4	1	0.995	0.007	0.05

mission 1	**sequence_base**	107	61	115	7	63	19	82	45	41	11	85										
	sequence_opt	115	7	63	19	82	45	41	11	61	107	85										
	sequence_grow	3	4	5	6	7	8	9	10	2	1	11										
	slotl_base	2	4	3	6	2	3	2	6	6	2											
	slotl_optimized	6	4	5	6	4	4	1	2	2	2											
	cost_base	2789.16							**reduction**							29.62%						
	cost_optimized	1962.95																				
mission 2	**sequence_base**	38	97	35	117	23	121	20	27	25	50	79	95	113	55	87	57	29	90	73	10	31
	sequence_opt	97	38	23	117	121	20	27	50	25	35	79	95	113	55	87	57	29	90	73	10	31
	sequence_grow	2	1	5	4	6	7	8	10	9	3	11	12	13	14	15	16	17	18	19	20	21
	slotl_base	6	6	2	6	6	2	6	5	6	6	5	3	3	6	6	4	6	4	6	3	
	slotl_optimized	3	6	2	6	5	5	6	5	5	6	4	6	6	5	6	5	6	1	5	4	
	cost_base	7880.56							**reduction**							12.75%						
	cost_optimized	6875.60																				
mission 3	**sequence_base**	71	65	66	43	28	69	4	8	64	102	72	77									
	sequence_opt	69	71	28	43	65	8	4	66	64	102	72	77									
	sequence_grow	6	1	5	4	2	8	7	3	9	10	11	12									
	slotl_base	3	3	3	6	6	2	4	5	4	4	4										
	slotl_optimized	3	3	6	3	5	2	6	5	1	6	4										
	cost_base	4723.06							**reduction**							8.73%						
	cost_optimized	4310.79																				
mission 4	**sequence_base**	114	2	26	32	47	22	119	104	108	24	37	112	75	3							
	sequence_opt	2	114	26	47	32	104	119	24	108	37	112	22	75	3							
	sequence_grow	2	1	3	5	4	8	7	10	9	11	12	6	13	14							
	slotl_base	6	5	4	5	5	4	2	6	2	6	5	5	5								
	slotl_optimized	6	4	5	3	6	6	2	4	4	6	6	3	5								
	cost_base	6027.08							**reduction**							18.79%						
	cost_optimized	4894.83																				
TOT	**cost_base**	21419.86							**reduction**							15.76%						
	cost_optimized	18044.17																				

Table 6.21: Optimization of case $4L\_2$

Case 4L_3				
alpha	**beta**	**el**	**dt**	**e**
4	1	0.99	0.007	0.05

mission 1	**sequence_base**	79	113	55	121	117	25	20	27	57	50	95	87	23	35	97	38
	sequence_opt	27	20	117	25	79	55	113	57	50	95	87	121	23	35	97	38
	sequence_grow	8	7	5	6	1	3	2	9	10	11	12	4	13	14	15	16
	slotl_base	6	6	6	4	4	6	3	1	6	4	5	5	2	5	1	
	slotl_optimized	5	6	3	6	1	4	4	6	4	4	3	5	6	6	1	
	cost_base	5221.61						**reduction**					18.72%				
	cost_optimized	4243.95															
mission 2	**sequence_base**	29	64	90	28	66	73	10	69	61	107	3	65	31			
	sequence_opt	29	64	90	28	66	73	10	61	107	3	69	65	31			
	sequence_grow	1	2	3	4	5	6	7	9	10	11	8	12	13			
	slotl_base	6	5	3	6	6	6	1	6	6	5	4	4				
	slotl_optimized	6	6	6	4	5	6	6	2	4	3	6	4				
	cost_base	2744.28						**reduction**					20.79%				
	cost_optimized	2173.70															
mission 3	**sequence_base**	71	43	72	19	8	4	115	77	102	112	7	41	82			
	sequence_opt	71	43	72	8	19	4	115	77	102	112	7	41	82			
	sequence_grow	1	2	3	5	4	6	7	8	9	10	11	12	13			
	slotl_base	2	4	6	1	3	6	6	6	3	6	3	4				
	slotl_optimized	6	6	3	2	2	6	4	2	5	6	5	3				
	cost_base	6945.00						**reduction**					8.87%				
	cost_optimized	6329.07															
mission 4	**sequence_base**	11	26	2	114	32	47	85	119	104	108	24	37	22	63	75	45
	sequence_opt	2	114	26	11	32	47	85	104	119	24	108	37	63	22	75	45
	sequence_grow	3	4	2	1	5	6	7	9	8	11	10	12	14	13	15	16
	slotl_base	6	2	6	6	3	4	6	1	2	6	4	4	5	6	4	
	slotl_optimized	6	6	3	2	3	6	4	3	4	4	1	5	6	6	6	
	cost_base	7398.90						**reduction**					21.36%				
	cost_optimized	5818.26															
TOT	**cost_base**	22309.79						**reduction**					16.79%				
	cost_optimized	18564.98															

Table 6.22: Optimization of case $4L\_3$

Case 4L_4				
alpha	**beta**	**el**	**dt**	**e**
4	1	0.99	0.007	0.25

mission 1	**sequence_base**	2	26	47	85	11	41	45	19	115	82	71	43									
	sequence_opt	2	26	47	85	11	41	19	45	82	115	71	43									
	sequence_grow	1	2	3	4	5	6	8	7	10	9	11	12									
	slotl_base	4	6	6	3	6	6	4	6	6	3	4										
	slotl_optimized	6	6	6	6	2	4	3	6	5	6	4										
	cost_base	3470.59						**reduction**							17.81%							
	cost_optimized	2852.55																				
mission 2	**sequence_base**	38	117	23	121	97	20	27	25	50	79	113	95	35	55	57	29	87	61	107	31	
	sequence_opt	38	97	117	23	121	20	27	25	50	79	35	95	113	55	87	29	61	107	57	31	
	sequence_grow	1	5	2	3	4	6	7	8	9	10	13	12	11	14	17	16	18	19	15	20	
	slotl_base	6	6	5	2	4	5	3	5	5	3	1	5	4	6	5	2	5	6	6		
	slotl_optimized	2	2	5	5	3	1	6	5	6	5	4	3	6	6	5	6	3	6	5		
	cost_base	7960.78						**reduction**							14.15%							
	cost_optimized	6834.45																				
mission 3	**sequence_base**	65	28	69	66	4	8	10	73	90	102											
	sequence_opt	66	69	28	65	8	4	73	10	90	102											
	sequence_grow	4	3	2	1	6	5	8	7	9	10											
	slotl_base	4	5	6	6	6	6	4	6	5												
	slotl_optimized	6	6	2	6	6	4	6	6	6												
	cost_base	2421.54						**reduction**							21.66%							
	cost_optimized	1897.02																				
mission 4	**sequence_base**	77	64	72	3	7	112	75	63	22	37	108	24	119	104	32	114					
	sequence_opt	77	64	72	3	7	75	22	63	112	119	24	108	37	104	32	114					
	sequence_grow	1	2	3	4	5	7	9	8	6	13	12	11	10	14	15	16					
	slotl_base	5	5	2	6	1	4	6	3	3	3	3	4	1	4	1						
	slotl_optimized	6	6	6	1	5	3	2	4	4	3	2	1	4	2	2						
	cost_base	9904.18						**reduction**							21.44%							
	cost_optimized	7781.18																				
TOT	**cost_base**	23757.09						**reduction**							18.49%							
	cost_optimized	19365.20																				

Table 6.23: Optimization of case $4L\_4$

Case 4L_5					
alpha 1	**alpha 2**	**beta**	**el**	**dt**	**e**
5	4	1	0.98	0.01	0.05

mission 1	**sequence_base**	19	7	63	115	107	61	82	45	11	41	85	47	26	2	71			
	sequence_opt	63	7	115	107	61	19	82	45	11	41	85	47	26	71	2			
	sequence_grow	3	2	4	5	6	1	7	8	9	10	11	12	13	15	14			
	slotl_base	6	4	4	5	4	4	5	6	5	4	1	3	4	6				
	slotl_optimized	4	6	3	4	5	3	5	6	5	6	6	6	1	1				
	cost_base	3050.17						**reduction**						23.28%					
	cost_optimized	2340.09																	
mission 2	**sequence_base**	38	117	23	121	97	20	27	25	50	79	113	95	35	55	29	87	57	31
	sequence_opt	117	38	23	121	97	20	27	25	50	79	95	113	35	55	29	87	57	31
	sequence_grow	2	1	3	4	5	6	7	8	9	10	12	11	13	14	15	16	17	18
	slotl_base	6	6	2	5	5	4	6	2	1	5	3	4	6	6	5	4	1	
	slotl_optimized	2	5	4	2	1	3	5	6	6	5	2	6	6	5	5	6	2	
	cost_base	7409.75						**reduction**						11.34%					
	cost_optimized	6569.55																	
mission 3	**sequence_base**	65	66	43	28	69	90	8	4	73	10	102							
	sequence_opt	66	65	69	28	43	90	4	8	73	10	102							
	sequence_grow	2	1	5	4	3	6	8	7	9	10	11							
	slotl_base	5	6	5	6	6	6	3	6	5	5								
	slotl_optimized	3	6	5	6	3	6	6	6	6	6								
	cost_base	2369.06						**reduction**						24.56%					
	cost_optimized	1787.21																	
mission 4	**sequence_base**	77	64	72	3	75	112	22	37	108	24	119	104	32	114				
	sequence_opt	77	64	72	3	75	112	22	119	24	108	37	104	32	114				
	sequence_grow	1	2	3	4	5	6	7	11	10	9	8	12	13	14				
	slotl_base	6	6	4	5	6	4	4	4	2	6	2	1	2					
	slotl_optimized	2	5	6	6	5	4	4	3	2	3	2	6	4					
	cost_base	8828.60						**reduction**						23.00%					
	cost_optimized	6798.19																	
TOT	**cost_base**	21657.58						**reduction**						19.22%					
	cost_optimized	17495.03																	

Table 6.24: Optimization of case $4L\_5$

Case 4L_6						
alpha 1	**alpha2**	**beta**	**el**	**dt**	**e**
1	4	1	0.98	0.01	0.05

mission 1	**sequence_base**	19	7	63	115	107	61	45	11	41	85	47	26	2							
	sequence_opt	63	7	115	107	61	19	45	11	41	85	47	26	2							
	sequence_grow	3	2	4	5	6	1	7	8	9	10	11	12	13							
	slotl_base	2	4	5	6	4	6	6	4	5	4	5	4								
	slotl_optimized	6	6	6	6	1	6	6	2	6	3	1	6								
	cost_base	2405.06						**reduction**							14.88%						
	cost_optimized	2047.07																			
mission 2	**sequence_base**	117	38	97	23	121	20	27	25	50	79	35	95	113	55	87	29	90	10	73	31
	sequence_opt	117	38	97	23	121	20	27	25	50	79	95	113	35	55	87	29	73	31	90	10
	sequence_grow	1	2	3	4	5	6	7	8	9	10	12	13	11	14	15	16	19	20	17	18
	slotl_base	6	4	4	2	3	2	6	4	4	6	3	6	6	3	5	5	4	3	3	
	slotl_optimized	4	2	4	3	4	5	6	5	5	5	4	6	3	6	3	6	3	2	3	
	cost_base	7967.09						**reduction**							9.55%						
	cost_optimized	7206.59																			
mission 3	**sequence_base**	71	28	69	65	43	8	4	64	57	102	66	72	77	3						
	sequence_opt	71	69	28	43	65	8	4	66	57	64	102	72	77	3						
	sequence_grow	1	3	2	5	4	6	7	11	9	8	10	12	13	14						
	slotl_base	6	2	5	5	6	3	5	5	3	5	3	3	6							
	slotl_optimized	2	6	5	3	1	1	3	6	6	6	6	6	6							
	cost_base	7287.88						**reduction**							30.29%						
	cost_optimized	5080.71																			
mission 4	**sequence_base**	114	32	22	119	24	108	37	104	112	75	82									
	sequence_opt	82	112	75	22	119	24	108	37	104	32	114									
	sequence_grow	11	9	10	3	4	5	6	7	8	2	1									
	slotl_base	6	6	6	5	5	6	1	6	2	3										
	slotl_optimized	6	3	6	6	3	6	1	5	6	4										
	cost_base	5380.23						**reduction**							46.60%						
	cost_optimized	2872.82																			
TOT	**cost_base**	23040.26						**reduction**							25.32%						
	cost_optimized	17207.20																			

Table 6.25: Optimization of case $4L\_6$

Case 4L_7				
alpha	**beta**	**el**	**dt**	**e**
4	1	0.99	0.007	0.05

mission 1	**sequence_base**	20	117	27	3	25	121	79	55	113	102	50	95	87	23	38	97
	sequence_opt	3	25	121	113	79	55	20	27	102	50	95	87	117	23	38	97
	sequence_grow	4	5	6	9	7	8	1	3	10	11	12	13	2	14	15	16
	slotl_base	1	5	1	4	1	5	5	6	5	4	5	1	5	5	5	
	slotl_optimized	6	5	4	3	5	3	6	5	1	4	1	2	4	6	3	
	cost_base	5079.96						**reduction**					21.98%				
	cost_optimized	3963.55															
mission 2	**sequence_base**	63	11	31	7	47	85	2	26	77	8	41	45	82	4	115	
	sequence_opt	63	11	31	7	85	47	2	26	77	8	82	45	41	4	115	
	sequence_grow	1	2	3	4	6	5	7	8	9	10	13	12	11	14	15	
	slotl_base	4	2	4	6	6	5	6	4	4	3	4	6	4	4		
	slotl_optimized	4	4	3	3	4	5	4	6	6	4	6	5	2	6		
	cost_base	3933.54						**reduction**					18.94%				
	cost_optimized	3188.65															
mission 3	**sequence_base**	29	107	61	73	10	90	71	43	65	28	69	66	19	64	57	72
	sequence_opt	61	107	29	73	10	90	71	43	65	28	69	66	19	64	57	72
	sequence_grow	3	2	1	4	5	6	7	8	9	10	11	12	13	14	15	16
	slotl_base	6	2	6	6	3	3	5	3	6	4	6	6	5	4	5	
	slotl_optimized	5	4	6	2	6	3	6	6	4	1	6	6	5	4	6	
	cost_base	4906.10						**reduction**					4.03%				
	cost_optimized	4708.43															
mission 4	**sequence_base**	114	32	22	119	104	24	108	37	112	75	35					
	sequence_opt	24	104	119	108	37	22	75	35	112	32	114					
	sequence_grow	6	5	4	7	8	3	10	11	9	2	1					
	slotl_base	4	4	5	5	6	3	6	3	6	5						
	slotl_optimized	4	4	6	5	6	6	3	6	5	2						
	cost_base	4886.97						**reduction**					28.04%				
	cost_optimized	3516.51															
TOT	**cost_base**	18806.57						**reduction**					18.24%				
	cost_optimized	15377.15															

Table 6.26: Optimization of case $4L\_7$

Case 4L_8				
alpha	beta	el	dt	e
4	1	0.990	0.007	0.25

mission 1	sequence_base	20	117	25	121	79	55	113	27	102	50	95	87	23	38	97	35							
	sequence_opt	27	20	117	25	113	79	55	121	50	95	87	102	38	97	35	23							
	sequence_grow	8	1	2	3	7	5	6	4	10	11	12	9	14	15	16	13							
	slotl_base	6	5	2	3	4	6	6	4	4	3	2	2	5	6	4								
	slotl_optimized	4	5	6	4	2	2	6	4	2	6	2	6	4	3	6								
	cost_base	5086.80								reduction							20.38%							
	cost_optimized	4050.30																						
mission 2	sequence_base	82	85	26	7	2	63	77	8															
	sequence_opt	82	85	7	2	26	63	77	8															
	sequence_grow	1	2	4	5	3	6	7	8															
	slotl_base	6	3	6	5	2	3	6																
	slotl_optimized	6	6	3	4	3	6	3																
	cost_base	1352.19								reduction							22.48%							
	cost_optimized	1048.25																						
mission 3	sequence_base	57	29	90	61	107	73	10	31	69	66	65	71	28	43	4	19	64	3	115	72	112	45	
	sequence_opt	29	90	61	107	73	10	31	28	69	71	66	43	65	57	4	64	19	72	115	3	112	45	
	sequence_grow	2	3	4	5	6	7	8	13	9	12	10	14	11	1	15	17	16	20	19	18	21	22	
	slotl_base	3	5	6	2	4	6	3	6	3	5	1	3	4	4	5	6	5	3	6	6	5		
	slotl_optimized	6	1	4	6	4	6	3	5	6	5	2	3	3	5	2	6	6	3	6	6	3		
	cost_base	10906.96								reduction							14.12%							
	cost_optimized	9366.42																						
mission 4	sequence_base	114	32	11	47	119	104	24	108	37	75	41	22											
	sequence_opt	11	32	47	114	104	37	108	24	119	22	75	41											
	sequence_grow	3	2	4	1	6	9	8	7	5	12	10	11											
	slotl_base	6	3	5	6	4	4	6	6	6	4	3												
	slotl_optimized	6	6	6	6	6	3	2	3	6	5	4												
	cost_base	4476.76								reduction							13.52%							
	cost_optimized	3871.37																						
TOT	cost_base	21822.72								reduction							15.98%							
	cost_optimized	18336.35																						

Table 6.27: Optimization of case $4L\_8$

It is clear the great improvement obtained, with all the cases being characterized by a total cost reduction of at least the 12%; the case that was subjected to the greatest improvement is $4L\_6$ that presents an overall cost reduction even of the 25%. Analysing the numerical values, however, the best case is the $4L\_7$ that, with a 18.24% total cost reduction, it gets really near to the JPL proposed cost (it is only about the 10% higher). These good results can be explained by the fact that the algorithm applied to the single missions considers a random transfers time sequence that changes at every repetition, giving the possibility to find better solutions. For a clearer and more immediate visualization of these that are the main results obtained by this thesis, in the following pages are reported some bar charts (one for each case) indicating the single missions and total cost before the optimization (in blue) and after the local optimization (in orange) with an indication of the percentage reduction; at the end (from figure 6.53 to figure 6.56), a more detailed visualization of the single transfers of case $4L\_7$ is given.

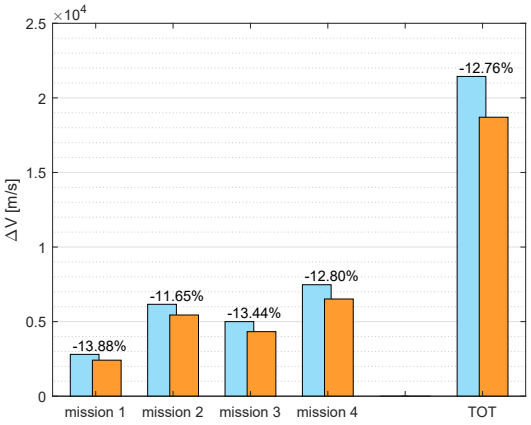

Figure 6.45: Case 4*L*_1 optimized

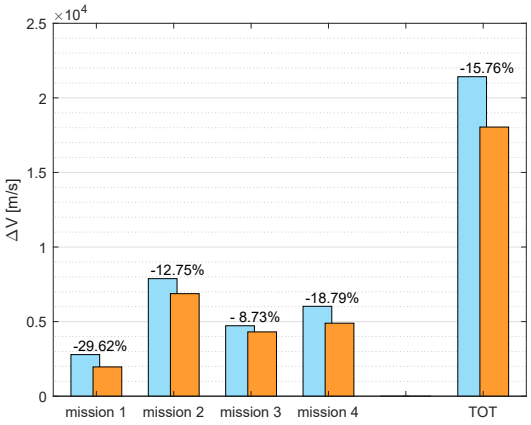

Figure 6.46: Case 4*L*_2 optimized

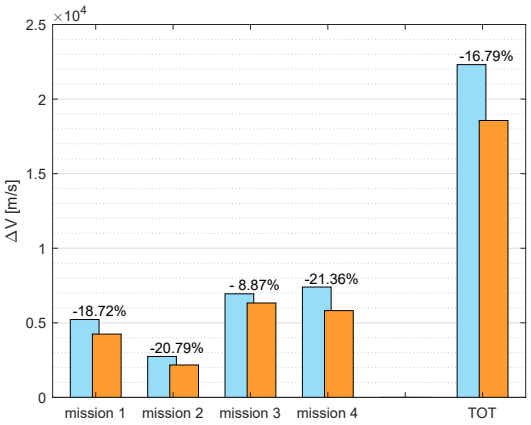

Figure 6.47: Case 4*L*_3 optimized

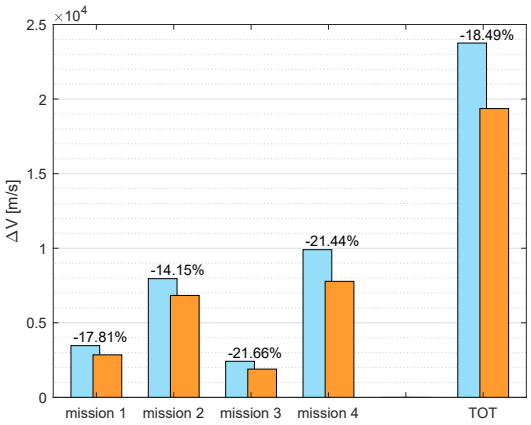

Figure 6.48: Case 4*L*_4 optimized

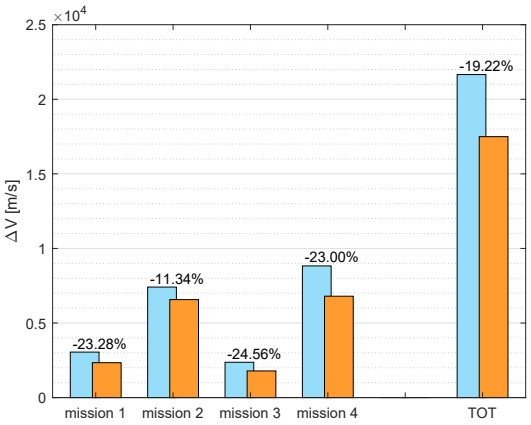

Figure 6.49: Case 4*L*_5 optimized

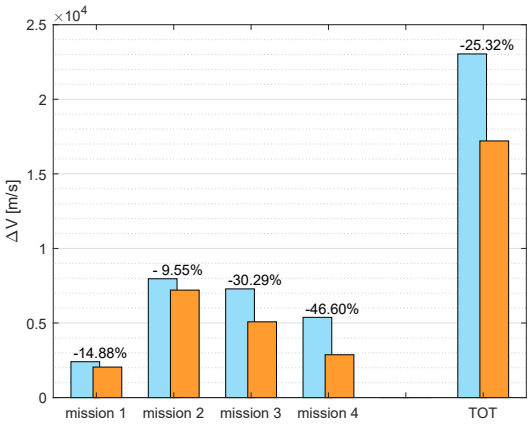

Figure 6.50: Case 4*L*_6 optimized

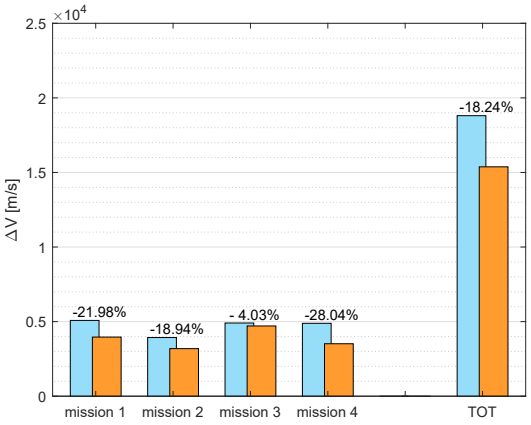

Figure 6.51: Case 4*L*_7 optimized

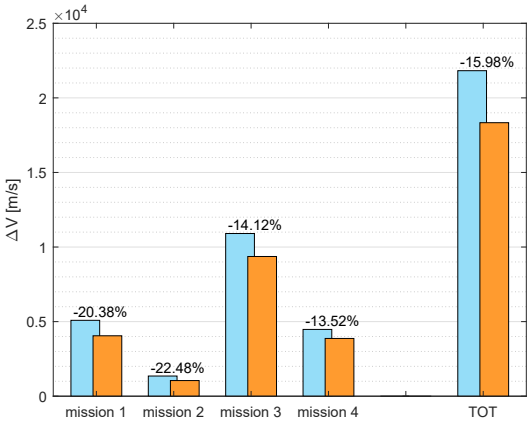

Figure 6.52: Case 4*L*_8 optimized

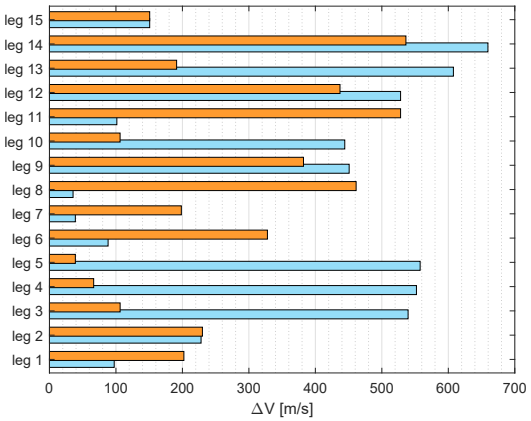

Figure 6.53: First mission of case 4*L*_7

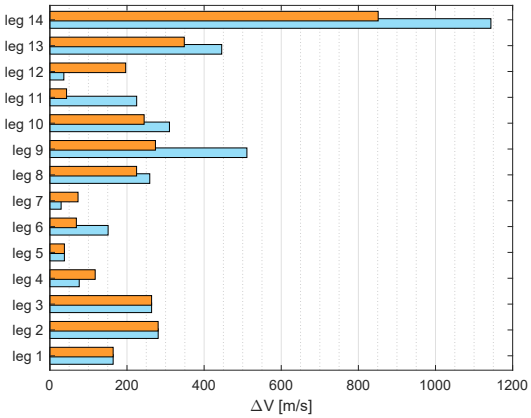

Figure 6.54: Second mission of case 4*L*_7

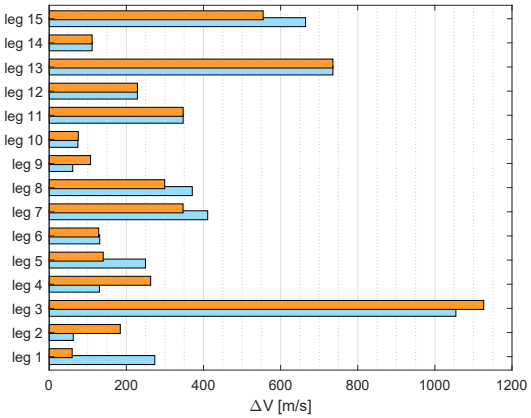

Figure 6.55: Third mission of case 4*L*_7

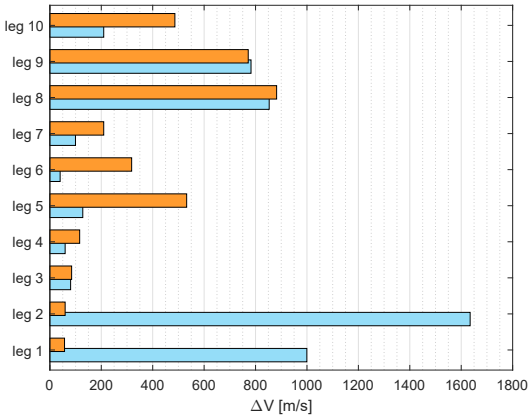

Figure 6.56: Fourth mission of case 4*L*_7

Analysing more in details how the optimization has changed the transfers cost of the case $4L\_7$, it is possible to note an interesting aspect: some of the single legs, after the optimization (represented in orange), have a higher cost, however, the algorithm has been able to cleverly distribute the legs cost variations in order to obtain an overall reduction of the cost. Another interesting aspect is that the optimization tended to reduce the ΔV of the first legs and to increase that of the last legs: from a designing point of view this is a winning and efficient move, since at the end of a mission the spacecraft mass is lower (because of the propellant consumed and the de-orbit packages delivered) and this means that to obtain the same ΔV, less propellant is required.

Chapter 7

Conclusions

Space debris today represents a concerning problem and a real threat for the present and the future of the space activities; there is the need to take action and, since the PMD policy has shown to be not enough, the implementation of ADR missions becomes necessary to avoid the space environment becoming unusable. This thesis focuses on one of the possible ADR techniques for the LEO environment being the rendezvous with a series of debris objects and the delivery of de-orbit packages to make them re-enter into the atmosphere. The work done analyses the use of ACO algorithm to optimize, in term of ΔV cost, the sequence of debris pieces that has to be visited with a variable transfer time; the first part of the study had the goal of analysing how different parameters influenced the algorithm behaviour and how they affected the results obtained; in the second part, an increase in the number of debris bodies to rendezvous with was considered with the further optimization of the single missions determined, thanks to the use of the same ACO algorithm. The results obtained are promising, with the best optimization having a reduction of the campaign ΔV cost of 25% after the individual optimization and with the best solution being only the 10% higher than the exact JPL's solution. These results show the potential of ACO algorithm and, in particular, its good performances in tackling this specific problem in a rapid and effective way; the optimization can be further improved with the change of the ACO algorithm used, like implementing some aspects of ACS or like using a hybrid version. However, already with this work, the debris problem would see an initial solution since the results obtained would make the removal of 16 debris per year (that would actually be 33 debris every two year, given the results obtained) possible, a number further beyond the sought 5 debris per year. The analysis can be continued with the introduction of new debris pieces and new missions and, if the trend observed in this thesis continues, it is possible to predict a further improvement of the solutions obtained with the growing of the problem dimensions (with a limit posed by too big instances that would make this method too slow and inefficient).

Of course, this is only a preliminary study on finding the best sequence possible and on understanding if this type of campaigns would be a possible solution to the space debris problem; a deeper feasibility analysis needs to be done and further studies need to be conducted about the type of propulsion and the type of propellant that can be used and about the mission profile. The electric propulsion is an option that can be evaluated in future studies: it would radically change the problem resulting in a more prolonged time to conclude a campaign and a stronger influence of the J2 effect, given the longer manoeuvres time; however, it would have the benefit of a reduced propellant consumption, resulting in a smaller and lighter spacecraft (even if there would still be the need of bringing the de-orbit packages on board, representing a fixed weight). About the propellant, it would be possible to study the use of some green propellants like the LMP-103S: it would guarantee better performances, lower costs and a much lower toxicity with respect to the more commonly used hydrazine. Considering the implementation of this solution, a great result would be the possibility of adopting a reusable spacecraft that, after having concluded a mission, would came back to Earth for refuelling and loading new de-orbit packages with an important reduction in operating costs; another interesting hypothesis would be the use of an orbiting tank with which the spacecraft would rendezvous at the end of each mission, without the need of launching a new spacecraft. Even if these two solutions may seem science fiction scenarios, it is unquestionable that today they are made closer to reality thanks to the recent achievements of SpaceX's Starship and thanks to the program of the future NASA's Artemis III.

Appendix A

The IJK coordinate system

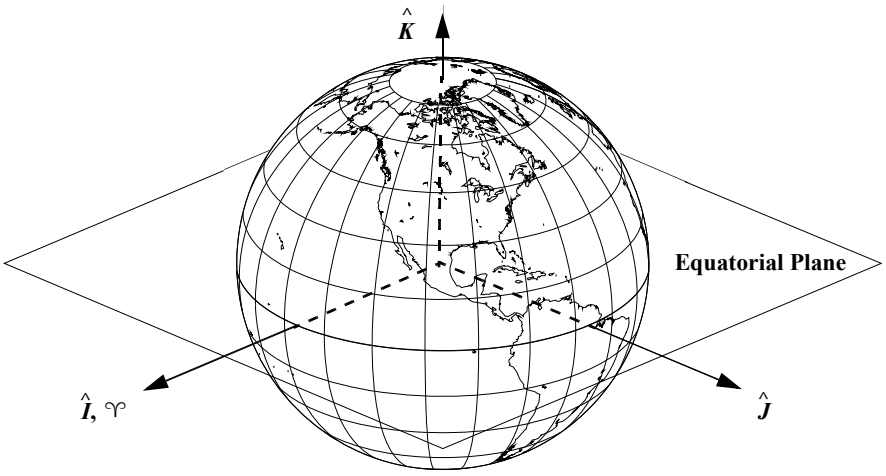

Figure A.1: The geocentric equatorial system (IJK) [17]

The first step before making any orbital mechanics study is to clearly establish a coordinate system with which any calculation is made. The most used coordinate system for satellites orbiting the Earth is the geocentric equatorial system, also called IJK system; its origin is at the centre of the Earth (geocentric) and its fundamental plane is the Earth's equatorial plane. The I axis is defined by the intersection of the ecliptic plane with the equatorial plane during the Vernal equinox; the direction is such that, during the Vernal equinox, the Earth sees the Sun in the Aries constellation. The K axis is perpendicular to the equatorial plane with direction towards the hemisphere which contains Polaris. The J axis completes the right-hand triad. Sometimes confused with the Earth-Centred Inertial system (ECI) it actually is not inertial because the equinox and the plane of the equator slightly move over time; however, considering this system inertial is not a big error.

Appendix B

Combinatorial Optimization Problems

Combinatorial optimization problems are problems that, to be solved, require finding an optimal solution among a set of finite and discrete solutions; to solve a combinatorial optimization problem, it is useful to know how difficult it is to find a solution and a way of measuring this difficulty is correlated to the time required for solving it. First of all, there is the need of introducing the concept of a Touring Machine (TM): it can be considered a primitive computer that is easy to be studied; it consists in a set of internal states, an unbounded tape made of cells and a set of rules. The TM, starting from an initial state given by the input on one tape cell, executes the rules until it runs into a rule that makes it stop; for a standard TM every combination of internal state and tape symbol has exactly one single rule that corresponds to it, meaning that the next move depends uniquely by that pair. There are several TM variants and the most important one is the non-deterministic TM: for this type of TM, every combination of internal state and tape symbol has a set of possible rules that correspond to it and so the TM has a choice of ways to continue. Another essential concept is the one of a problem that can be solved in a polynomial time: it means that there is an algorithm to solve it that takes a number of steps that is a polynomial in the number of digits.

Combinatorial optimization problems are classified into two complexity classes: P and NP problems. P problems can be solved in a polynomial number of steps on a standard TM; NP problems can be solved in a number of steps that is a polynomial function of the size of the input on a non-deterministic TM that always makes the correct choice; another explanation is that NP problems are the ones that can only be verified in polynomial time. Then, it is possible to identify other two categories: NP-hard problems that are at least as hard as the hardest problem

in *NP*, if it is possible to solve these problems in polynomial time, any *NP* problem can be solved; however, these problems are not necessarily *NP* problems meaning that it may not be possible to verify their solution in polynomial time. The other category is the one of *NP* complete problems that are both *NP* and *NP*-hard: if it is possible to solve these problems, any *NP* problem can be solved and the solutions to these problems can be verified in polynomial time. Today, there is still the open question "$P = NP$?" even if most scientists tend to accept that $P \neq NP$; among the most famous *NP*-complete problems there is also the TSP.

Combinatorial optimization problems may be solved using two different classes of algorithms: exact and approximate algorithms. Exact algorithms can find the optimal solution but for most *NP*-hard problems they have pretty bad performances; on the other hand, approximate algorithms trade optimality for efficiency and can be used to obtain solutions in less time. This second class is often referred to as heuristic algorithms and can use two different techniques: constructive or local search methods. Constructive algorithms build a solution in an incremental way, adding solution components; local search methods are based on the iterative exploration of neighbourhoods of solutions in order to improve the current solution with local changes; a negative aspect of this second type of methods is that, even if they can be used to solve hard combinatorial optimization problems in a reduced amount of time, they require a good starting solution: it is for this reason that the two methods are often combined applying firstly the constructive approach to find an initial solution and then the local search to improve it.

A disadvantage of the before indicated single-run algorithms is that they generate a limited number of different solutions (construction heuristics) or stop at unsatisfactory local optima (iterative improvement methods); to solve these problems a series of general approaches, called metaheuristic, have been proposed. They can be considered as a general algorithm that can be applied to different combinatorial optimization problems with little modifications to make them adapted to a specific problem; in other words, they can be considered as general-purpose heuristic methods used to guide a problem-specific heuristic [18].

Appendix C

Debris orbital elements

Here is presented the content of the *.txt* file of the GTOC9 displaying the classical elements of the 123 debris and the epochs at which they have been measured; the first line indicates the content of each column and the measurement unit adopted, in order: the debris id, the reference epoch, the semimajor axis, the eccentricity, the inclination, the RAAN, the argument of perigee and the mean anomaly.

id	ref epoch [mjd2000]	a [m]	e	i [rad]	Ω [rad]	ω [rad]	M [rad]
0	2.1947649637665050E+04	7.1657396824464779E+06	1.4872294030037296E-03	1.7084949743764815E+00	5.4251494477699103E+00	5.1896466191474777E-01	3.2208883569328890E+00
1	2.2167216339714400E+04	7.1194824568500286E+06	1.6818826066925901E-02	1.7190324556571761E+00	4.0302319446772756E+00	2.2497345785659948E+00	4.8807277888575742E+00
2	2.1971814991607400E+04	7.1596212552715428E+06	3.7928260515825026E-03	1.6950996273137624E+00	2.9287068301393302E+00	4.4933242266297109E+00	6.2437606565086217E+00
3	2.2169543272808445E+04	7.1105112426873706E+06	6.6662989696863410E-03	1.6942903799536431E+00	6.2336478358175662E-01	3.4119092650909670E+00	4.7714199815539757E+00
4	2.2052222441592254E+04	7.1020000939046489E+06	1.8296158479309513E-03	1.7498728280660838E+00	2.6225638296225968E+00	2.3970723874904802E+00	3.1329207586641292E+00
5	2.1974981005491496E+04	7.1734650347685460E+06	8.5007296809300539E-03	1.7250021365460082E+00	4.7168822657255580E+00	2.9873237970074014E+00	5.4944812707940045E+00
6	2.2148092594213187E+04	7.0580417103809919E+06	8.7234352836937229E-03	1.7206738530599246E+00	3.5746425158521933E+00	4.9814352991997808E+00	4.1956188833732098E+00
7	2.2142824876524191E+04	7.0596020528455991E+06	2.4932447158364495E-03	1.7069135576765333E+00	1.4559862537354920E+00	4.3020929502250089E+00	5.3481532423694276E+00
8	2.2128717858909135E+04	7.1343239397846498E+06	1.6271597009714870E-02	1.7445269197014779E+00	1.3297786145266177E-01	5.8382098923205268E+00	5.5621781601339935E+00
9	2.2037559358191760E+04	7.1472079797105445E+06	8.0077227049872458E-03	1.7054359870027067E+00	3.3787314329735190E+00	1.2760194010266370E+00	5.2234270395895157E+00
10	2.2187763624733412E+04	7.1622151761647547E+06	2.4022908192228684E-03	1.7179524541970677E+00	2.6044168759567419E+00	1.8942795035536908E+00	4.3848444989363751E+00
11	2.2091992956061134E+04	7.2325076497609392E+06	1.1773575210463410E-03	1.7066308859386896E+00	3.0516552852502272E+00	1.7076541122844591E+00	3.3574832589913597E+00
12	2.1928718422188100E+04	7.1586430111981770E+06	1.0040189006720379E-02	1.7320255324625642E+00	7.2170125435764443E-01	2.9454391014605554E+00	3.2835498420677034E+00
13	2.2178426502743732E+04	7.2364943577317204E+06	3.3123508976602113E-03	1.7137497162075539E+00	1.8043660156735728E+00	4.1480720014348309E+00	2.2581703181417367E+00
14	2.2134431225703171E+04	7.1834394254642036E+06	5.8116054059847893E-03	1.6983761271184348E+00	1.3049702380875483E+00	4.9906874011610523E+00	3.5562531992810604E+00
15	2.2057921381551841E+04	7.1828607044945257E+06	7.2677718502275265E-03	1.7253514550779128E+00	1.2035298909060050E+00	5.5176308702359096E+00	4.0513937316575852E+00
16	2.2029071784023829E+04	7.0894689928508550E+06	8.9326888889894128E-03	1.7152239407832581E+00	1.2304416110682046E+00	2.9125171649255796E+00	1.4008509098039548E+00
17	2.1976563697352434E+04	7.1720225944849178E+06	7.5893483630202667E-03	1.7123965415036928E+00	4.1231617147467006E+00	2.7235734264056872E+00	1.1697634274344053E+00
18	2.1975694539661748E+04	7.1160540084790485E+06	8.9459158777377718E-03	1.7201869268629908E+00	1.8279761920424498E+00	9.1080302919982903E-01	3.2999093640193995E+00
19	2.1931586760054113E+04	7.1303163416429311E+06	1.1013165668174162E-02	1.7213767664138027E+00	2.4191384654330679E+00	2.1026039581904379E+00	1.0309483985080592E+00
20	2.1956811664258676E+04	7.0123578015429014E+06	3.7306380068279953E-03	1.7145647888784965E+00	4.7679056701808413E+00	2.2242109725930712E+00	1.4407588641131199E+00
21	2.2075496256256381E+04	7.0595214196055979E+06	5.3035724008734580E-03	1.7212739396318075E+00	3.2737188088473581E+00	3.3286802852617283E+00	3.5355657675244623E+00
22	2.2069343848537206E+04	7.0625550915621240E+06	4.3442870408157983E-03	1.7274807156156051E+00	5.7747057927675343E+00	5.5322087355228531E+00	5.9103830148672429E+00
23	2.1948744829845527E+04	7.1573978226773487E+06	1.5212151785574607E-02	1.7216539017764789E+00	5.6363586292055992E+00	2.6108330779745432E+00	2.8271977566834545E+00
24	2.2029251106989806E+04	7.1555331719438899E+06	1.3321444405024063E-02	1.7174360733542935E+00	4.0525068916629250E+00	7.2403243072993662E-01	5.5759592098961139E+00
25	2.2130244426204234E+04	7.1464835814257395E+06	8.8690120247721140E-03	1.7159961448710592E+00	3.1149672619883688E+00	4.9101235612376826E+00	1.9099320863932947E+00
26	2.2061290194591929E+04	7.1039263464457355E+06	5.8569091102657986E-03	1.6951486894980508E+00	3.4127281819364517E+00	3.5456193218613050E+00	5.6164298976873681E-02
27	2.2031785631728311E+04	7.1790690163070457E+06	1.2466361831497469E-02	1.7272417777180353E+00	6.0033713676831582E+00	4.2489596845890985E+00	3.1308889128759659E-01
28	2.2106503602448225E+04	7.1548926144156400E+06	8.5901282030945436E-03	1.7120961575913876E+00	2.4572206030974217E+00	4.3217101229759586E-01	4.3437959455053639E+00
29	2.1979331806257043E+04	7.2122805333583979E+06	5.3956273119150225E-03	1.7242717175613382E+00	5.0395440741529400E+00	5.1225128189834539E+00	1.2919866064654601E-02
30	2.2171949104583124E+04	7.0431049324577386E+06	6.4494782640898366E-03	1.7131987270766398E+00	7.8965530147945362E-01	5.5593420114028174E+00	1.5533958461281466E-01
31	2.2100945181434621E+04	7.0511735148911076E+06	6.4404280075398591E-03	1.7420043786805250E+00	5.4463005936920865E+00	8.3721710495148161E-01	2.3101662836450814E+00
32	2.2087473578509675E+04	7.1383156311670616E+06	1.5510661800150968E-02	1.7236853831563850E+00	2.3591664859976991E+00	5.9022304190593484E+00	5.8196021023314177E+00
33	2.2089365771485533E+04	7.1733325035796296E+06	1.7588786078658327E-04	1.7438626369040473E+00	5.3942322768045923E+00	2.6724698576601229E+00	3.9194811262667328E+00
34	2.1983510862905558E+04	7.0779741771415481E+06	1.4009942129800680E-02	1.7215325437741333E+00	1.1823804809187488E+00	2.4169663867550462E+00	3.3484602935716228E+00
35	2.2190319956868829E+04	7.1815335356525052E+06	8.2694096670929921E-03	1.6872536314195152E+00	4.1953711487235674E+00	4.7248177184707432E+00	1.9828268904413309E+00
36	2.2090616310520716E+04	7.1266443595469426E+06	1.8884742998232167E-02	1.7320881079442307E+00	4.6361372304766943E+00	1.8936129053661557E+00	1.9648682839730347E+00
37	2.2009128889703745E+04	7.0522455231495667E+06	1.0226105517608826E-03	1.7045167205637233E+00	5.6055751997810201E+00	3.6164072587258722E-01	5.3431740930722107E+00
38	2.1931689936687369E+04	7.2156436338522844E+06	7.6753809657671562E-03	1.7188962371369039E+00	7.3520127753738185E-01	3.4025158235750408E+00	4.7063636408505069E+00
39	2.2073480116883646E+04	7.2155867520766146E+06	7.1447854891607595E-03	1.7428349992255205E+00	1.2067432088736836E+00	1.1585490122341995E+00	2.9091196055806097E+00
40	2.2106597160092482E+04	7.1155445662984997E+06	3.4822798542468746E-03	1.7177296660679058E+00	3.3414080979386287E+00	5.4941099459201643E+00	5.5670277741425456E-01

id	ref epoch [mjd2000]	a [m]	e	i [rad]	Ω [rad]	ω [rad]	M [rad]
41	2.2181546561241721E+04	7.0537312368787061E+06	3.7862236257196992E-03	1.7035488797357139E+00	2.8474057854962371E+00	3.6608319638678997E+00	3.8182791770148365E+00
42	2.2072358466858957E+04	7.1600584675016981E+06	5.8170487663027487E-03	1.7222866047584235E+00	2.4941440448754115E-01	2.4964511089227650E+00	5.8140788801379308E+00
43	2.2072354706048889E+04	7.0562341483805571E+06	8.3186072168059365E-03	1.7248401261454507E+00	2.7727456320765680E+00	5.4730275482522117E+00	5.6640929684694878E+00
44	2.2055219696911659E+04	7.2285245139823500E+06	1.6432740854238829E-03	1.7425014513366612E+00	5.7897048728397511E+00	4.7090007348192708E+00	6.2728250610625018E+00
45	2.1970940786550811E+04	7.1967875745517286E+06	8.9620265989971380E-03	1.7131061997439556E+00	5.7168231729127674E+00	9.9388397107801385E-01	5.2860493835605329E+00
46	2.2044226375825379E+04	7.1728480968989916E+06	7.9159186812811607E-04	1.7332902080040073E+00	5.8397411393420162E+00	1.2834637264579531E+00	5.6396537589788720E-01
47	2.2116530205686773E+04	7.1983810963819930E+06	7.0110951916878305E-04	1.7039179284859733E+00	3.6556430044342076E+00	3.5753756946842765E+00	1.9953739732575226E-01
48	2.2155193984658359E+04	7.2260747106473614E+06	3.2078681129155948E-03	1.7040592632195255E+00	3.9881908170829217E+00	3.3815011786417442E+00	3.5585393734014956E+00
49	2.1919258898316097E+04	7.1636298433968909E+06	6.0022204845783956E-03	1.6940426588185797E+00	2.8896213047682268E-01	1.0664187967062160E+00	4.4035533535287996E+00
50	2.2182664370105940E+04	7.2298836862790585E+06	2.9917620092200794E-03	1.7134303650042442E+00	5.6926197217389527E+00	1.2233136774674289E+00	4.1318990297592326E-02
51	2.2044920207572985E+04	7.2739820311951246E+06	4.5501936582343245E-04	1.6984418143865772E+00	6.0695146770589146E+00	2.5126745662421355E+00	4.0860220181482437E-01
52	2.2073359216226632E+04	7.1840646567192953E+06	1.2200894059330541E-02	1.7032379552587862E+00	4.3875259731814475E+00	4.2857308477606502E+00	2.2649606756697751E+00
53	2.2205209609883474E+04	7.1206047619816754E+06	1.8748484639598464E-02	1.7243522402183677E+00	1.1940441927132608E+00	6.0338292424834350E+00	2.3180748141847425E+00
54	2.2178806845173607E+04	7.0827093171032118E+06	5.4624296859097409E-03	1.7260128697659984E+00	7.6512910206348372E-01	3.8751061612825590E+00	4.1741915005385852E+00
55	2.1919141218682595E+04	7.1119544452803489E+06	7.2193999746037766E-03	1.7008450549301035E+00	2.2287562039418822E+00	3.0204626824881009E+00	2.4608001081360684E-01
56	2.2166542627464853E+04	7.1328845283907494E+06	1.5710587455467794E-02	1.7218054617786223E+00	1.3992166343807633E+00	2.8127235385722593E+00	2.1255691897846543E+00
57	2.2178469846282238E+04	7.1143762048009802E+06	3.0421126849487285E-04	1.6930494943764807E+00	1.5193391565747167E+00	1.5599742418151235E+00	5.6825470758277430E-01
58	2.2006332507567706E+04	7.1056280441766176E+06	1.1732939476348967E-02	1.7262279765290676E+00	3.1441764475246430E+00	5.2611532849012335E+00	2.5663829610793720E+00
59	2.2163240281393657E+04	7.2712467703733621E+06	3.7621960354441167E-04	1.7212799166847672E+00	4.8395782921675762E-01	2.2160044247743689E+00	5.0772463754078387E+00
60	2.2177320616762518E+04	7.1716012040374856E+06	2.1047874933081073E-04	1.7275989015732440E+00	1.1663700094786258E+00	3.9608426165574842E+00	5.2466952870077899E+00
61	2.2017124740562955E+04	7.0085967511928463E+06	9.6657821225086700E-04	1.7246480834680864E+00	1.4474464886844627E+00	1.3160281382469714E+00	2.1844062662362118E+00
62	2.2211036326393703E+04	7.0819101487611402E+06	1.4223022718280010E-02	1.7181056414718701E+00	4.1357457757784761E+00	4.5125407881632258E+00	4.7150846681953178E+00
63	2.1948368543193159E+04	7.0282159997846913E+06	3.3813812507357444E-03	1.7018642596525826E+00	5.1547319645647347E+00	6.0194532582543605E+00	3.4102941141740866E+00
64	2.2189004682927152E+04	7.0891769168093726E+06	1.1094715846474828E-02	1.7011298552037972E+00	5.2725641283662759E+00	5.8736657019993128E+00	2.6358901555757273E+00
65	2.1985511836499572E+04	7.1821031446048273E+06	1.4540395437083150E-03	1.7200544253523042E+00	5.0991392141449134E+00	6.2489941242111229E+00	1.0770567821776937E+00
66	2.2079395819412173E+04	7.1687288234295696E+06	8.1745810104903917E-03	1.7118881025766945E+00	2.2351058161744106E+00	6.1633980114305968E+00	1.2800966525662680E+00
67	2.1997984183882658E+04	7.1633269926687032E+06	1.3373183859161334E-02	1.7059777602540207E+00	4.7252840425713183E-01	3.2814162358718839E+00	5.5138732706838125E+00
68	2.2045994762104783E+04	7.0867899522829605E+06	5.3141553993309018E-03	1.7355722160723295E+00	4.9926834967080058E+00	3.0247680333777667E+00	2.1255078945244210E+00
69	2.2045557194956789E+04	7.0431946071981397E+06	8.8599667139060648E-03	1.7060479901576877E+00	1.0007467177243383E+00	1.6051909074038720E-01	3.0469359063417198E+00
70	2.2093406321657600E+04	7.0480234701131647E+06	9.3019444788688260E-03	1.7105222032478846E+00	5.7590824068411042E+00	7.7546768833529622E-01	5.3222221475105336E+00
71	2.2184960029949372E+04	6.9961042701278944E+06	1.6195224821454204E-03	1.7210822050247361E+00	4.7763457420678730E+00	2.7696818579916922E+00	5.0531882245756576E-01
72	2.2186506727661585E+04	7.1586608796730023E+06	8.8093103111976170E-03	1.7049922072391817E+00	5.2148345224712571E+00	2.6463789090242815E+00	3.6333320001306896E+00
73	2.2176187952287721E+04	7.0997443373522386E+06	1.0022275901682637E-02	1.7140108243844197E+00	2.3039176302152424E+00	4.8418211596697578E+00	3.6025465702163886E+00
74	2.2090756786585865E+04	7.1365075652298192E+06	1.9318060962718084E-02	1.7624919151168126E+00	3.8052584717681466E+00	1.6532789006091402E+00	3.0137669349616565E+00
75	2.2020123357027613E+04	7.0955686484739427E+06	1.1772361985212523E-02	1.7146347629642993E+00	3.7361493756263959E+00	2.7575974229800186E+00	6.3578365412810645E-01
76	2.2069039197899721E+04	7.0440736948122876E+06	3.8167773124460724E-03	1.7269158049937028E+00	3.2398209555803703E+00	9.7847934284866156E-02	5.1640747953863830E-01
77	2.2137636871397644E+04	7.1175384406800950E+06	1.0915119339331225E-02	1.7251715951096656E+00	4.2823553590123149E+00	6.9395098319210136E-01	5.8438457313897221E+00
78	2.2209547485415889E+04	7.1109906600534106E+06	3.8565218749051443E-03	1.7178475070344257E+00	3.2997546040568797E+00	5.4804048988930809E+00	3.6099256074234982E+00
79	2.2009653278978960E+04	7.0958242874252126E+06	1.4582049263723295E-02	1.7059189934667947E+00	2.4165867791564595E+00	5.0206313578910420E+00	5.6361900556679290E+00
80	2.1948912499956517E+04	7.0914633510917975E+06	9.6641139622932366E-03	1.7123365971163147E+00	1.3612865409546255E+00	6.2796954716614914E+00	8.4065067387618064E-01
81	2.1993439972648222E+04	7.1319174665910909E+06	1.4624954360824376E-02	1.7304222775526015E+00	5.0832991374551106E+00	4.2515961487354259E-01	9.1457019973320197E-01
82	2.2068730606255926E+04	7.1667229436290581E+06	7.2855383648181013E-03	1.7118659052980396E+00	8.0676295252394914E-01	5.5780118411717980E+00	4.2157304137638274E+00
83	2.2186920695821791E+04	7.0452730690178890E+06	1.2055927176520007E-03	1.7352783426273417E+00	5.2287798382216417E+00	3.6456990858463647E+00	4.7946769138740226E+00
84	2.2183126261371559E+04	7.1688227550771963E+06	8.7944941814681200E-03	1.7319518833884155E+00	1.4051043004545718E+00	2.2048195488435027E+00	3.3710490411276611E-01
85	2.2199447334976554E+04	7.2326969750298122E+06	9.0471773767734020E-04	1.7083959100774138E+00	4.4715006952838880E+00	4.3363978788567916E+00	4.2947628179948794E+00
86	2.2159200221347182E+04	7.1640805910059214E+06	4.8558076134916448E-03	1.7429814532121297E+00	4.6633765351924339E+00	1.9933853377993427E+00	4.2962177907899024E+00
87	2.2012963799731206E+04	7.1347437131959293E+06	1.7972542171495187E-02	1.6903589325124464E+00	1.6118829302766163E-01	1.5583972332967269E-01	5.5820969403177347E+00
88	2.2012679626211182E+04	7.1480170031832065E+06	1.6163769764606806E-02	1.7206069452035428E+00	3.4084613046222954E+00	2.6428412096696001E+00	7.3016285773200396E-01
89	2.2142048184397634E+04	7.2066042702119499E+06	1.7080045147391503E-03	1.7156196429772856E+00	7.4320315571008078E-01	4.3263792920130104E+00	5.5010823424141959E+00
90	2.2100853440830062E+04	7.2364403247203296E+06	4.7855129948774786E-03	1.7181879133869626E+00	2.3718533924912508E+00	6.2527984950062487E+00	4.4683225431172939E+00
91	2.2096126117240376E+04	7.1312035441568093E+06	5.7492976726698403E-03	1.7479532116032237E+00	5.4432006530001686E+00	2.7732881182542057E-01	3.2398795672527632E+00
92	2.2137840884012039E+04	7.0728773408125304E+06	1.7498203979812602E-03	1.7005523181555344E+00	3.3875792540865401E-01	1.2800686160039740E+00	6.0943937408199407E+00
93	2.2196704127081510E+04	7.1222652922248837E+06	9.9379692949495557E-03	1.7052791686055375E+00	5.3604697012136198E+00	2.4262837970310058E+00	4.5959398681615040E+00
94	2.2078773798168124E+04	7.0985778576443586E+06	6.4462931153876756E-03	1.7323900027585808E+00	3.3827778486909371E-01	7.7479518928343549E-01	4.4283860105720168E+00
95	2.1921771578919277E+04	7.2056114354656432E+06	7.8716644870463932E-03	1.7042082617249430E+00	3.1061071695453046E+00	1.9010241910924512E+00	3.9181627643965085E+00
96	2.1959443768936169E+04	7.1017104353711102E+06	2.8986025214346105E-03	1.7311066739265173E+00	3.0462850210516739E+00	2.0478382195513030E+00	2.2383482806859384E-01
97	2.1977593507699592E+04	7.0899475992780998E+06	1.5993969373482495E-03	1.7019626977660338E+00	3.2988477592372596E+00	5.5248613572498140E-01	5.2378102292088009E+00
98	2.2092567948924211E+04	7.2588711307795681E+06	2.5978142527248284E-03	1.7201556992141955E+00	5.6666218536714412E+00	4.9445371149564412E+00	4.3991351594269119E+00
99	2.1998196132537287E+04	7.1510842673991937E+06	1.0309155791164525E-02	1.7153443549008842E+00	3.1952938240664239E+00	2.4574958739073454E+00	5.2868953408200241E+00
100	2.2149374413090936E+04	7.1652280903818859E+06	1.3383384270878484E-02	1.7216907588303647E+00	5.5064988026377415E-01	3.3987073688977572E+00	4.9931133866366704E+00
101	2.2165269690097237E+04	7.0692867927575335E+06	4.8051230560654402E-03	1.7030360748582729E+00	8.4963089183265772E-01	4.0094993214479171E+00	1.2869051723859843E+00
102	2.2184404174064908E+04	7.1146699073704677E+06	7.6203646555481159E-03	1.7639595215680164E+00	1.3271059114527712E+00	7.5010646132919467E-01	3.7323443632963667E+00
103	2.2211358428428794E+04	7.1828228078946415E+06	1.3121882178922047E-04	1.7191575454172257E+00	5.0171299539534369E+00	5.1571293095340369E+00	1.4514145023718026E+00
104	2.2027282877856735E+04	7.1378151205907669E+06	4.3741423663386046E-03	1.7099007602062939E+00	5.9543052456394676E+00	6.1226460102772826E+00	5.1464486420502853E+00
105	2.2013340779681730E+04	7.1586530208477378E+06	5.2483164202037930E-03	1.7307732652215102E+00	5.7883013204191061E+00	4.3007246611212846E+00	8.0482639773526155E-01
106	2.2132901796983588E+04	7.1021730836894019E+06	1.2238235121960209E-02	1.7353442812874009E+00	9.0700698294148563E-01	3.8248618034002688E+00	2.6154307768775054E+00
107	2.2042676361728983E+04	7.0787447114419416E+06	1.0926894137701443E-02	1.7304588752794843E+00	1.8419231628655386E+00	1.0954462462362624E+00	5.7563854337945364E-01
108	2.1977382751816251E+04	7.1543581531256661E+06	1.3311866252980474E-02	1.7153861200817262E+00	3.8031578317423747E+00	3.8294186733432753E+00	2.7716788514284487E+00
109	2.2179647978757417E+04	7.0816056032247618E+06	6.6848616695973266E-03	1.6796369801682678E+00	1.7976276953897439E+00	1.7520617530039719E+00	3.7155389266165089E+00
110	2.2171542134845920E+04	7.0399828272993378E+06	8.0246151973830393E-03	1.7066398849824660E+00	3.3202457565355075E+00	1.0260665319926889E+00	5.0935780051250057E-01
111	2.2097837292221255E+04	7.1116691803758247E+06	3.9945400674119324E-03	1.7196257237148562E+00	5.3370927429813353E-01	4.0537404048670762E+00	3.0359102114114513E+00
112	2.1927288941126742E+04	7.1279406944167428E+06	6.2708096351464324E-03	1.6964051527852968E+00	2.5529766706451547E+00	3.7582283745148315E+00	4.9340755746347957E+00
113	2.2006029422436750E+04	7.1068472064248882E+06	1.3967797404851538E-03	1.7037453945063739E+00	2.9207407561315852E+00	3.6801831522152093E+00	6.0019507085513690E-01
114	2.2128601160391125E+04	7.1120055866450276E+06	1.3561981138585460E-02	1.7263915979294957E+00	1.5064075711549956E+00	3.0218371469877107E-02	4.0283762096609887E+00
115	2.2203068052243107E+04	7.1285734628544971E+06	6.9382589158470344E-04	1.7186620978213143E+00	1.2537677159116398E+00	7.1071385284506100E-02	5.7715629253636758E+00
116	2.2056732352276045E+04	7.1534623433983997E+06	1.2588526707125717E-02	1.7198750003376257E+00	2.2108528254934559E+00	8.8446228901499913E-01	3.2200450177407980E+00
117	2.2187674306585417E+04	7.0551211862821421E+06	3.3429292710779337E-03	1.7252913477749166E+00	1.3424448800805884E+00	5.5735697790101639E+00	3.4790134980232836E+00
118	2.2120680757028877E+04	7.1436814967498723E+06	5.2750640926571809E-03	1.7051952832434334E+00	5.1479055058387146E+00	4.6657931150205995E-01	3.8188656897403370E+00
119	2.1985467231746807E+04	7.1236066486014575E+06	1.9671672048720040E-03	1.7177855058331584E+00	2.4658155016064462E+00	5.7642962589185895E+00	3.2999201272266392E+00
120	2.2046861190029143E+04	7.1378410281004757E+06	6.7681479312739620E-03	1.7392207510691602E+00	4.5128692291610628E+00	5.9714662996213246E+00	2.1623307875177531E+00
121	2.2047241592465343E+04	7.0449162288662978E+06	1.3994745303859671E-03	1.7171004089978914E+00	2.1737679601795284E-01	4.8827391731757253E+00	2.8327649313298746E+00
122	2.1997682969749330E+04	7.1565544201999474E+06	8.8214761474042051E-03	1.7059858422924437E+00	4.6259954675669990E-01	9.6977896913311734E-01	4.9318283510214940E+00

Bibliography

[1] Donald J. Kessler, Nicholas L. Johnson, J.-C. Liou, and Mark Matney. «The Kessler syndrome: Implications to future Space Operations». In: *Advances in the Astronautical Sciences* (2010) (cit. on pp. 1, 3, 7–9).

[2] Jeffrey Stuart, Kathleen Howell, and Roby Wilson. «Application of multi-agent coordination methods to the design of space debris mitigation tours». In: *Advances in Space Research* (2016) (cit. on pp. 4, 5, 7).

[3] Lorenzo Casalino and Dario Pastrone. «Active debris removal missions with multiple targets». In: *AIAA/AAS Astrodynamics Specialist Conference* (2014) (cit. on p. 4).

[4] ESA Space Debris Mitigation WG. *ESSB-ST-U-007 Issue 1. ESA Space Debris Mitigation Requirements*. Tech. rep. ESA, 2023 (cit. on pp. 5, 8).

[5] T.S. Kelso and S. Alfano. «Satellite orbital conjunction reports assessing threatening encounters in space (SOCRATES)». In: *Proceedings of SPIE - The International Society for Optical Engineering* (2006) (cit. on p. 6).

[6] URL: `https://nanoavionics.com/blog/nanoavionics-mp42-satellite-survives-impact-with-object-in-orbit/` (cit. on p. 6).

[7] URL: `https://www.aftc.af.mil/News/On-This-Day-in-Test-History/Article-Display-Test-History/Article/2311875/september-13-1985-anti-satellite-missile-testing/` (cit. on p. 7).

[8] Nicholas L. Johnson, E. Stansbery, J.-C. Liou, M. Horstman, C. Stokely, and D. Whitlock. «The characteristics and consequences of the break-up of the Fengyun-1C spacecraft». In: *Acta Astronautica* (2008) (cit. on p. 7).

[9] URL: `https://nssdc.gsfc.nasa.gov/nmc/spacecraft/display.action?id=1982-092A` (cit. on p. 7).

[10] URL: `https://www.armscontrol.org/act/2022-12/news/un-first-committee-calls-asat-test-ban` (cit. on p. 7).

[11] Brent W. Barbee, Salvatore Alfano, Elfego Piñon, Kenn Gold, and David Gaylor. «Design of spacecraft missions to remove multiple orbital debris objects». In: *2011 Aerospace Conference* (2011) (cit. on pp. 7, 10).

[12] URL: https://www.space.com/space-exploration/satellites/worlds-1st-wooden-satellite-arrives-at-iss-for-key-orbital-test (cit. on p. 11).

[13] URL: https://www.heospace.com/ (cit. on p. 12).

[14] URL: https://clearspace.today/ (cit. on p. 13).

[15] URL: https://astroscale.com/missions/adras-j/ (cit. on p. 13).

[16] Roger R. Bate, Donald D. Mueller, and Jerry E. White. *Fundamentals of Astrodynamics*. Dover Publications, 1971 (cit. on p. 15).

[17] David A. Vallado. *Fundamentals of Astrodynamics and Applications*. Microcosm Press, 2013 (cit. on pp. 17, 21, 27, 30, 102).

[18] Marco Dorigo and Thomas Stützle. *Ant Colony Optimization*. A Bradford Book, The MIT Press, 2004 (cit. on pp. 38–40, 43, 46, 48, 77, 104).

[19] Marco Dorigo and Luca Maria Gambardella. «Ant Colony System: A Cooperative Learning Approach to the Traveling Salesman Problem». In: *IEEE Transactions on Evolutionary Computation* (1997) (cit. on p. 48).

[20] URL: https://sophia.estec.esa.int/gtoc_portal/ (cit. on p. 49).

[21] Dario Izzo and Marcus Märtens. «The Kessler Run: On the Design of the GTOC9 Challenge». In: *Acta Futura 11* (2018) (cit. on pp. 50, 51).

[22] Anastassios Petropoulos et al. «GTOC9: Results from the Jet Propulsion Laboratory (team JPL)». In: *Acta Futura 11* (2018) (cit. on pp. 51, 53).

[23] Hong-Xin Shen and Lorenzo Casalino. «Simple ΔV Approximation for Optimization of Debris-to-Debris Transfers». In: *Journal of Spacecraft and Rockets* (2020) (cit. on pp. 53, 55–58).